REPORT DOCUMENTATION PAGE

Form Approved
OMB No. 0704-0188

1. REPORT DATE *(DD-MM-YYYY)*	2. REPORT TYPE	3. DATES COVERED *(From - To)*
	Final Technical Report	23 Aug 2004 – 31 Aug 2006

4. TITLE AND SUBTITLE
Geopolymers for Structural Ceramic Applications

5a. CONTRACT NUMBER

5b. GRANT NUMBER
FA9550-04-C-0063

5c. PROGRAM ELEMENT NUMBER

6. AUTHOR(S)
Mr. Douglas C. Comrie

5d. PROJECT NUMBER

5e. TASK NUMBER

5f. WORK UNIT NUMBER

7. PERFORMING ORGANIZATION NAME(S) AND ADDRESS(ES)
Catawba Resources, Inc.
4281 Meadowlark Trail
Stow Ohio 44224

8. PERFORMING ORGANIZATION REPORT NUMBER

9. SPONSORING/MONITORING AGENCY NAME(S) AND ADDRESS(ES)
Air Force Office of Scientific Research (AFOSR)
875 N. Arlington St., Rm. 3112
Arlington, VA 22203
Dr Joan Fuller/NA

10. SPONSOR/MONITOR'S ACRONYM(S)
AFOSR

11. SPONSORING/MONITORING AGENCY REPORT NUMBER
AFRL-SR-AR-TR-07-0073

12. DISTRIBUTION AVAILABILITY STATEMENT
DISTRIBUTION A: Approved for public release; distribution unlimited.

13. SUPPLEMENTARY NOTES

14. ABSTRACT

Geopolymers show promise in a variety of structural ceramic based application including refractory adhesives for ceramics and metals, thermal shock resistant molds, fiber reinforced composites, and as a precursor in the formation of pure ceramic phases such as leucite ($KAlSi_2O_6$) and pollucite ($CsAlSi_2O_6$) with tailorable porosity and thermal expansion. In this work, the scientific details of using geopolymers in these emerging areas were explored via mechanical and structural testing, and within an industrial setting. A variety of techniques including shear strength testing, microstructural analysis, laser scanning confocal microscopy, and X-ray analysis were to characterize fabricated materials.

As adhesives, geopolymers were effectively used to bond low-carbon steel and borosilicate glass at ambient and elevated temperatures (450°C). The steel/geopolymer bonds had shear strengths between 2 - 3 MPa while the borosilicate/geopolymer bond strength was undetermined; during testing, fracture occurred within the glass itself, not within the geopolymer bond or at the interface.

15. SUBJECT TERMS

16. SECURITY CLASSIFICATION OF:			17. LIMITATION OF ABSTRACT	18. NUMBER OF PAGES	19a. NAME OF RESPONSIBLE PERSON
a. REPORT	b. ABSTRACT	c. THIS PAGE			19b. TELEPONE NUMBER *(Include area code)*
Unclassified	Unclassified	Unclassified	Unclassified	136	(703)

GEOPOLYMERS FOR STRUCTURAL CERAMIC APPLICATIONS

CONTRACT #FA9550-04-C-0063

CONTRACT PERIOD

2004 AUGUST 23

TO

2006 AUGUST 31

DR. TRUDY KRIVEN
DEPARMENT OF MATERIALS SCIENCE AND ENGINEERING
UNIVERSITY OF ILLINOIS, URBANA-CHAMPAIGN

CAROLYN A. KELLY
DOUGLAS C. COMRIE
CATAWBA RESOURCES, INC.
4281 MEADOWLARK TRAIL
STOW, OHIO 44224

GEOPOLYMERS FOR STRUCTURAL CERAMIC APPLICATIONS
FA9550-04-C-0063

Dr. Trudy Kriven
Department of Materials Science and Engineering
University of Illinois, Urbana-Champaign
Carolyn A. Kelly
Douglas C. Comrie
Catawba Resources, Inc.
4281 Meadowlark Trail
Stow, Ohio 44224

Abstract

Geopolymers, also called geo-cements and low-temperature synthesized glasses, are a class of cementious materials that do not depend on the presence of calcium. Geopolymers are formed by mixing aluminosilicate materials (e.g. metakaolin, fly ash) with alkali or alkali-silicate solutions.[1] MacKenzie and Barbosa hypothesized that geopolymers are formed from cross-linked AlO_4^- and SiO_4 tetrahedral, where charge-balancing cations are provided by hydrated alkali metal cations, i.e. Li^+, Na^+, K^+, Rb^+ or Cs^+.[2] Geopolymers have been the subject of numerous studies.[1-14] Applications of geopolymers have included ceramic matrix composites,[1, 3] waste encapsulation [9-11] and alternative cements.[7, 12, 14]

As adhesives, geopolymers may offer significant advantages over conventional organic glues. Geopolymers exhibit high chemical corrosion resistance to both acids and bases and unlike organic adhesives, are inflammable. Latella *et al.* reported the strain release rate of geopolymer adhesives, bonding glass to steel ranged from 0.38 – 1.02 J/m^2 (comparable to an epoxy resin).[15] In this work, geopolymers were used to bond 6061-T6 aluminum alloy, low-carbon steel and borosilicate glass at ambient and elevated temperatures (450°C). Shear strengths of the geopolymer bonds were determined using single and double lap-shear tests. The steel/geopolymer bonds had shear strengths between 2 - 3 MPa. The shear strengths of the borosilicate/geopolymer bonds were undetermined; during testing, fracture occurred within the glass itself, not within the geopolymer bond or at the interface. Subsequent heating of the glass and steel to 450°C did not affect the strength of the geopolymer bond. The geopolymer corroded the aluminum alloy severely and showed no adhesion. The compositions of the geopolymer adhesive interfaces were studied with scanning electron microscopy (SEM) and energy dispersive spectroscopy (EDS).

Durable materials with exceptional thermal shock resistance are needed to improve the efficiency of casting Fe_2Si for use in the specialty steel market. Continuous graphite-fiber reinforced geopolymer molds incorporating fillers of Al_2O_3, SiC, or molybdenum

were engineered for the net-shape casting of Fe_2Si. Molds were fabricated by either hand-lay up or cured in a hydraulic press operating at $\geq$ 21.5 MPa. Molten Fe_2Si (1428°C) was poured into the finished molds at Calvert City Metals and Alloys LLC (CCMA). SEM analysis of the molds showed no difference between molds using different filler phases. Without the use of pressure during curing, infiltration between the graphite-fibers was minimal. Pressure curing of the molds increased the density of the overall matrix as well as improved the infiltration of the geopolymer matrix between the individual graphite fibers. Crystallites, possibly of leucite, were found precipitating out of the geopolymer matrix in regions near the pour zone. The sheath-like morphology of the crystallites is similar to that which is found in some glass ceramics.[16]

Geopolymer molds reinforced with continuous graphite-fibers survived initial thermal shock testing at CMMA. Poor infiltration of the geopolymer matrix between graphite fibers however, led to significant spalling of the geopolymer matrix after thermal shock testing. In response, chopped-fiber reinforced geopolymer composites were processed as possible candidate mold materials for casting Fe_2Si. The resulting composite materials were produced into flat panels that could be machined into simple geometries. Limitations on scaling up the continuous and chopped-fiber reinforced composites to the necessary test sizes required by CCMA prevented additional field-testing. Thermal conversion of the chopped-fiber composites into glass ceramics resulted in severe microcracking of the composite materials.

Unlike conventional cements, geopolymers do not depend on the formation of a hydrated compound, e.g. calcium silicate hydrate. As such, it may be possible to create monolithic shapes of geopolymer and convert them into a ceramic phase by heating. A low water content geopolymer, having a molar composition of $K_2O{\bullet}Al_2O_3{\bullet}4SiO_2{\bullet}7.5\ H_2O$, reinforced with amorphous 500 nm silica spheres, was made and thermally converted into crystalline leucite $KAlSi_2O_6$, by heating above 900°C. Upon thermal conversion, the geopolymer exhibited macroscopic cracking. The microstructure consisted of a glazed surface with numerous spherical voids, caused by air entrapped in the geopolymer during mixing. Powders derived from crushed geopolymers with a molar composition of $K_2O \bullet Al_2O_3 \bullet 4\ SiO_2 \bullet 10\ H_2O$ were die-pressed into pellets, crystallized, and sintered at 1200°C into leucite. The resulting pellets exhibited no cracking upon conversion into leucite. SEM analysis of the resulting ceramic also showed a glazed surface. The interiors of both samples had microstructures characteristic of glass ceramics. TEM of the amorphous matrix phase showed a two-phase microstructure reminiscent of spinodal decomposition such as might be formed by a miscibility gap. Selected area diffraction (SAD) patterns of the continuous matrix phase suggested that the matrix was generally amorphous, with occasional incipient nanocrystals of leucite forming.

During thermal conversion of geopolymers into glass ceramics, capillary forces develop within dense geopolymer bodies, due to vaporization of entrapped water. These forces lead to cracking and failure of monolithic geopolymer bodies. Attempts were made to engineer controlled porosity into geopolymers in an effort to shorten the diffusion distance for entrapped water to leave the geopolymers, thereby reducing the build up of capillary forces during heating. Three routes for engineering porosity (i.e. making

geopolymer foams) were tested, using internal pressure, external pressure and fugitive phases. Internal pressure was created in geopolymer slurries by mixing slurries with hydrogen peroxide, which was allowed to decompose in sealed containers. The internal pressure within the containers was adjusted between 0.5 – 3.5 MPa to control the porosity of the geopolymer. A uniform size distribution of pores (~ 50 μm) was obtained at pressures of 3.5 MPa. Regardless of pressure, however, none of the geopolymer samples produced using this method could be extracted from the pressure vessels without being destroyed. A hydraulic press was used to form an aluminum-reinforced geopolymer under 4 MPa of pressure. The decomposition of aluminum in the high pH geopolymer slurry was used to form porosity within the geopolymer. The decomposition of aluminum also increased the curing pressure to 12 MPa. The resultant geopolymer was dense to the naked eye; SEM analysis showed a porous microstructure with an average pores size of 20 μm. Residual, unreacted aluminum in the geopolymer caused catastrophic failure of the geopolymer upon heating, however. Spherical wax powders were added to geopolymer slurries as a fugitive phase for creating macro porosity. The wax was removed by boiling the geopolymers in water. In the majority of cases, however, the removal process caused the geopolymer samples to crack.

Laser scanning confocal microscopy (LSCM) is a microscopy technique that has the capability of transmitting light through thin sections of material, to visualize a 2-dimensional plane of the sample interior. Computer software is then used to form 3-dimensional representations of the sample from multiple 2-dimensional scans. LSCM has been used to study conventional cementious materials, including *in-situ* monitoring of the alkali/silicate reaction near the cement/aggregate interface.[17, 18] LSCM was employed to resolve the distribution of the alkali-silicate and metakaolin precursors in geopolymers with varying molar ratios ($M_2O{\bullet}Al_2O_3{\bullet}xSiO_2$, where x = 0, 1, 2 and M = Na^+, K^+, or Na/K = 1) and make correlations between the observed distributions and the degree of reaction between the two precursors. The alkali-silicate solutions were dyed with fluorescein isocyanate and mixed with metakaolin powder that had been dyed with rhodamine-B. The dyes were added to improve the visualization of the sample interior and distinguish the precursors from one another in the final geopolymer. The resulting slurries were allowed to cure between glass slides and cover slips and observed using laser scanning confocal microscopy (LSCM). Due to rearrangement of the metakaolin particles during curing, LSCM was unable to resolve the microstructure of the geopolymer *in-situ*. LSCM analysis of the post-cured samples, however, agreed with results in NMR studies presented in literature- increasing concentrations of silica and higher sodium to potassium ratios resulted in less reaction between metakaolin particles and alkali-silicate solutions.

The leucite family of ceramics ($MAlSi_2O_6$, where M is an alkali, K^+, Rb^+, Cs^+) have a wide range of thermal expansion coefficients.[19] The cesium-leucite compound, pollucite ($CsAlSi_2O_6$), is of particular interest. Pollucite is the most refractory silicate known, T_{melt} > 1900°C and has exceptional creep resistance between 1400 – 1500°C, comparable to mullite and yttrium-aluminum garnet (YAG).[20] In addition, the coefficient of thermal expansion (CTE) of pollucite is quite low [21-24]. The lattice parameter expansion of pollucite has been reported to be ~ 0.45% from 25 – 1000°C.[24] The CTE of pollucite can

be altered significantly by substituting different alkali-cations for cesium and/or doping with additional SiO_2.[22, 24] A cesium-based geopolymer (Cs-geopolymer) with a molar composition of $1.23Cs_2O{\bullet}Al_2O_3{\bullet}3.95SiO_2$ was fabricated by mixing a cesium-silicate solution with synthetic metakaolin (SynMK) powder derived from a steric entrapment method.[25] Ex-situ XRD analysis of Cs-geopolymer powders heated between 100 – 1400°C for 1 hour indicated the onset of crystallization into pollucite at 900°C. Heating at 1000°C for 1 hour was necessary to create well-formed crystallites of pollucite. Dynamic scanning calorimetery (DSC) of the Cs-geopolymer indicated two exotherms at 1050 and 1170°C. Both exotherms are thought to be crystallization events in the Cs-geopolymer powder, however only one phase, pollucite, crystallized. Thermal gravimetric analysis (TGA) measured cesia volitization above 1250°C. *In-situ* high temperature X-ray diffraction (HTXRD) was also performed on the cesium geopolymer using synchrotron radiation. Results show that the geopolymer-derived pollucite had a thermal expansion close to literature values for pollucite at lower temperatures 1.8×10^{-4} $\%\Delta a/a_o$ (500 – 1180°C) but at higher temperatures (1180 – 1480°C) the thermal expansion increased by more than 3-fold due to cesia loss.

Pair distribution function (PDF) analysis is a method for determining short to medium range order in amorphous or crystalline structures using data gathered from X-ray or neutron scattering experiments. Data for PDF analysis was performed on cesium-based geopolymer powders with a molar ratio of $1.23Cs_2O{\bullet}Al_2O_3{\bullet}3.95SiO_2$. The X-ray diffraction data for the analysis was obtained using synchrotron radiation on unheated geopolymer powders and powders that were heated *ex-situ* to 500, 900, 1000, and 1400°C. PDF analysis of diffraction data showed that structural ordering within the geopolymer was limited to ~8Å. It was determined that pollucite and the Cs-geopolymer precursor have similar short-range structures (<5Å), however the position of the cesium cation varied between the geopolymer and pollucite structures.

Although the thermal expansion of pollucite has been widely studied, the thermal expansion of other cesium aluminosilicate compounds (that geopolymers could potentially be converted into) has not. Powders with the nominal compositions of leucite ($KAlSi_2O_6$), pollucite ($CsAlSi_2O_6$), Cs-zeolite ($CsAlSi_5O_{12}$), Cs-feldspar ($CsAlSi_3O_8$), and Cs-mica ($CsAl_3Si_3O_{11}$) were synthesized using the steric entrapment method.[25] HTXRD determined that the latter two phases were not equilibrium phases. Thermal expansion studies showed that Stoichiometric pollucite had the lowest observed thermal expansion of all the powders, 1.00% $\Delta V/V_o$ (25 – 1472°C). Leucite had the highest thermal expansion, 6.98 % $\Delta V/V_o$ (20 – 1494°C), followed by the Cs-zeolite 4.68% (20 – 1408°C).

Research Objectives

The objectives of this research were: (1) To develop low cost, thermal shock resistant, graphite-fiber reinforced geopolymer composites which that can fit a variety of applications, including casting molds for the near-net shape solidification of Fe_2Si. (2) To study the conversion process of amorphous geopolymers into crystalline pollucite and/or leucite compounds via thermal conversion. (3) To measure the thermal expansion behavior of pollucite and leucite based ceramics. (4) To characterize the use of geopolymers as an adhesive on metal and ceramic surfaces using both mechanical testing and microstructural analysis. (5) To study the intrinsic microstructure of geopolymers using SEM, XRD, synchrotron radiation.

References

[1]J. Davidovits, "Geopolymers - inorganic polymeric new materials," *Journal of Thermal Analysis*, **37**[8] 1633-1656 (1991).

[2]V. F. F. Barbosa and K. J. D. MacKenzie, "Thermal behaviour of inorganic geopolymers and composites derived from sodium polysialate," *Materials Research Bulletin*, **38**[2] 319-331 (2003).

[3]C. G. Papakonstantinou, P. Balaguru and R. E. Lyon, "Comparative study of high temperature composites," *Composites Part B-Engineering*, **32**[8] 637-649 (2001).

[4]R. E. Lyon, J. Davidovits and P. N. Balaguru, "Fire resistant aluminosilicate composites," *Fire and Materials*, **21** 67-73 (1997).

[5]V. F. F. Barbosa, K. J. D. MacKenzie and C. Thaumaturgo, "Synthesis and characterization of materials based on inorganic polymers of alumina and silica: sodium polysialate polymers," *International Journal of Inorganic Materials*, **2**[4] 309-317 (2000).

[6]V. F. F. Barbosa and K. J. D. MacKenzie, "Synthesis and thermal behaviour of potassium sialate geopolymers," *Materials Letters*, **57**[9-10] 1477-1482 (2003).

[7]T. W. Cheng and J. P. Chiu, "Fire-resistant geopolymer produced by granulated blast furnace slag," *Minerals Engineering*, **16**[3] 205-210 (2003).

[8]W. M. Kriven, J. Bell and M. Gordon, "Microstructure and microchemistry of fully-reacted geopolymers and geopolymer matrix composites"; pp. 227-250 in Ceramic Transactions, Vol. 153, *Advances in Ceramic Matrix Composites IX*. Edited by N. P. Bansal, J. P. Singh, W. M. Kriven and H. Schneider, The American Ceramic Society, Westerville, OH, 2003.

[9]J. W. Phair, J. S. J. van Deventer and J. D. Smith, "Effect of Al source and alkali activation on Pb and Cu immobilization in fly-ash based "geopolymers"," *Applied Geochemistry*, **19**[3] 423-434 (2004).

[10]J. G. S. van Jaarsveld, J. S. J. van Deventer and L. Lorenzen, "The potential use of geopolymeric materials to immobilize toxic metals .1. Theory and applications," *Minerals Engineering*, **10**[7] 659-669 (1997).

[11]J. G. S. van Jaarsveld, J. S. J. van Deventer and A. Schwartzman, "The potential use of geopolymeric materials to immobilize toxic metals: Part II. Material and leaching characteristics," *Minerals Engineering*, **12**[1] 75-91 (1999).

[12]H. Xu and J. S. J. van Deventer, "Geopolymerisation of multiple minerals," *Minerals Engineering*, **15**[12] 1131-1139 (2002).

[13]H. Xu, J. S. J. van Deventer and G. C. Lukey, "Effect of alkali metals on the preferential geopolymerization of stilbite/kaolinite mixtures," *Industrial & Engineering Chemistry Research*, **40**[17] 3749-3756 (2001).

[14]J. G. S. van Jaarsveld and J. S. J. van Deventer, "Effect of the alkali metal activator on the properties of fly ash-based geopolymers," *Industrial & Engineering Chemistry Research*, **38**[10] 3932-3941 (1999).

[15]B. A. Latella, D. S. Perera, T. R. Escott and D. J. Cassidy, "Adhesion of glass to steel using a geopolymer," *Journal of Materials Science*, **41**[4] 1261-1264 (2006).

[16]W. Höland and G. Beall, *Glass-Ceramic Technology*. Westerville, OH The American Ceramic Society. 2002

[17]K. E. Kurtis, N. H. El-Ashkar, C. L. Collins and N. N. Nalk, "Examining cement-based materials by laser scanning confocal microscopy," *Cement & Concrete Composites*, **25**[7] 695-701 (2003).

[18]C. L. Collins, J. H. Ideker and K. E. Kurtis, "Laser scanning confocal microscopy for in situ monitoring of alkali-silica reaction," *Journal of Microscopy-Oxford*, **213** 149-157 (2004).

[19]D. Taylor, "The thermal expansion of the leucite group of minerals," *American Mineralogist*, **53**[9-10] 1476-1488 (1968).

[20]R. S. Hay, T. A. Parthasarathy and J. R. Welch, "Creep and stability of pollucite"; pp. 89-104 in Ceramic Transactions, Vol. 52, *Low-Expansion Materials* Edited by D. P. Stinton and S. Y. Limayme, American Ceramic Society, Westerville, OH, 1995.

[21]D. W. Richerson and H. F. A., "Synthesis and thermal expansion of polycrystalline cesium minerals," *Journal of the American Ceramic Society*, **55** 269-272 (1972).

[22]H. Kobayashi, T. Terasaki, T. Mori, H. Yamamura and T. Mitamura, "preparation and thermal-expansion behavior of excess SiO2 pollucite powders," *Nippon Seramikkusu Kyokai Gakujutsu Ronbunshi-Journal of the Ceramic Society of Japan*, **100**[1] 91-93 (1992).

[23]I. Yanase, S. Tamai and H. Kobayashi, "Sintering of pollucite using amorphous powder and its low thermal expansion property," *Journal of the Ceramic Society of Japan*, **111**[8] 533-536 (2003).

[24]I. Yanase, S. Tamai and H. Kobayashi, "Low-thermal-expansion properties of sodium- and lithium-substituted cubic cesium leucite compounds," *Journal of the American Ceramic Society*, **86**[8] 1360-1364 (2003).

[25]M. A. Gulgun, M. H. Nguyen and W. M. Kriven, "Polymerized organic-inorganic synthesis of mixed oxides," *Journal of the American Ceramic Society*, **82**[3] 556-560 (1999).

Acknowledgements/Disclaimer

This work was supported by the Air Force Office of Scientific Research, USAF, under grant/contract number FA95550-04-0063, by an Australian-American Fulbright Postgraduate Scholarship and a University of Melbourne Postgraduate Overseas Research Experience Scholarship, both awarded to JLP, as well as through the Particulate Fluids Processing Centre (a Special Research Centre of the Australian Research Council) and the National Science Foundation, Grant number (DMR 02-11139). Experimental work was conducted at NSLS, Brookhaven National Laboratory, which is supported by the U.S. Department of Energy under Contract No. DE AC02-98CH10886, APS, Argonne

National Laboratory supported by the US DOE, BES-Materials Sciences, under Contract No: W-31-109-ENG-38 and the Center for Microanalysis of Materials, University of Illinois at Urbana-Champaign, which is partially supported by the U.S. Department of Energy under grant DEFG02-91-ER45439. We acknowledge the assistance of Margrit Martin of Chemetall Chemical Products, Inc. for contributing the cesium hydroxide to this research, Dr. Yongjae Lee and Dr. Thomas Vogt (NSLS beamline X7A) in obtaining experimental data, Dr. Matthew Rowles for supplying a copy of his Ph.D. thesis, Dr. Maria Martínez-Iñesta (University of Delaware) for suggestions regarding data analysis, and Dr. Thomas Proffen (Los Alamos National Laboratory, NM) for guidance in the use of the PDFFIT software. The views and conclusions contained herein are those of the authors and should not be interpreted as necessarily representing the official policies or endorsements, either expressed or implied, of the Air Force Office of Scientific Research or the U.S. Government.

Personnel Supported

Matthew Gordon	Graduate Student, University of Illinois, Urbana-Champaign
Jonathan L. Bell	Graduate Student, University of Illinois, Urbana-Champaign
Seth Mallicoat	Graduate Student, University of Illinois, Urbana-Champaign
Dong K. Kim	Post-doctorial Research Assistant, University of Illinois, Urbana-Champaign
Trudy W. Kriven	Professor, University of Illinois, Urbana-Champaign
Carolyn A. Kelly	CEO, Catawba Resources, Inc.
Douglas C. Comrie	Principle Investigator, Catawba Resources, Inc.

Publications

[1]D. C. Comrie and W. M. Kriven, "Composite cold ceramic geopolymer in a refractory application"; pp. 211-225 in Ceramic Transactions, Vol. 153, *Advances in Ceramic Matrix Composites IX*. Edited by N. P. Bansal, J. P. Singh, W. M. Kriven and H. Schneider, The American Ceramic Society, Westerville, OH, 2003.

[2]W. M. Kriven, J. Bell and M. Gordon, "Microstructure and microchemistry of fully-reacted geopolymers and geopolymer matrix composites"; pp. 227-250 in Ceramic Transactions, Vol. 153, *Advances in Ceramic Matrix Composites IX*. Edited by N. P. Bansal, J. P. Singh, W. M. Kriven and H. Schneider, The American Ceramic Society, Westerville, OH, 2003.

[3]J. Bell and W. M. Kriven, "Nanoporosity in geopolymeric cements"; pp. 590-591 in Microscopy and Microanalysis, Vol. 10, *The Proceedings of the 62nd Annual Meeting of Microscopy Society of America*. Edited by I. M. Anderson, R. Price, E. Hall, E. Clark and S. McKarnan, Press Syndicate of the University of Cambridge, New York, NY, 2004.

[4]M. Gordon, J. Bell and W. M. Kriven, "Comparison of naturally and synthetically derived, potassium based geopolymers"; pp. 95-103 in Ceramic Transactions, Vol. 165, *Advances in Ceramic Matrix Composites X*. Edited The American Ceramic Society, Westerville, OH, 2004.

[5]W. M. Kriven and J. Bell, "Effect of alkali choice on geopolymer properties"; pp. 99-104 in Ceramic Engineering and Science Proceedings, Vol. 25 [3], *The 28th International Conference on Advanced Ceramics & Composites:B*. Edited by E. Lara-Curzio and M. Readey, J., The American Ceramic Society, Westerville, OH, 2004.

[6]W. M. Kriven, J. Bell and M. Gordon, "Geopolymer refractories for the glass manufacturing industry"; pp. 57-79 in Ceramic Engineering and Science Proceedings, Vol. 25, *The 64th Annual Conference on Glass Problems*. Edited by W. M. Kriven, The American Ceramic Society, Westerville, OH, 2004.

[7]W. M. Kriven, M. Gordon and J. Bell, "Geopolymers: nanoparticulate, nanoporous ceramics made under ambient conditions"; pp. 404-405 in Microscopy and Microanalysis, Vol. 10, *The Proceedings of the 62th Annual Meeting of the Microscopy Society of America*. Edited Press Syndicate of the University of Cambridge, New York, NY, 2004.

[8]J. Bell, M. Gordon and W. M. Kriven, "Use of geopolymeric cements as a refractory adhesive for metal and ceramic joins"; pp. 407-413 in Ceramic Engineering and Science Proceedings, Vol. 26 [3], *The 29th International Conference on Advanced Ceramics and Composites*. Edited by D. Zhu, K. Plucknett and W. M. Kriven, The American Ceramic Society, Westerville, OH, 2005.

[9]P. Duxson, S. Mallicoat, G. Lukey, W. M. Kriven and J. S. J. van Deventer, "Microstructural characterization of metakaolin-based geopolymers"; pp. 71-85 in Ceramic Transactions, Vol. 165, *Advances in Ceramic Matrix Composites*. Edited by J. P. Singh, N. P. Bansal and W. M. Kriven, The American Ceramic Society, Westerville, OH, 2005.

[10]P. Duxson, J. L. Provis, G. C. Lukey, S. W. Mallicoat, W. M. Kriven and J. S. J. van Deventer, "Understanding the relationship between geopolymer composition, microstructure and mechanical properties," *Colloids and Surfaces A-Physicochemical and Engineering Aspects*, **269**[1-3] 47-58 (2005).

[11]M. Gordon, J. Bell and W. M. Kriven, "Thermal conversion and microstructural evaluation of geopolymers or "Alkali-bonded ceramics" (ABCs)"; pp. 215-224 in Ceramic Transactions, Vol. 175, *Advances in Ceramic Matrix Composites XI*. Edited by N. P. Bansal, J. P. Singh and W. M. Kriven, The American Ceramic Society, Westerville OH, 2005.

[12]S. W. Mallicoat, P. Sarin and W. M. Kriven, "Novel alkali-bonded ceramic filtration membranes"; pp. 37-44 in Ceramic Engineering and Science Proceedings, Vol. 26 [8], *The 29th International Conference on Advanced Ceramics and Composites*. Edited by M. E. Brito, P. Filip, C. Lewinsohn, A. Sayir, M. Opeka, W. M. Mullins, D. Zhu and W. M. Kriven, The American Ceramic Society, Westerville, OH, 2005.

TABLE OF CONTENTS

Section A - Geopolymer Adhesives

Introduction

Joseph Davidovits coined the term "geopolymer" in 1979 for mineral binders formed by adding an aluminosilicate source to a high pH, concentrated alkali solution.[1] Since this time, geopolymers have been used in a variety of applications such as structural blended cements, fiber reinforced composites and toxic waste encapsulation.[2-9] More recently, geopolymers are being examined for adhesive applications. Latella et al. reported the strain release rate of geopolymer adhesives, bonding glass to steel range from 0.38 – 1.02 J/m^2 (comparable to an epoxy resin) depending on the particle size and particle size distribution of the metakaolin used.[10]

The goal of this study was to explore the use of geopolymer adhesives on aluminum, steel and borosilicate glass in order to determine which materials may be suitable adherents for geopolymer adhesives. The microstructure and diffusion across the geopolymer / substrate interface was also studied using a scanning electron microscope (SEM) and energy dispersive analysis (EDS).

Experimental Procedures

A potassium silicate solution was prepared by dissolving EH-5 fumed silica (Cabot, Tuscola, IL) 0.2 – 0.3 μm dia, and 380 ± 30 m^2/g surface area) and potassium hydroxide pellets in deionized water to make an alkali-silicate solution with molar ratios of $K_2O \bullet 2\ SiO_2 \bullet 13\ H_2O$. The solution was stirred overnight to dissolve the fumed silica completely. Polestar 400 metakaolin, 0.6 μm dia, 16 m^2/g, (Imerys Minerals) was mixed into the potassium silicate solution using a high speed mixer with a weight ratio of 2.2 : 1 (solution : metakaolin). After mixing, the geopolymer paste was applied to the respective samples and cured 36 hours at 50°C. The overlap of the geopolymer adhesive was 12.7 mm x 25.4 mm for the lap-shear testing. All single lap-shear glass samples failed within the glass region rather than in the adhesive or at the interface region. As a result, the

overlap region for the geopolymer adhesives on glass samples for the double lap-shear tests was decreased to 3 x 25.4 mm.

Raw materials, suppliers and cleaning procedures for adhesion are given in Table I. Single lap-shear test samples were prepared using ASTM D1002-01 testing requirements; likewise, double lap-shear tests were prepared using ASTM D3528-96 standards. Water-based dye was applied to pre-cleaned and post-cleaned samples to qualitatively evaluate the wetting characteristics to the surface of the substrates.

Table 1: Materials tested for adhesive bonding of geopolymers.

Material Tested	Supplier	Sheet thickness (in.)	Single lap-shear testing	Double lap-shear testing	Cleaning Procedure
1008/1010 Steel	McMaster-Carr	0.062	Yes	Yes	ASTM D2651
6061-T6 Aluminum alloy	McMaster-Carr	0.0625	Yes	No	ASTM D2651
Borosilicate glass (Borofloat)	Schott glass	0.064	Yes	Yes	70% H_2SO_4, 30% H_2O_2 for 2 hours

After cleaning, each sample was dipped into the geopolymer slurry to ensure adequate surface coverage. A 400 g weight was then placed on each sample once it was loaded into the furnace to cure. All samples were placed on a Mylar® sheet to prevent them from adhering to the bottom of the furnace.

Surface rough nesses were characterized before and after cleaning using a Dektak 3030 surface profilometer (Veeco Instruments Inc., Woodbury NY) and a Hitachi S-4700 scanning electron microscope (SEM) (Hitachi, Osaka, Japan) equipped with an energy dispersive spectrometer (EDS). The same equipment was used to analyze the fracture surfaces of post mortem specimens. Shear strengths of the adhesive joins were measured with an Instron universal testing machine using a 10 kN load cell (Instron). The upper

fixtures on the lap-shear samples were given two degrees of freedom; the bottom fixture was fixed.

X-ray diffraction (XRD) on the metakaolin powder before and after mixing and curing was performed using a Rigaku D-Max X-ray diffractometer operated at 25 KeV and 40mA (Phillips, Tokyo, Japan).

Results

The diffraction pattern of the PoleStar 400 metakaolin indicates the presence of poorly crystallized mullite, as shown in Fig. 1. The diffuse peak at 22° 2-theta is characteristic of metakaolin. After curing, the intensity of all the mullite peaks in the diffraction pattern decreased, indicating the dissolution of mullite during the reaction. As a result of the reaction, the diffuse peak shifted to 28° 2-theta; the diffuse peak at 28° 2-theta is characteristic of metakaolin-based geopolymers.[3]

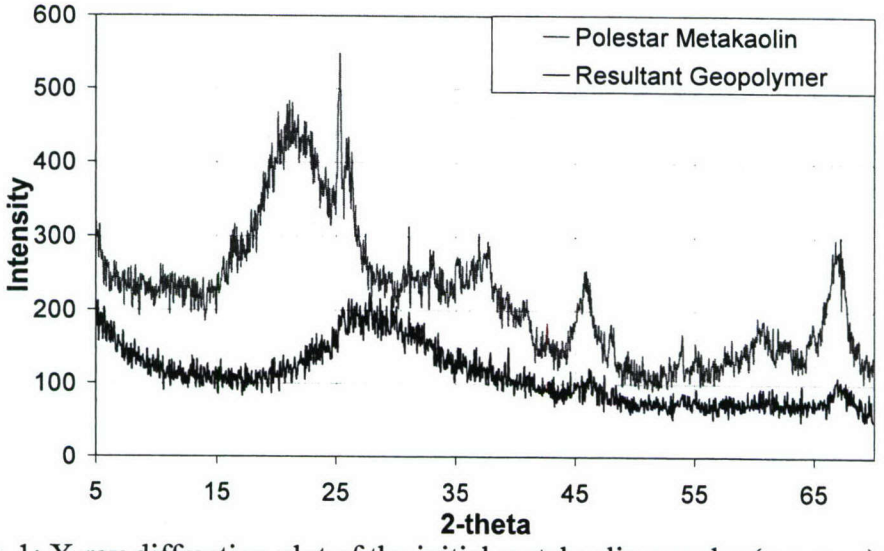

Fig. 1: X-ray diffraction plot of the initial metakaolin powder (top scan) and the corresponding geopolymer. (bottom scan).

The cleaning of steel and aluminum leads to the creation of porous surfaces, with pores ranging from 1 – 10 μm, as shown in Fig. 2. Sample surface profile variations were ± 2 - 3 μm for steel and ± 1.5 – 2 μm for aluminum before and after cleaning. The height

variations on glass were ± 0.08 μm and ± 0.05 μm before after cleaning. The wetting characteristics on steel and aluminum, shown in the top right box of each SEM image in Fig. 2, improved significantly after cleaning.

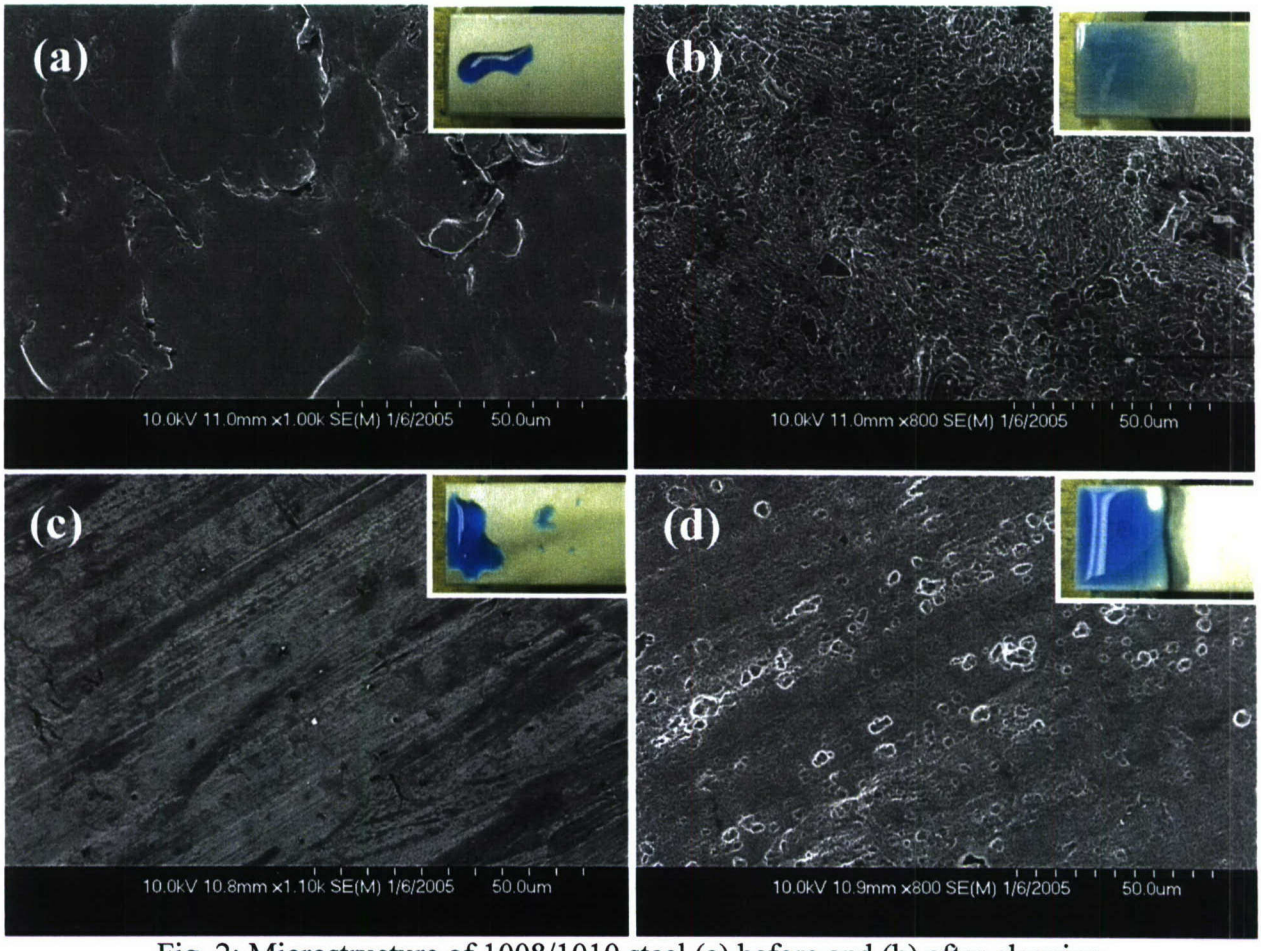

Fig. 2: Microstructure of 1008/1010 steel (a) before and (b) after cleaning. Microstructure of 6061-T6 aluminum alloy (c) before and (d) after cleaning.

SEM micrographs for steel and aluminum geopolymer bonded samples are shown in Fig. 2. The aluminum substrate was significantly corroded, due to the high pH of the geopolymer adhesive. The geopolymer adhesive did not significantly alter the steel substrate and the geopolymer / steel interface was clearly distinguishable. SEM images of the geopolymer bonded glass are given in Fig. 4. The interfacial region between the geopolymer and glass is somewhat ambiguous, however. Heating the bonded glass to 450°C appeared to reduce the overall porosity of the interface.

The EDS line scan of the geopolymer-steel interface (Fig. 5) showed no noticeable long range diffusion of Fe, Si, K, or Al across the interface. An EDS line scan was not done on the aluminum samples; the bond between the aluminum was too weak to withstand mechanical polishing. An EDS line scan of the geopolymer-borosilicate glass interface, Fig. 6 also suggested that there is no significant diffusion across the adhesive interface. The results from the shear strength tests are summarized in Table 2.

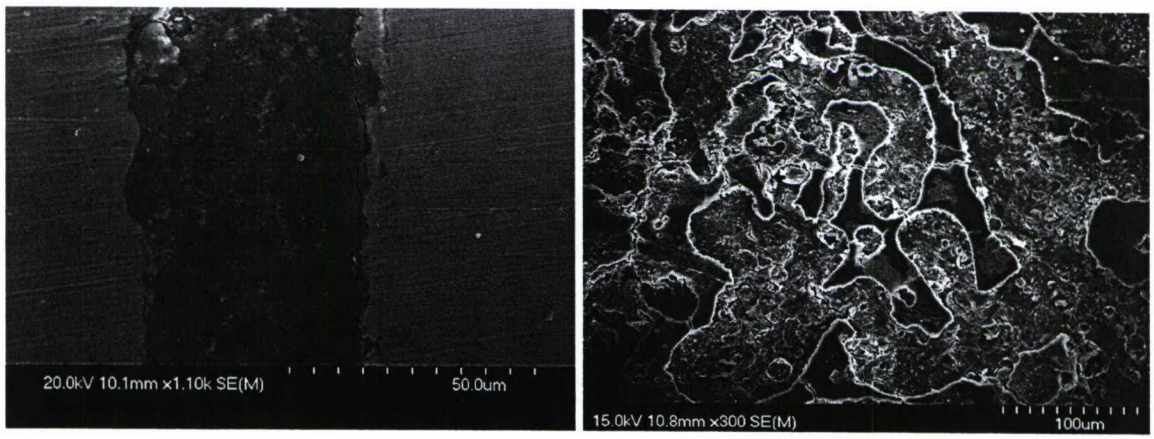

Fig. 3: SEM image of the interfacial region of geopolymer bonded steel (left) and the surface of geopolymer bonded aluminum alloy (right).

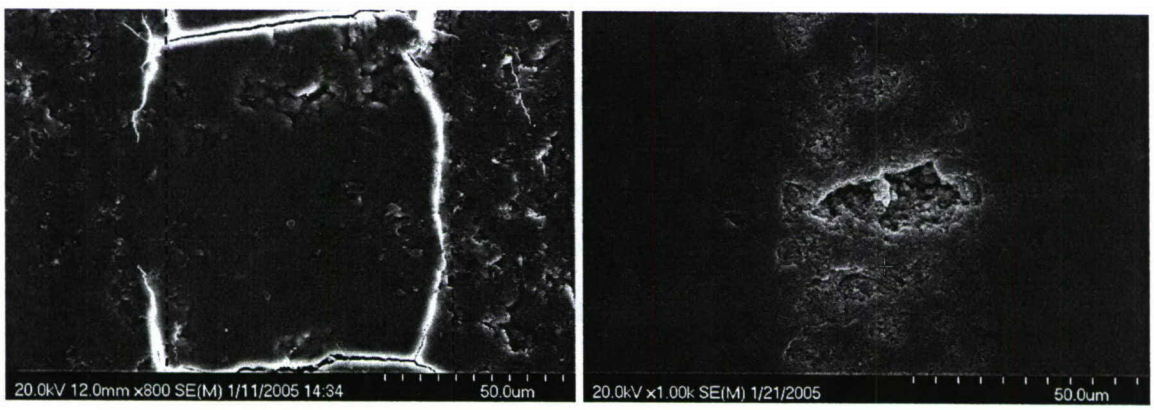

Fig. 4: Cross sectional SEM images of the geopolymer borosilicate glass interfaces for glass without heat treatment (left) and heated to 450°C for one hour (right). Dotted line indicates estimated geopolymer-glass interface (is running vertically).

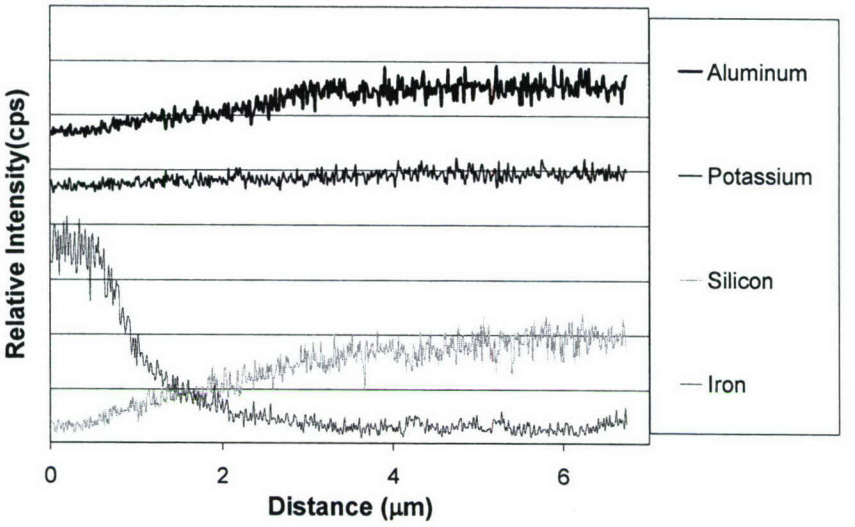

Fig. 5: EDS scan of the geopolymer / steel interface. Intensity values were scaled for each element for the sake of clarity.

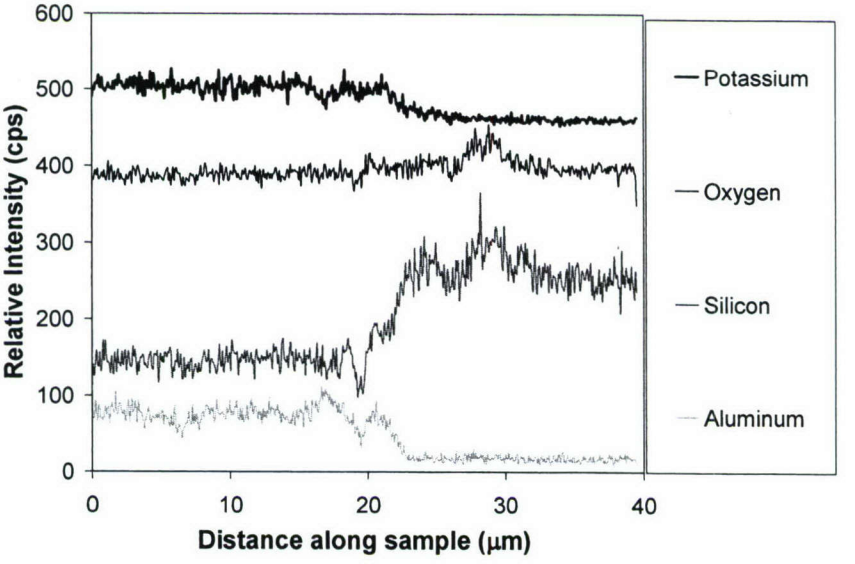

Fig. 6: EDS scan of the geopolymer / glass interface Intensity values were scaled for each element for the sake of clarity.

Table 2: Shear strengths for geopolymer bonded materials

Material Tested	Average Max Shear Strength Value in MPa (# of samples tested)		
	Sample post heat temp.	Single lap-shear test D1002-01	Double lap-shear test D3528-96
1008/1010 Steel	RT	3.12 (7)	3.79 (6)
	450°C	-	3.45 (3)
6061-T6 Al alloy	RT	0.81 (6)	-
Borosilicate glass*	RT	1.27 (4)	1.91 (2)
	450°C	3.40 (1)	2.05 (2)

Discussion

During testing of the glass samples, premature fracture always occurred within the glass samples rather than within the geopolymer adhesive or at the interface. The testing protocol used was inadequate to evaluate the bond with glass and will be revised in future testing. The shear strength of the aluminum–geopolymer bond was poor, (< 1 MPa). Upon examination of the fracture surface of the aluminum, it became clear the highly alkaline geopolymer adhesive strongly reacted with the surface of the aluminum, which led to poor bonding. Geopolymers adhered to the steel samples; the shear strength of the bond was limited to 3 – 4 MPa, however. Heating of the bonded glass and steel samples to 450°C did not affect the shear strength of the geopolymer adhesive.

Conclusions

The steel / geopolymer bond had a low shear strength of 2 - 3 MPa. The shear strength of borosilicate glass was not determined from the present study, but showed good potential as a substrate for geopolymer bonding. Shear testing always resulted in fracture within the glass rather than within the adhesive or at the interface. Heating of the glass and steel to 450°C did not affect the strength of the geopolymer bond. The use of geopolymer adhesive was not suitable for aluminum due to the high alkalinity of the geopolymer, which corroded the aluminum detrimentally.

References

[1]J. Davidovits, "Geopolymers and geopolymeric materials," *Journal of Thermal Analysis*, **35**[2] 429-441 (1989).

[2]J. Davidovits, "Geopolymers - inorganic polymeric new materials," *Journal of Thermal Analysis*, **37**[8] 1633-1656 (1991).

[3]C. G. Papakonstantinou, P. Balaguru and R. E. Lyon, "Comparative study of high temperature composites," *Composites Part B-Engineering*, **32**[8] 637-649 (2001).

[4]J. W. Phair, J. S. J. van Deventer and J. D. Smith, "Effect of Al source and alkali activation on Pb and Cu immobilization in fly-ash based "geopolymers"," *Applied Geochemistry*, **19**[3] 423-434 (2004).

[5]J. G. S. van Jaarsveld, J. S. J. van Deventer and L. Lorenzen, "The potential use of geopolymeric materials to immobilize toxic metals .1. Theory and applications," *Minerals Engineering*, **10**[7] 659-669 (1997).

[6]J. G. S. van Jaarsveld, J. S. J. van Deventer and A. Schwartzman, "The potential use of geopolymeric materials to immobilize toxic metals: Part II. Material and leaching characteristics," *Minerals Engineering*, **12**[1] 75-91 (1999).

[7]H. W. Xu, A. Navrotsky, M. L. Balmer and Y. L. Su, "Crystal chemistry and phase transitions in substituted pollucites along the CsAlSi2O6-CsTiSi2O6.5 join: A powder synchrotron X-ray diffractometry study," *Journal of the American Ceramic Society*, **85**[5] 1235-1242 (2002).

[8]T. W. Cheng and J. P. Chiu, "Fire-resistant geopolymer produced by granulated blast furnace slag," *Minerals Engineering*, **16**[3] 205-210 (2003).

[9]J. G. S. van Jaarsveld and J. S. J. van Deventer, "Effect of the alkali metal activator on the properties of fly ash-based geopolymers," *Industrial & Engineering Chemistry Research*, **38**[10] 3932-3941 (1999).

[10]B. A. Latella, D. S. Perera, T. R. Escott and D. J. Cassidy, "Adhesion of glass to steel using a geopolymer," *Journal of Materials Science*, **41**[4] 1261-1264 (2006).

Section B – Continuous Fiber Reinforced Composites

Introduction

The production of diferrous silicide (Fe_2Si) and diferrous manganese (Fe_2Mn) products for the specialty steel market includes the casting of final molten metal products into nickel molds approximately 6 x 4 x 1.5 feet at a temperature of 1428°C (Fig. 1). The product is allowed to cool in the mold prior to its extraction. Once de-molded, the material is crushed into < 5 cm chunks for shipment to the end use customer. It is during this crushing process that fines are generated (< 0.6 cm) which can comprise 20 – 30% of the finished product. The fines have little value and can only partially be recycled through the furnace. The postulation was therefore formulated, that if the molten metal could be cast into exact forms suitable to the end user, this could significantly save costs of material crushing and in the management of fines.

Fig. 1: Molten Fe_2Si being poured into a nickel cast.

Any candidate mold would need to retain high strength at high temperature 1428°C, maintain dimensional shape, transmit heat quickly away from the molten metal, and

facilitate gravitational discharge of the solidified, molded metal form. In addition, the mold would have to be durable so that it could be subjected to multiple pour cycles.

Thermal shock is the key engineering parameter for any potential Fe_2Si casting mold. Under moderate thermal shock, the maximum temperature drop that a material can withstand is given in Equation 1 where σ_f is the material's fracture strength; ν, Poisson's ratio; k, thermal conductivity; E, elastic modulus and α_T the coefficient of thermal expansion.

Equation 1: $$\Delta T = \frac{\sigma_f (1-\upsilon) k}{E \alpha_T}$$

In cases of extreme thermal shock, however, the design parameters change from preventing cracking to incorporating microcracking in order to prevent catastrophic failure. The maximum thermal shock that a material can survive is given in Equation 2, where γ is the surface fracture energy and N is the number of circular and non-interacting cracks of equal diameter (l) / unit volume.[1]

Equation 2: $$\Delta T = \left(\frac{2\gamma}{\pi E \alpha_T^2 l} \right)^{1/2} (1 + 2\pi N l^2)$$

By substituting in Equation 3 (from a combined Griffith-Orowan-Irwin approach) and simplifying, the intrinsic material properties to optimize for extreme thermal shock are grouped in the expression outside the brackets in Equation 4.

Equation 3: $$\gamma \approx \left(\frac{K_{IC}^2}{2E} \right)$$

Equation 4: $$\Delta T = \left(\frac{K_{IC}}{E\alpha_T}\right)\left[\left(\frac{1}{\pi\, l}\right)^{1/2}(1+2\pi N l^2)\right]$$

The final constraint on a Fe_2Si casting mold would then be the operating temperatures and the fabrication cost of the mold. Under STTR-Phase I, a series of geopolymer molds were tested as possible candidates for Fe_2Si casting molds. This section of the report covers the progress made towards using geopolymers for Fe_2Si casting applications.

Experimental Procedures

Three separate designs of geopolymer molds for casting molten Fe_2Si were developed. The first mold design was a simple crucible shape. A plastic positive of the crucible was machined from Type-I PVC (McMaster-Carr, Chicago, IL), Fig. 2. The positive was then fitted onto a hollow cardboard cylinder using a small groove machined into the flat-side of the plastic positive. The positive was then covered with a thin layer of geopolymer having a molar composition of $K_2O \bullet Al_2O_3 \bullet 4\ SiO_2 \bullet 10\ H_2O$ that incorporated 10 volume percent filler (fillers are listed in Table-1). After the initial coating, one-inch wide plain weave graphite-fiber tape (Fibre Glast Developments Corp. Brookville, OH) was coated with geopolymer and draped over the bottom of the positive. The ends of the fabric were attached to the cardboard with electrical tape. Additional lengths of graphite-fiber tape were coated with geopolymer and arranged in a [0/90°, ± 45°] pattern for a total of 20 lengths of graphite-tape; only the initial four layers of graphite were attached to cardboard tubing using electrical tape. Once completed, clear Plastic-Wrap® was repeatedly wrapped around the mold. Rubber-bands were used to keep the Plastic-Wrap® in place. The mold was then cured in an oven at 50°C for a minimum of 72 hours. After curing, the plastic positive was removed from the mold and the outer lip of the crucible was sanded down. Additional geopolymer was then poured into a plastic container and the bottom of the crucible was set into the slurry, forming a flat bottom for the crucible.

The second mold design was a graphite-fiber reinforced composite plate fabricated without the use of external pressure. A positive mold of the pouring region was machined from Type-I PVC (McMaster-Carr) and attached to a 12 x 12 inch base plate, also made of Type-I PVC, as shown in Fig. 2. The pour zone is approximately ½ inch high, and 3 – ¾ inch in diameter with a tapered edge to allow graphite fiber weaves to conform to the surface of the pour zone. As in the case of the crucible-shaped mold, a thin layer of geopolymer was applied directly to the surface of the mold before adding any graphite-fibers. After the first coating of geopolymer, bi-directional weaves of graphite fiber with a 6HS weave (Fibre Glast Developments Corp.) coated with additional geopolymer and were laid up on the mold in a [0/90°, ± 45°] pattern for a total of 20 layers of graphite fiber weave. Excess geopolymer was removed from the mold using a rubber squeegee. After lay up was complete, the mold and attached base plate were wrapped in Plastic-Wrap® and cured in an oven at 50°C for a minimum of 168 hours.

The third mold design was a graphite-fiber reinforced geopolymer composite cured under pressure. A circular mold, also shown in Fig. 2, was machined from steel and coated with diamond impregnated chromium (The Armoloy Corp. Dekalb, IL) The coating was applied as a protective and non-adherent layer. (Previous work done in during STTR-I demonstrated that geopolymer cured under pressure is adherent to steel.) Ten layers of bi-directional plain weave graphite fiber (Fibre Glast) were cut in two inch diameter sections and an additional 20 layers were cut with 1 ¾ inch diameter sections. Boron nitride release agent (McMaster-Carr) was sprayed onto the interior surfaces of the die-mold (McMaster-Carr) before mold fabrication. Geopolymer, with a molar composition of $K_2O \cdot Al_2O_3 \cdot 4\ SiO_2 \cdot 8\ H_2O$ and mixed with 15 volume percent filler phase was then applied to the bottom surface of the die. Sections of two inch diameter graphite weave, coated with geopolymer, were then hand pressed onto the bottom of the geopolymer coated mold. Alternate layers of geopolymer and two inch diameter weave were then applied to the bottom of the mold after which 1.75 inch diameter layers of graphite weave were used. A total of 30 layers of graphite weaves were incorporated into the composites with molybdenum and silicon carbide fillers. The die was then pressure cured using a

hydraulic driven press at 43 MPa for four hours while being heated using a Fisher Scientific heating tape operating at 50% power. The high viscosity of the geopolymer with a sub-micron alumina filler phase prevented 30 layers of graphite weave from being incorporated in the mold. In this latter case, the mold contained only 20 layers of graphite weave and was pressed at 21.5 MPa.

It was found during the fabrication of the molds that SiC powders from (Superior Graphite, Chicago, IL) and (Great Lakes Finishing Equipment Inc., Melrose Park, IL) reacted with the alkali-silicate solutions. Silicon carbide is an inert substance. Elemental silicon may have been present in the powders which rapidly oxidized in the extreme pH of the alkali-silicate solutions. The result was significant bubbling in the geopolymer during mixing and casting (presumably from the evolution of H_2 gas). As a result, silicon carbide could only be incorporated into the pressure-cure mold where the externally applied pressure prevented the geopolymer from foaming.

Table-1: Filler Materials Used for Fabrication of Geopolymer Refractory Molds

Mold Type	Filler Type	Particle Size	Thermal Conductivity, k (W/s.m..°C)	Oxidization Temp.(°C)	Melting Temp. (°C)
Crucible, Plate, Pressure cured	α-Al_2O_3[a]	0.8 μm	20	N/A	2050
Crucible, Plate, Pressure cured	Molybdenum[b]	< 45 μm (-325 mesh)			
Crucible	Molybdenum[b]	2 – 8 μm	135	300	2623
Plate, Pressure Cured	Molybdenum[b]	1 – 5 μm			
Pressure Cured	α-SiC[c]	0.7 1 μm	100	1200	2700

[a] (A16-SG) Almatis, New Milford, CT
[b] Atlantic Equipment Engineers, Bergenfield, NJ
[c] (HSC490N) Superior Graphite, Chicago, IL

Fig. 2: Mold designs (positives) for Fe_2Si castings

Two high-alumina crucibles with two inch wide mouths and a 4 x 4 x 3 inch piece of SALI® board (Zircar Ceramics Inc., Florida, NY) with a two inch diameter, one inch deep machined cavity were also tested for comparison purposes.

All of the molds were then field-tested at Calvert City Metals and Alloys LLC (CCMA) steel company (Calvert, Kentucky). Boron nitride release agent was applied to all of the molds, immediately prior to use. Molten Fe_2Si was then poured into the molds at 1425°C. With the exception of the pressure-cured molds, which were quenched, the Fe_2Si was allowed to air cool in the molds before ejection. The Fe_2Si failed to eject from the crucible shaped molds. After testing, selected molds were sectioned, sputter coated with a gold-palladium alloy and viewed using a JOEL JSM-6060LV (Joel USA, Peabody, MA) scanning electron microscope (SEM). SEM analysis was not performed on the crucible molds or on the pressure cured mold with -325 mesh molybdenum filler.

Results

The completed geopolymer molds prior to Fe_2Si addition are shown in Fig. 3 – Fig. 5. Surface cracking, due to water dry out, was visible in the pouring regions of the crucibles and the plate-shapes molds but was not present on the pressure cured molds. In contrast to the geopolymer molds, theSALI® mold was extremely fragile (Fig. 6). Neither the geopolymer molds nor the SALI® mold failed during testing (Fig. 7 – Fig. 12). The alumina crucibles shattered as expected, however. Solidified Fe_2Si was easily ejected from the plate-shaped and the pressure cured geopolymer molds as well as from the SALI® mold. Fe_2Si could not be ejected from the crucible shaped molds shown in Fig. 3. Furthermore, the exteriors of the crucible molds were heavily cracked. By visual examination, the pressure cured mold reinforced with -325 mesh molybdenum appeared to be more damaged than the pressure cured mold with the smaller (1 – 5 μm) molybdenum reinforcements. The SEM analysis of selected molds is given in Fig. 13 – Fig. 67.

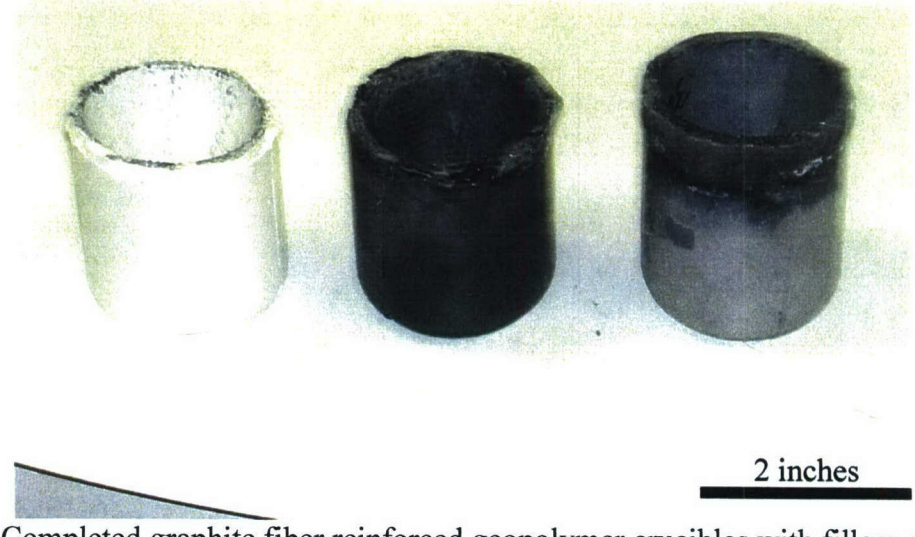

Fig. 3: Completed graphite fiber reinforced geopolymer crucibles with fillers of Al_2O_3 (left), 1 – 5 μm diameter molybdenum powder (center), -325 mesh molybdenum powder (right).

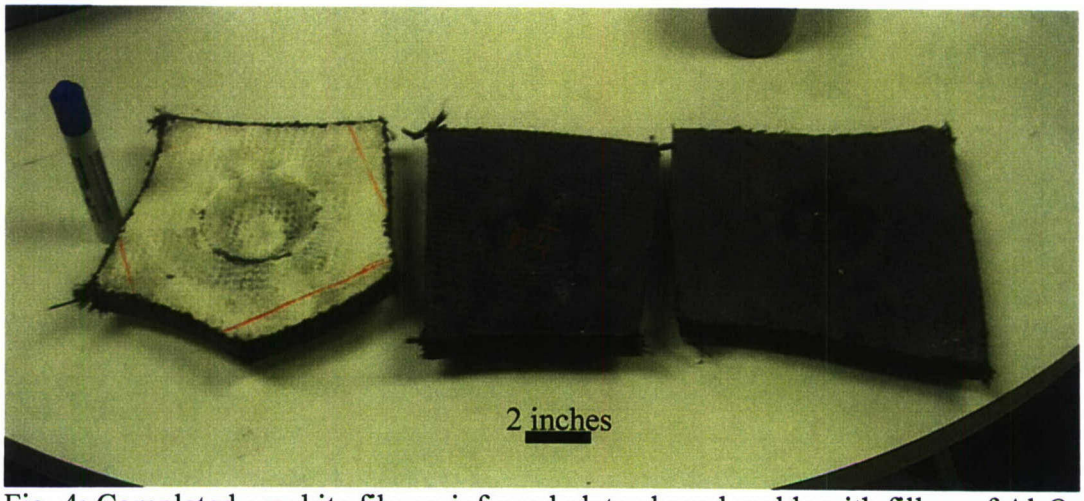

Fig. 4: Completed graphite fiber reinforced plate-shaped molds with fillers of Al_2O_3 (left), 1 – 5 μm diameter molybdenum powder (center), -325 mesh molybdenum powder (right).

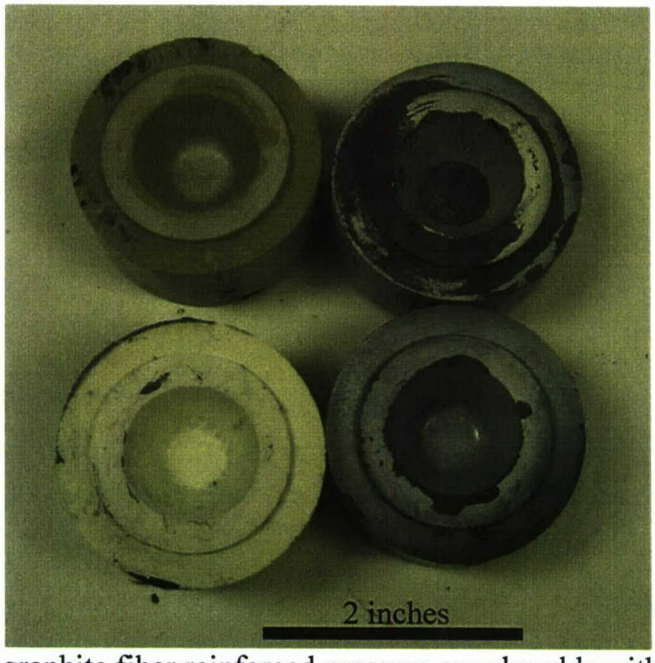

Fig. 5: Completed graphite fiber reinforced pressure cured molds with fillers of SiC (top left), 1 – 5 μm diameter molybdenum powder (top right), Al_2O_3 (bottom left), -325 mesh molybdenum powder (bottom right).

Fig. 6: SALI® fibrous ceramic foam casting mold.

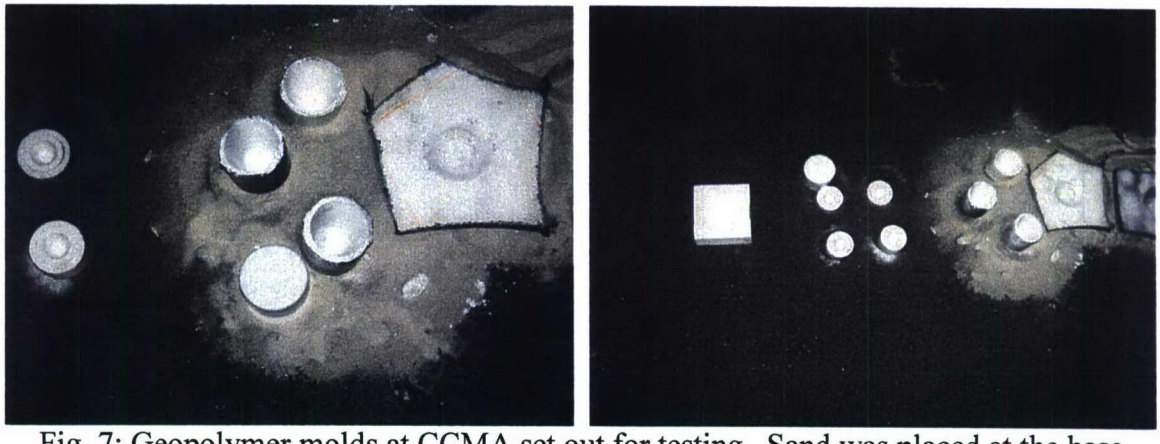
Fig. 7: Geopolymer molds at CCMA set out for testing. Sand was placed at the base some of the molds to stabilize them during pouring.

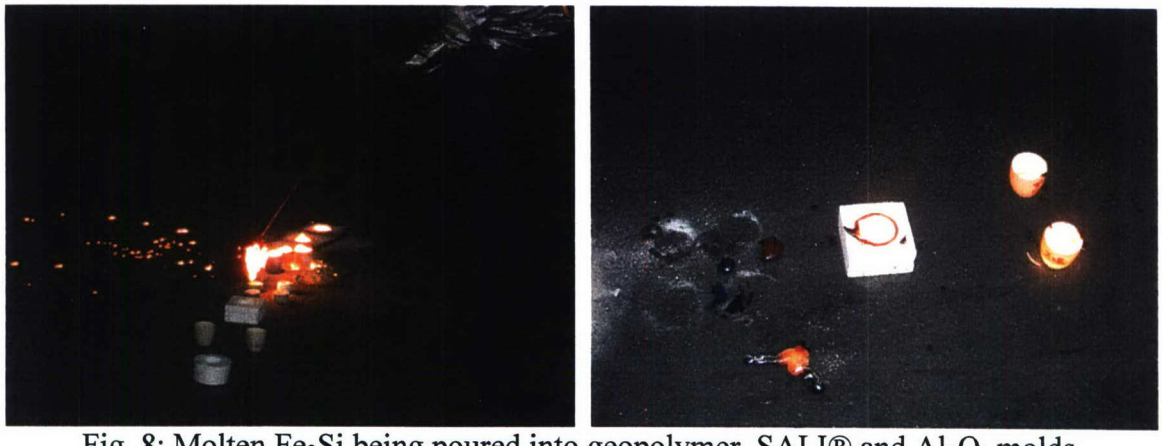
Fig. 8: Molten Fe_2Si being poured into geopolymer, SALI® and Al_2O_3 molds.

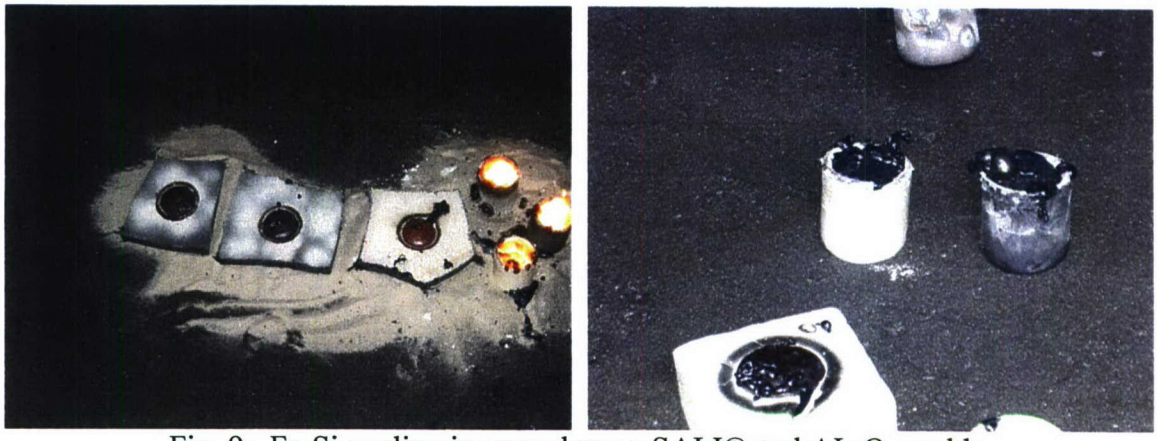

Fig. 9: Fe_2Si cooling in geopolymer, SALI® and AL_2O_3 molds.

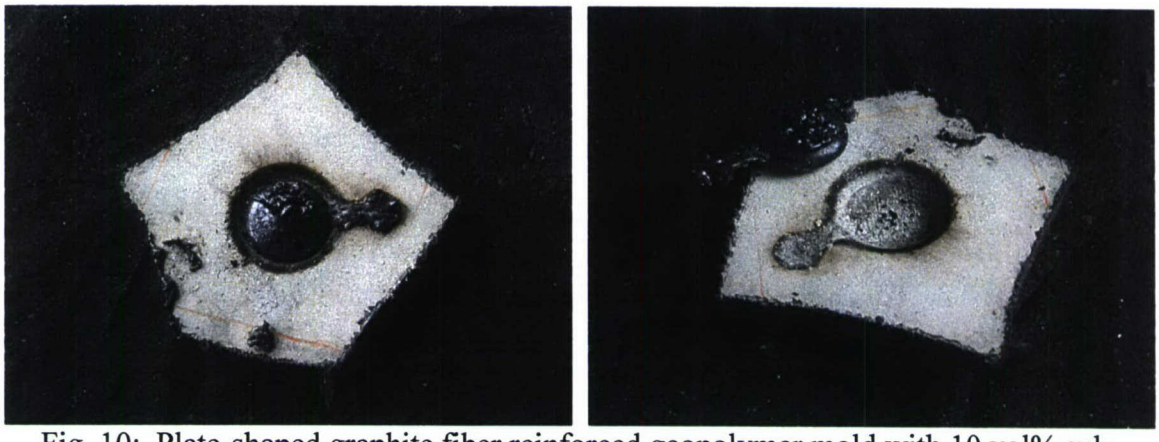

Fig. 10: Plate-shaped graphite fiber reinforced geopolymer mold with 10 vol% sub-micron Al_2O_3 before and after ejection of solidified Fe_2Si.

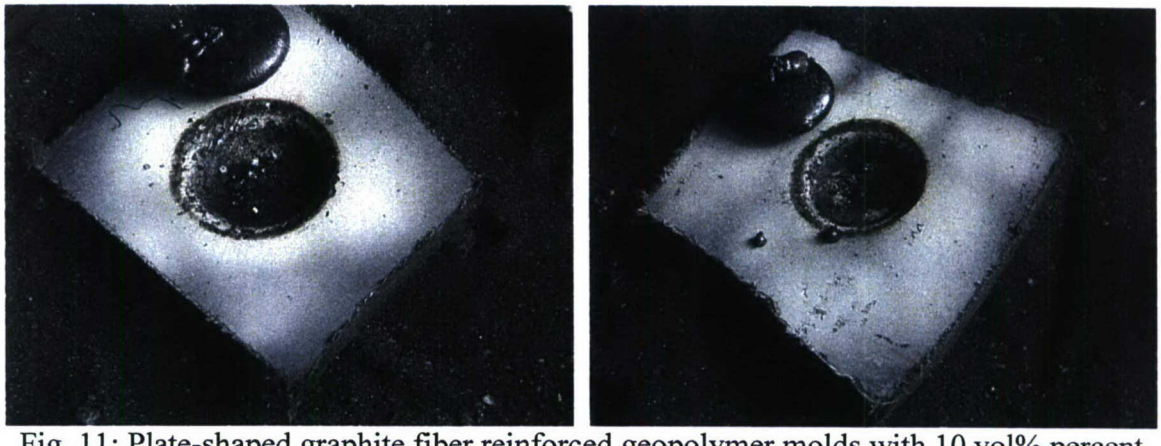

Fig. 11: Plate-shaped graphite fiber reinforced geopolymer molds with 10 vol% percent molybdenum particles, (1 – 5 μm) (left) and (-325 mesh) (right) after ejection of solidified Fe_2Si.

Fig. 12: Pressure cured molds quenched in water (top). Ejection of solidified Fe_2Si from the SALI® casting mold (bottom).

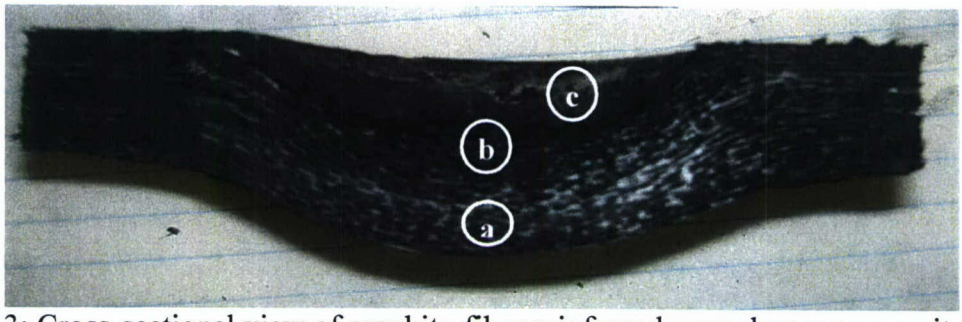

Fig. 13: Cross-sectional view of graphite-fiber reinforced geopolymer composite plate with 10 vol% (1 – 5 μm diameter) molybdenum particles. The labels correspond to a) a cross section away from the damage surface, b) cross section near the damage surface and c) top view of the damage surface. The SEM results for analysis of these areas are shown in Fig. 14 – Fig. 21.

Fig. 14: Cross-section of an undamaged section of graphite-fiber reinforced geopolymer composite plate with 10 vol% (1 – 5 μm diameter) molybdenum particles. The [0°, 90°, ±45°] orientation of the fiber mesh lay-up can be seen in the figure. The area shown in the figure is well below the pour zone.

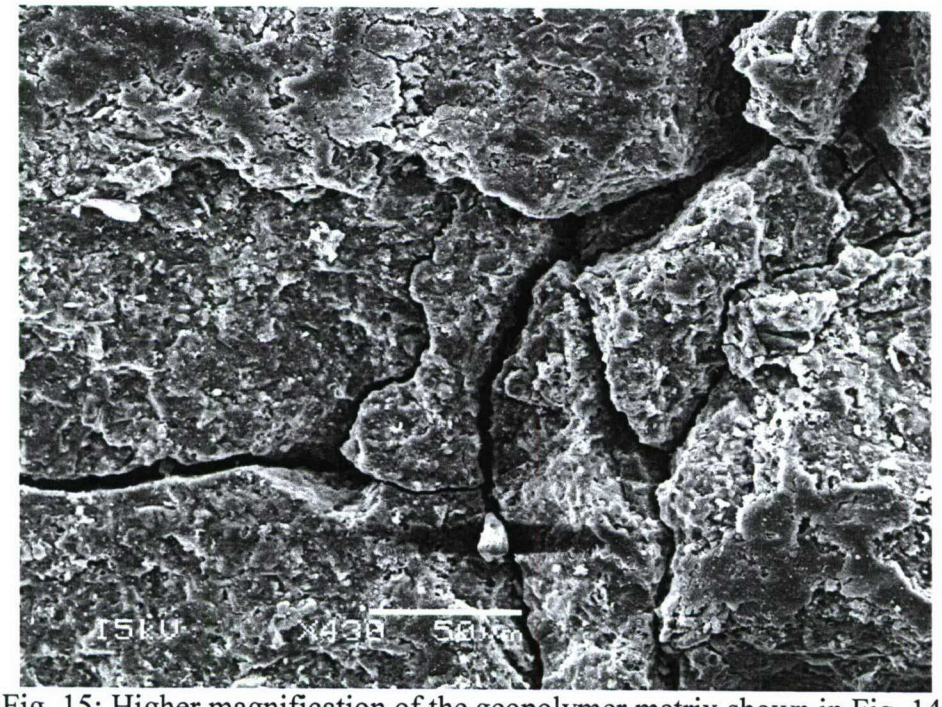

Fig. 15: Higher magnification of the geopolymer matrix shown in Fig. 14.

Fig. 16: Cross sectional view of the damaged area for the graphite-fiber reinforced geopolymer composite plate with 10 vol% (1 – 5 µm diameter) molybdenum particles. The top surface of the pour region was located at the bottom of the micrograph.

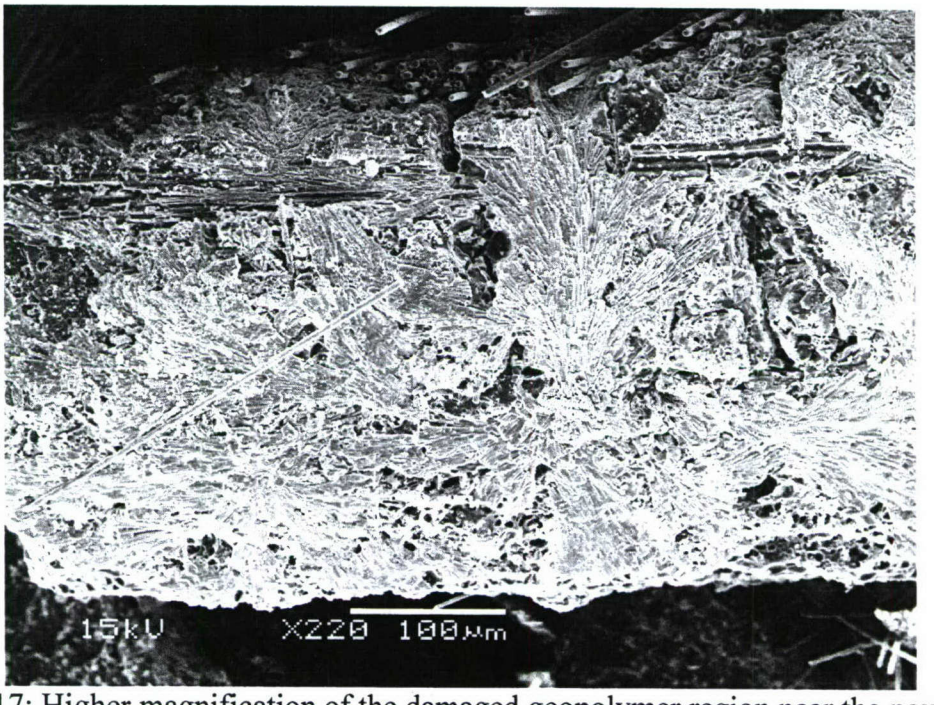

Fig. 17: Higher magnification of the damaged geopolymer region near the pouring interface shown in Fig. 16. The top surface of the pour region was located at the bottom of the micrograph.

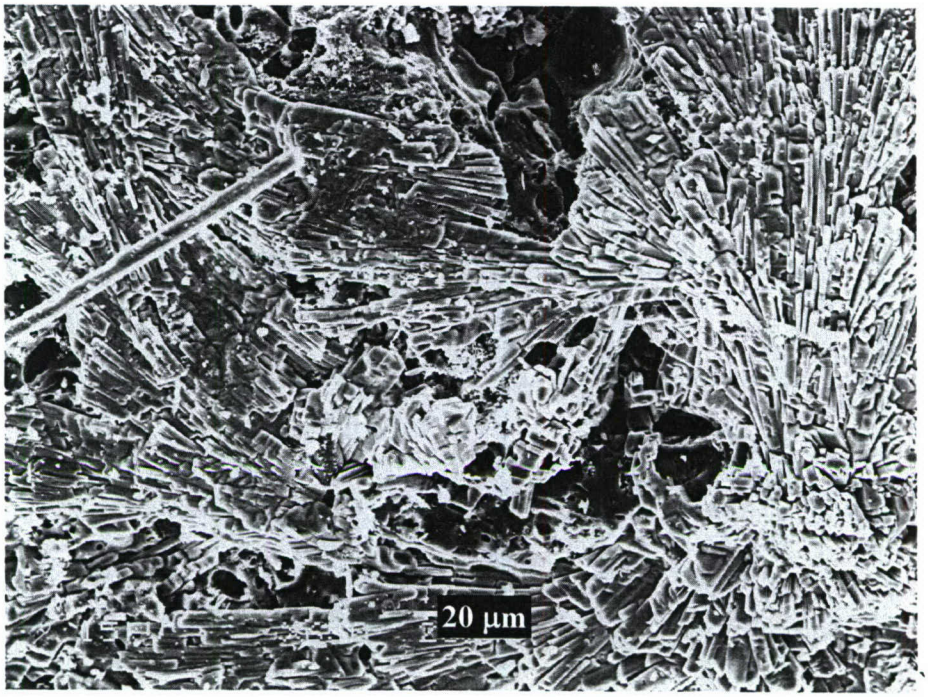

Fig. 18: Closer view of the micrograph region shown in Fig. 17. The texturing in this figure is may be indicative of crystallization.

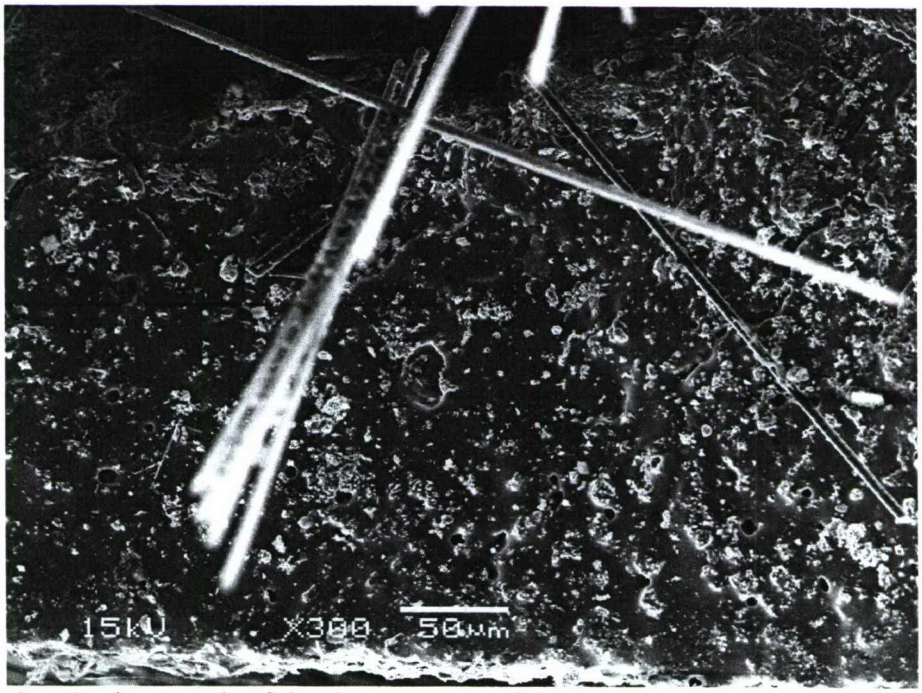

Fig. 19: SEM micrograph of the damage area of the geopolymer near the surface of the pour zone showing possible melting of the geopolymer phase.

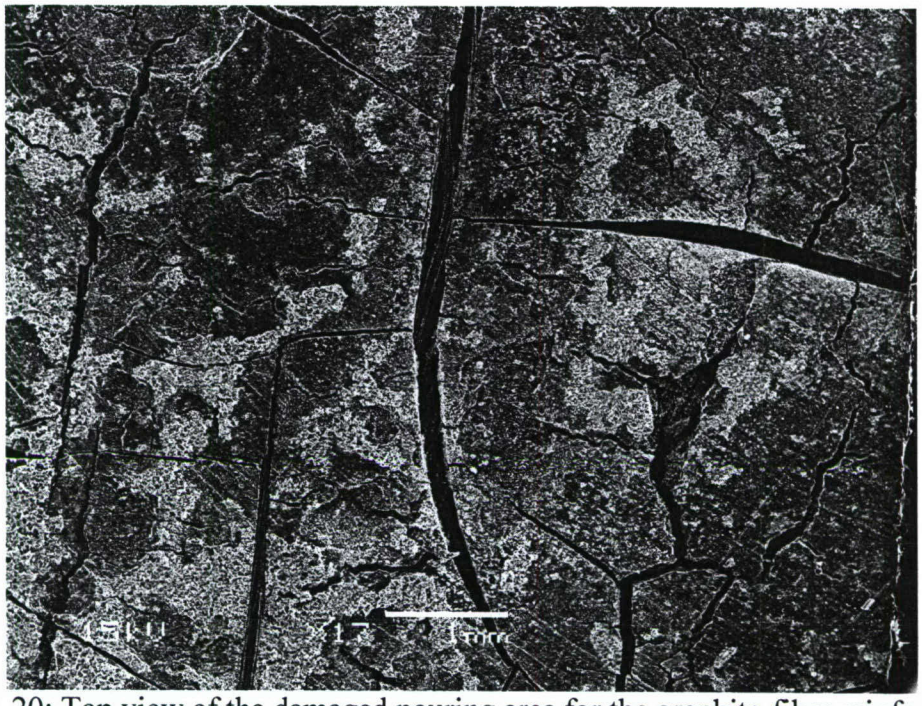

Fig. 20: Top view of the damaged pouring area for the graphite-fiber reinforced geopolymer plate composite with 10 volume % filler molybdenum (1 – 5 μm diameter).

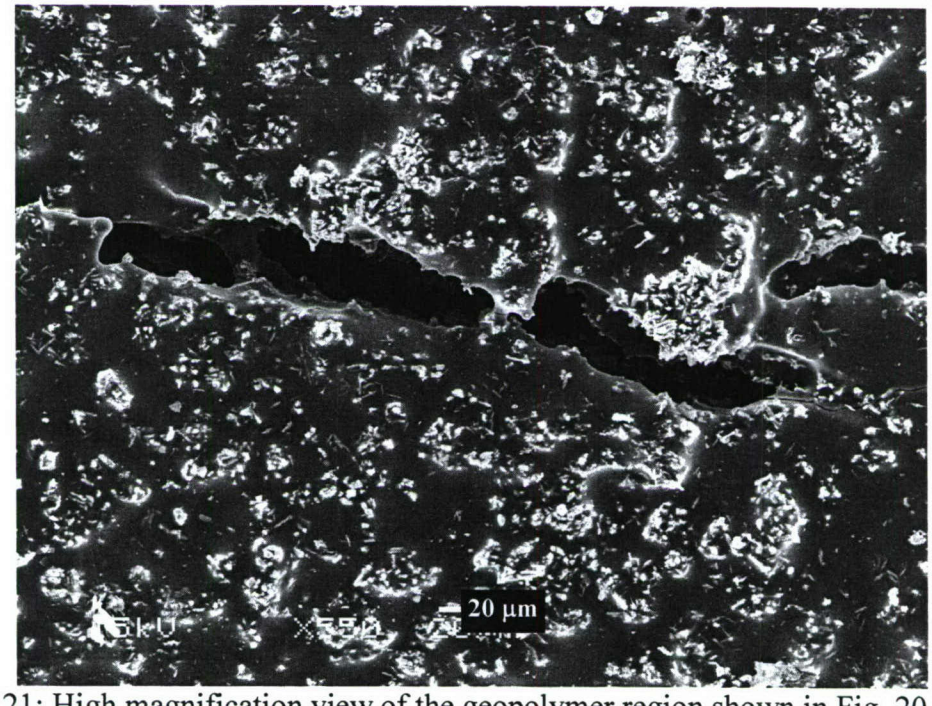

Fig. 21: High magnification view of the geopolymer region shown in Fig. 20. The structure shown may be evident of melting.

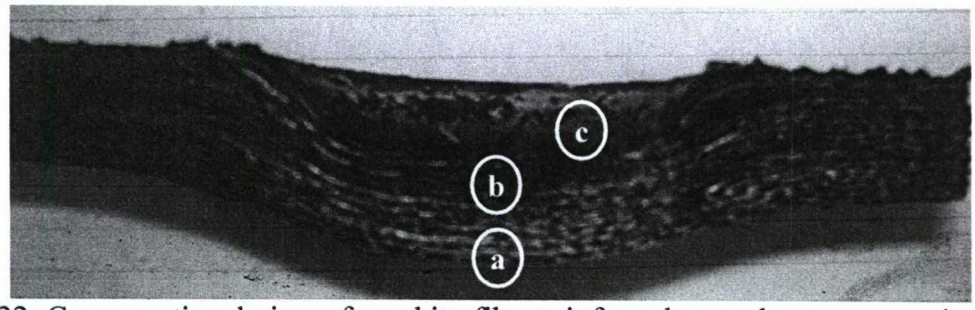

Fig. 22: Cross-sectional view of graphite-fiber reinforced geopolymer composite plate with 10 vol% (44 μm diameter) molybdenum particles. The labels correspond to a) a cross section away from the damage, b) cross section near the damage surface and c) top view of the damage surface. The SEM results for analysis of these areas are shown in Fig. 23 - Fig. 33.

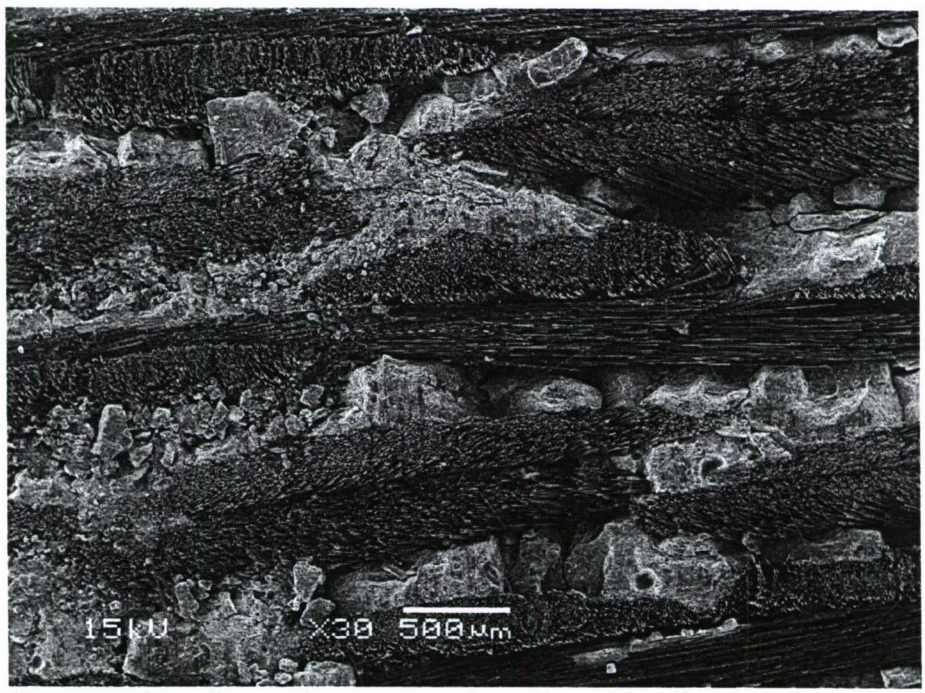

Fig. 23: Cross-section of an undamaged section of graphite-fiber reinforced geopolymer composite plate with 10 vol% (44 μm diameter) molybdenum particles. The [0°, 90°, ±45°] orientation of the fiber mesh lay-up can be seen in the figure. The area shown in the figure was sufficiently far from the pouring interface area to not be affected by the molten Fe_2Si.

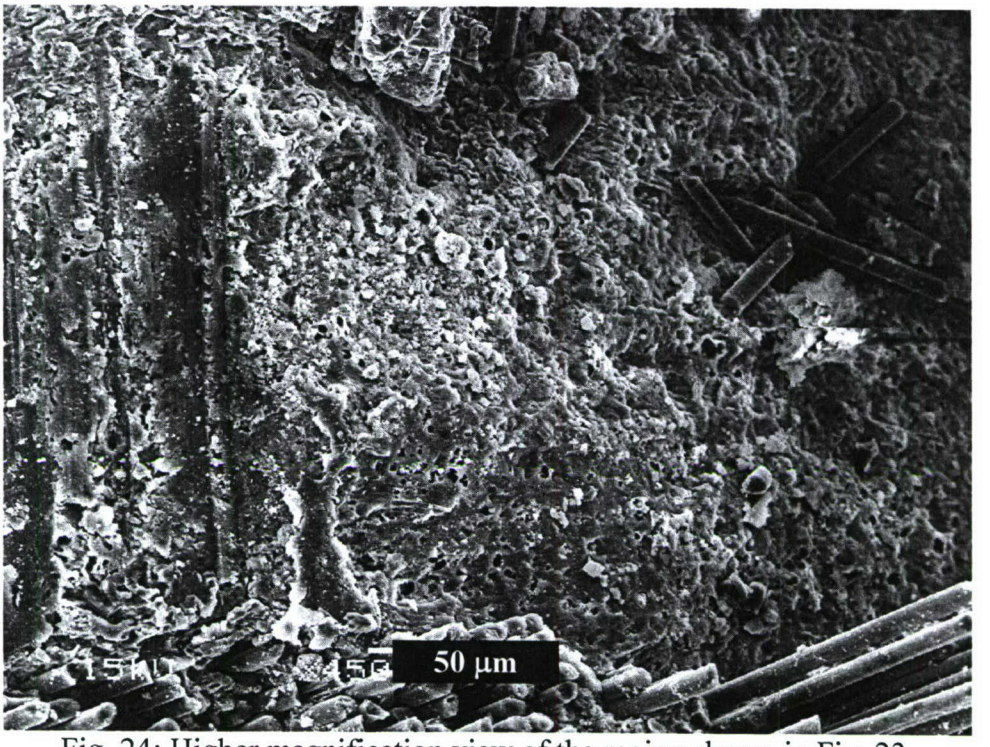

Fig. 24: Higher magnification view of the region shown in Fig. 23.

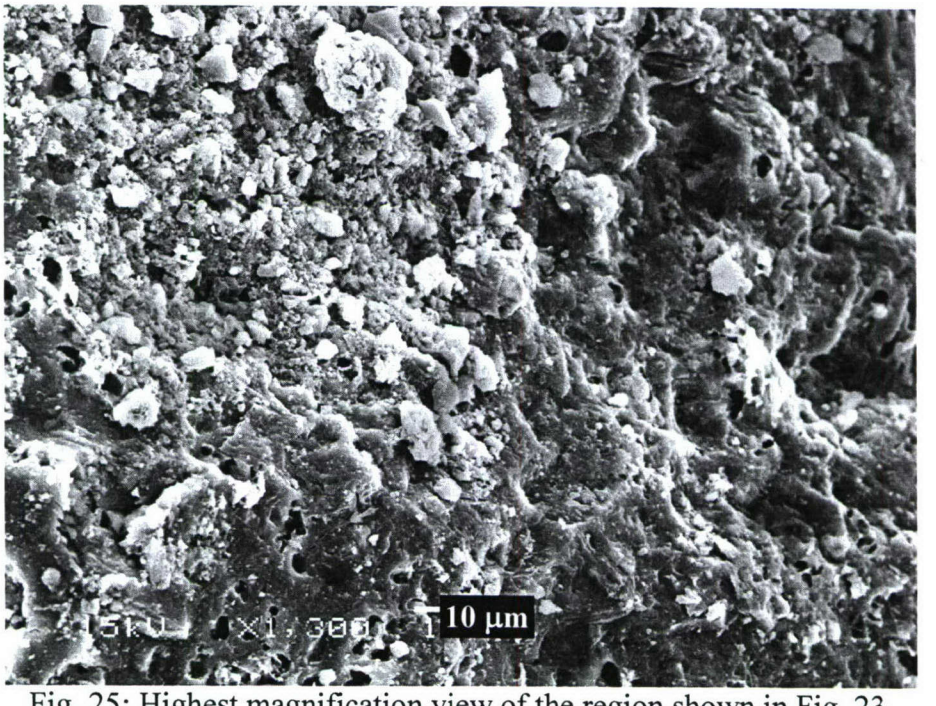

Fig. 25: Highest magnification view of the region shown in Fig. 23.

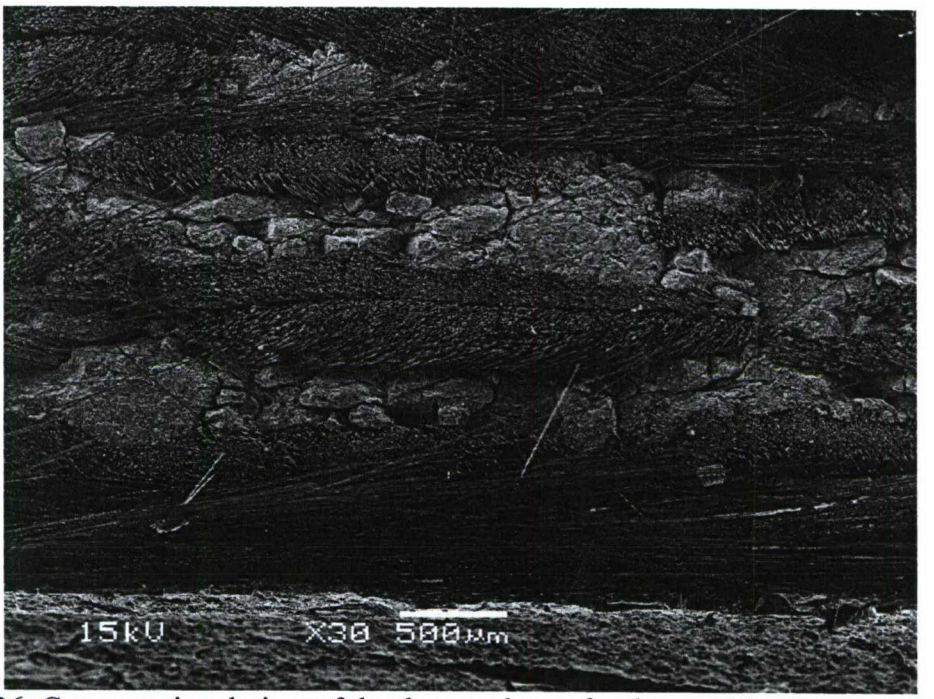

Fig. 26: Cross sectional view of the damaged area for the graphite-fiber reinforced geopolymer composite plate with 10 vol% -325 mesh molybdenum particles. The top surface of the pour region is located at the bottom of the micrograph.

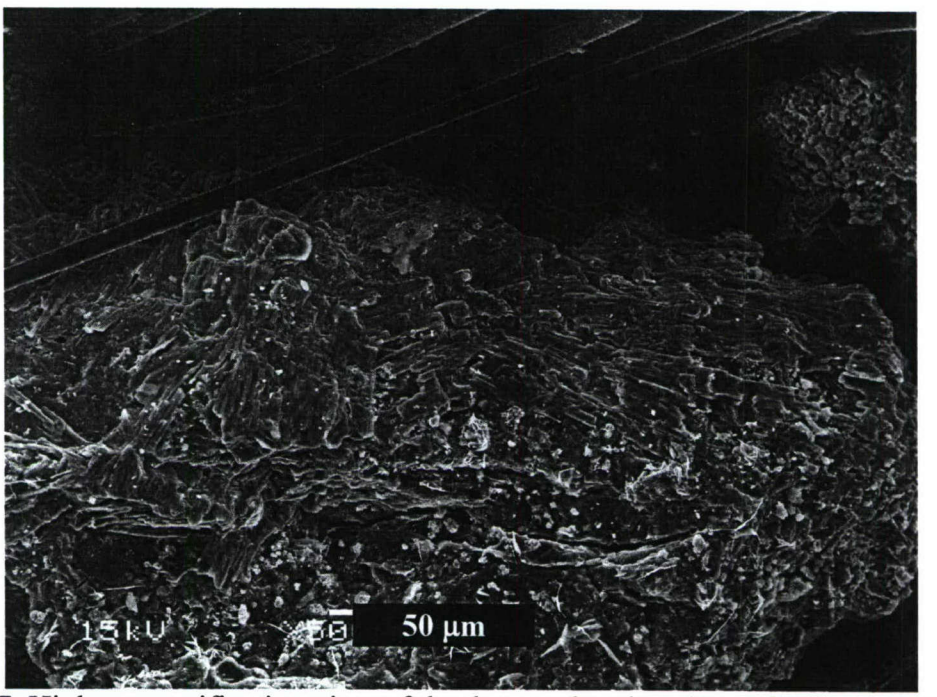

Fig. 27: Higher magnification view of the damaged region shown in Fig. 26 near the pouring interface showing the presence of needle-shaped crystals.

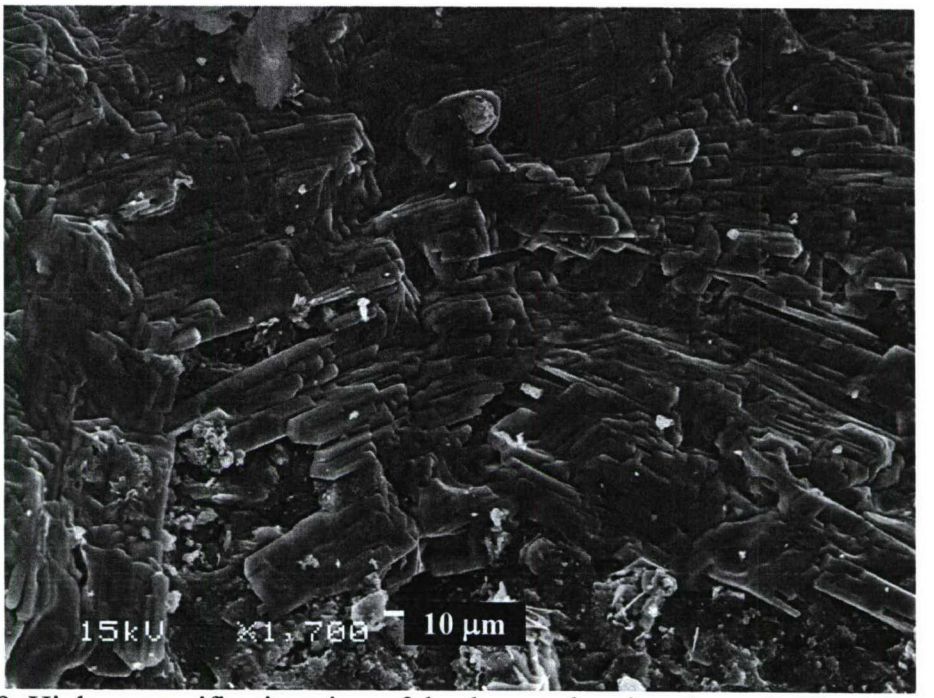

Fig. 28: Higher magnification view of the damaged region shown in Fig. 26 near the pouring interface showing the presence of needle-shaped crystals.

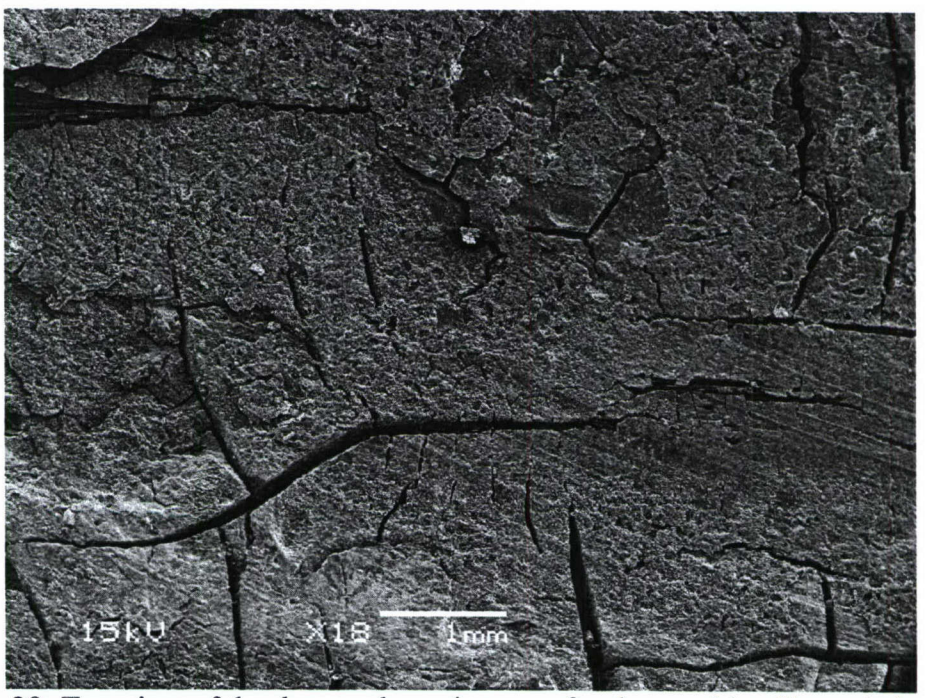

Fig. 29: Top view of the damaged pouring area for the graphite-fiber reinforced geopolymer composite plate with 10 volume % filler -325 mesh molybdenum .

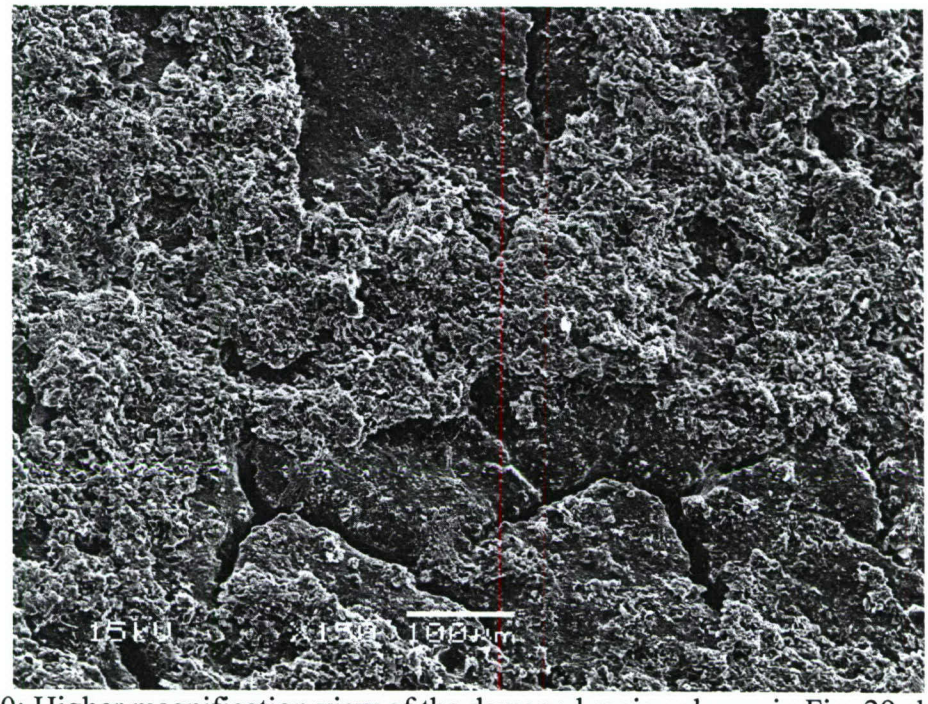

Fig. 30: Higher magnification view of the damaged region shown in Fig. 29 showing inhomogeneous regions of geopolymer matrix.

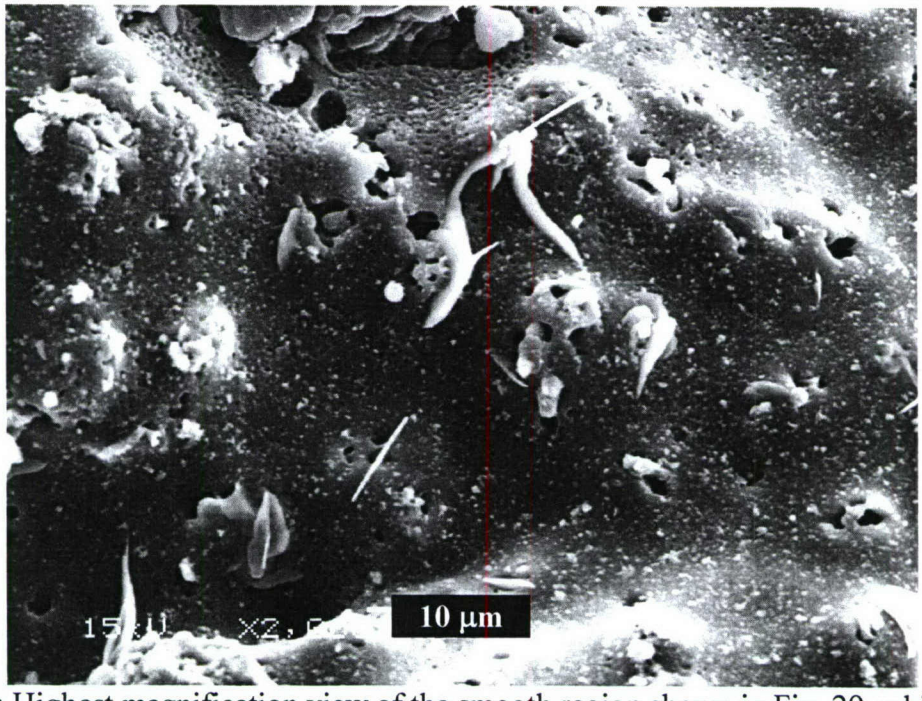

Fig. 31: Highest magnification view of the smooth region shown in Fig. 29, which may indicate localized melting.

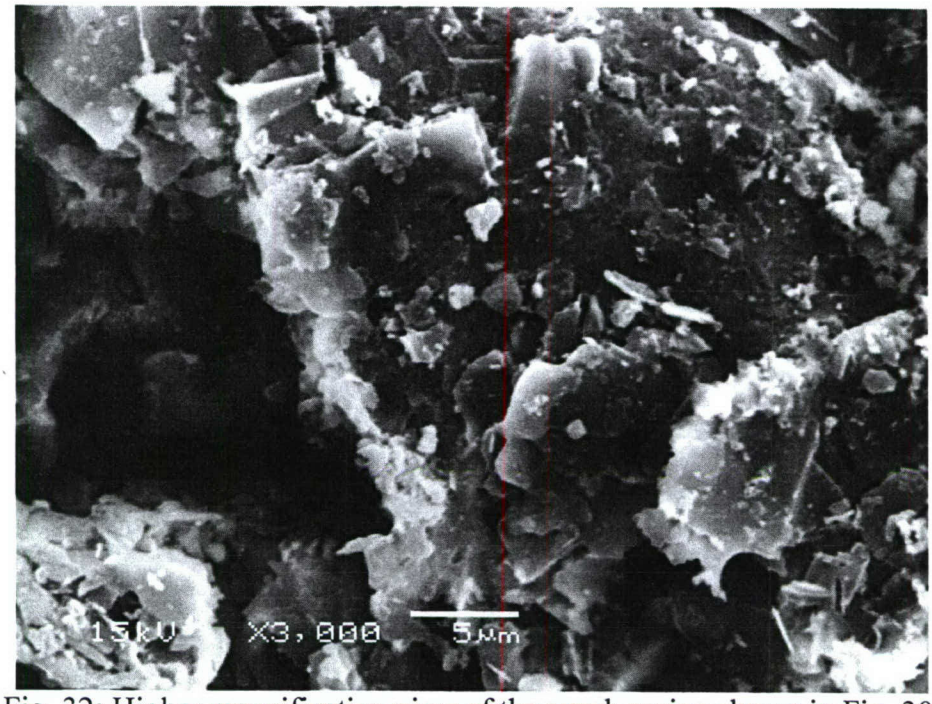

Fig. 32: Higher magnification view of the rough region shown in Fig. 30.

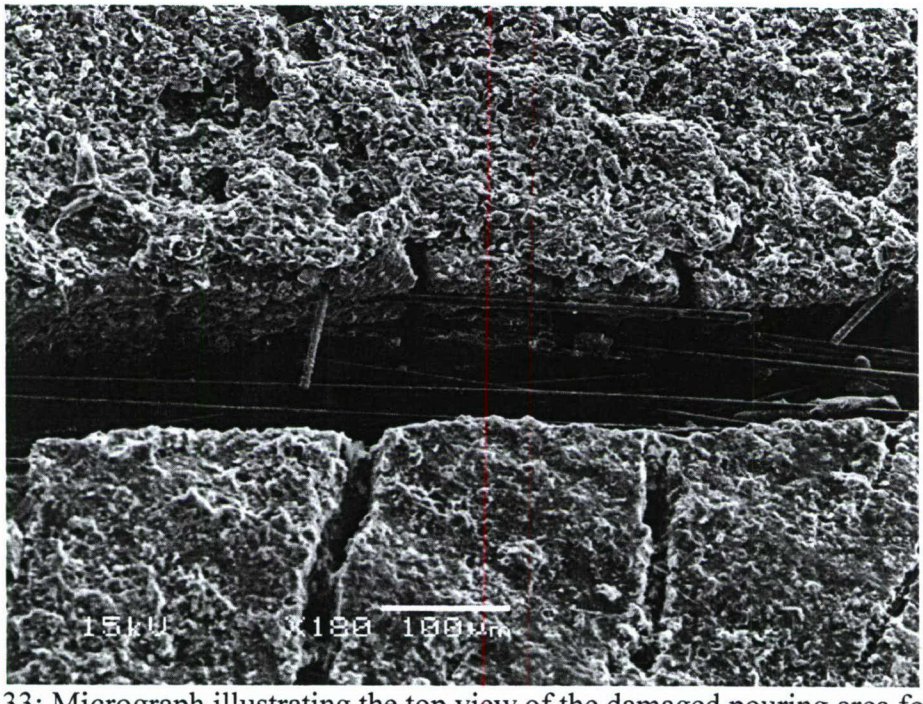

Fig. 33: Micrograph illustrating the top view of the damaged pouring area for the graphite-fiber reinforced geopolymer composite plate with 10 volume % filler molybdenum (44 μm diameter). The fibers at the surface remained intact despite cracking of the matrix phase.

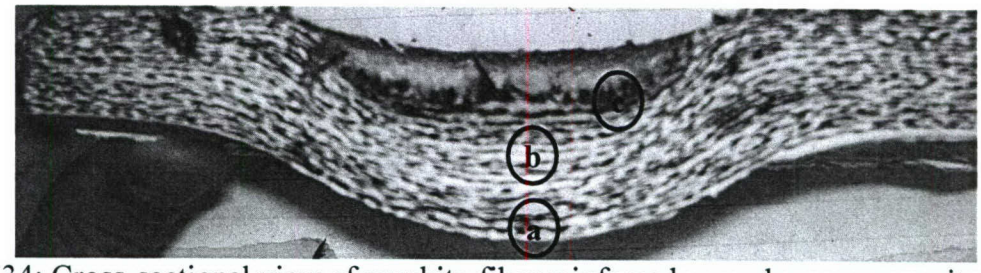

Fig. 34: Cross-sectional view of graphite-fiber reinforced geopolymer composite plate with 10 vol% Al_2O_3 particles. The labels correspond to a) a cross section away from the damage surface, b) cross section near the damage surface and c) top view of the damage surface. The SEM results for analysis of these areas are shown in Fig. 35 - Fig. 41.

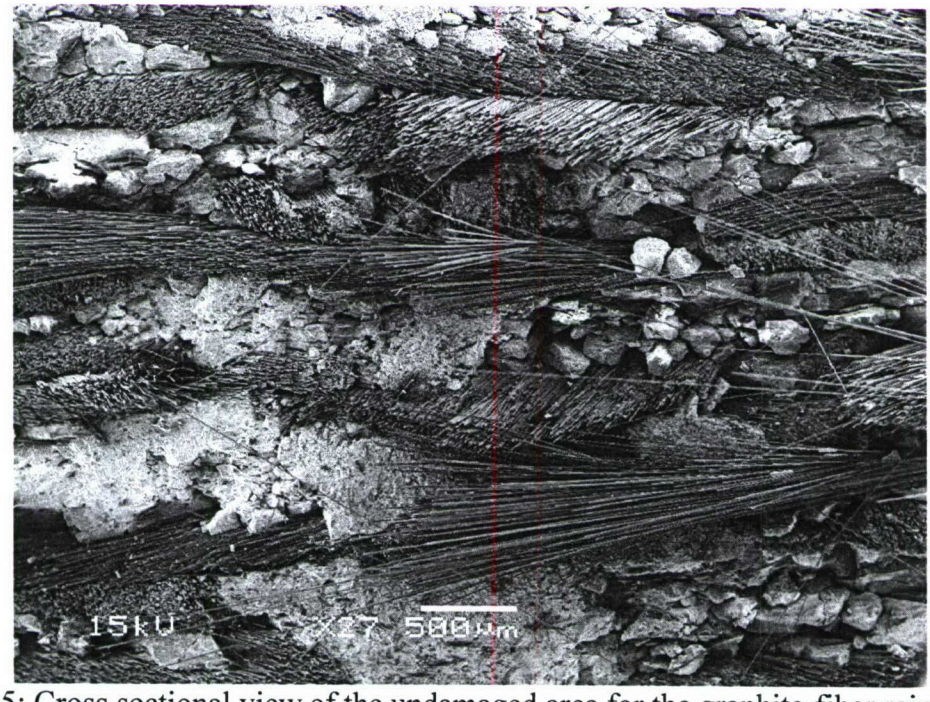

Fig. 35: Cross sectional view of the undamaged area for the graphite-fiber reinforced geopolymer composite plate with 10 vol% Al_2O_3 particles. The area shown in the figure was sufficiently far from the pouring interface area to not be affected by the molten Fe_2Si.

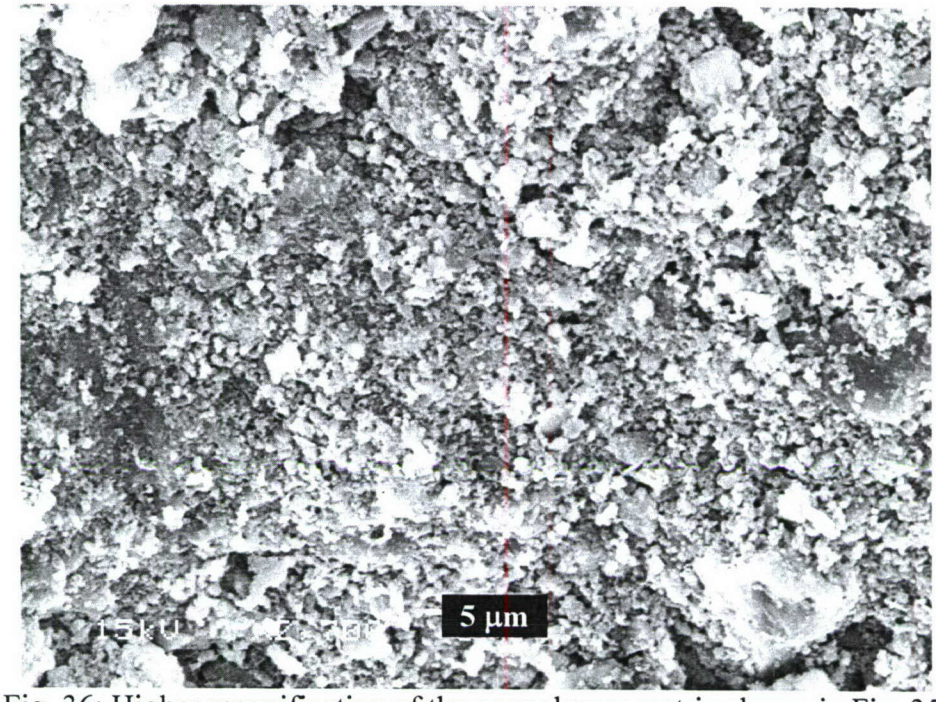

Fig. 36: Higher magnification of the geopolymer matrix shown in Fig. 35.

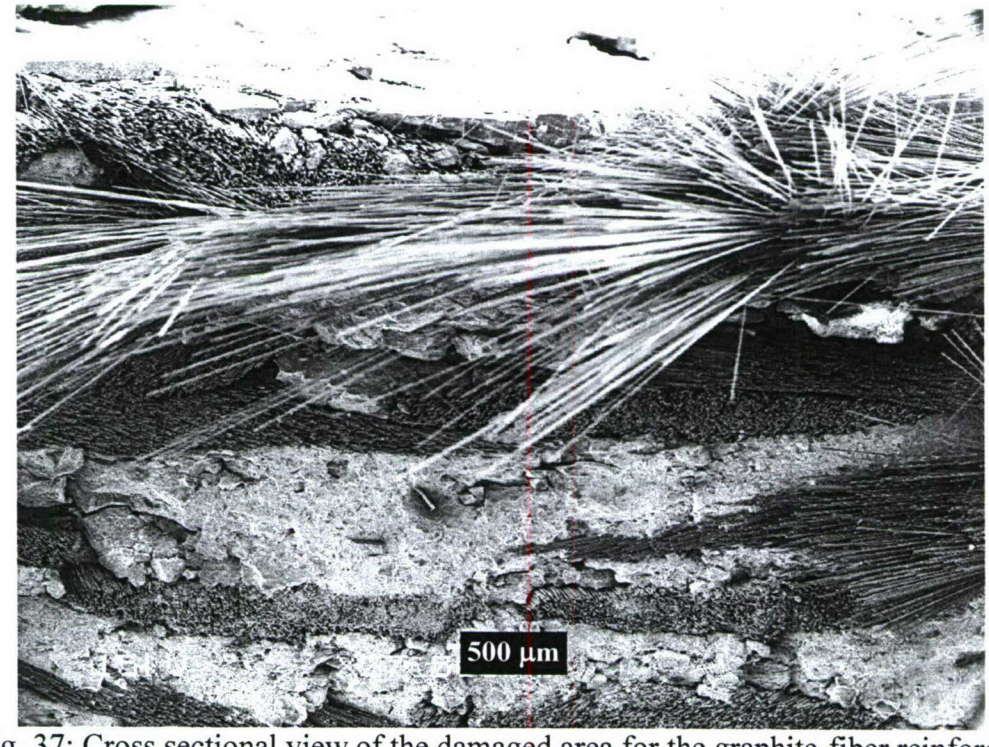

Fig. 37: Cross sectional view of the damaged area for the graphite-fiber reinforced geopolymer composite plate with 10 vol% Al_2O_3 particles. The pour region was located at the bottom of this micrograph. There was extensive fiber pullout near the pour region during cutting of the mold for preparation.

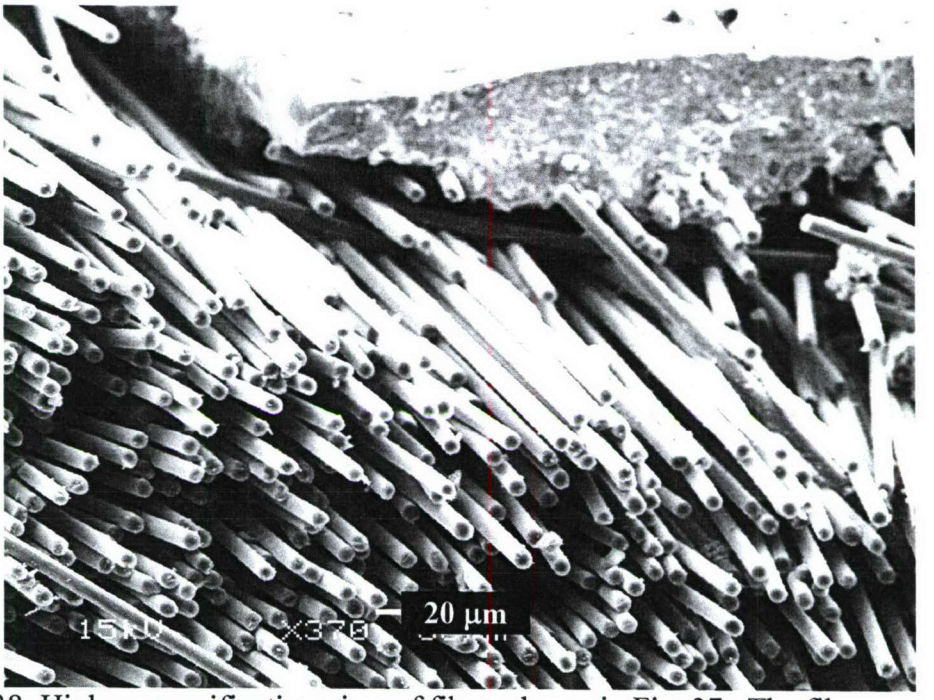

Fig. 38: Higher magnification view of fibers shown in Fig. 37. The fibers near the interface are intact despite weakening of the matrix phase.

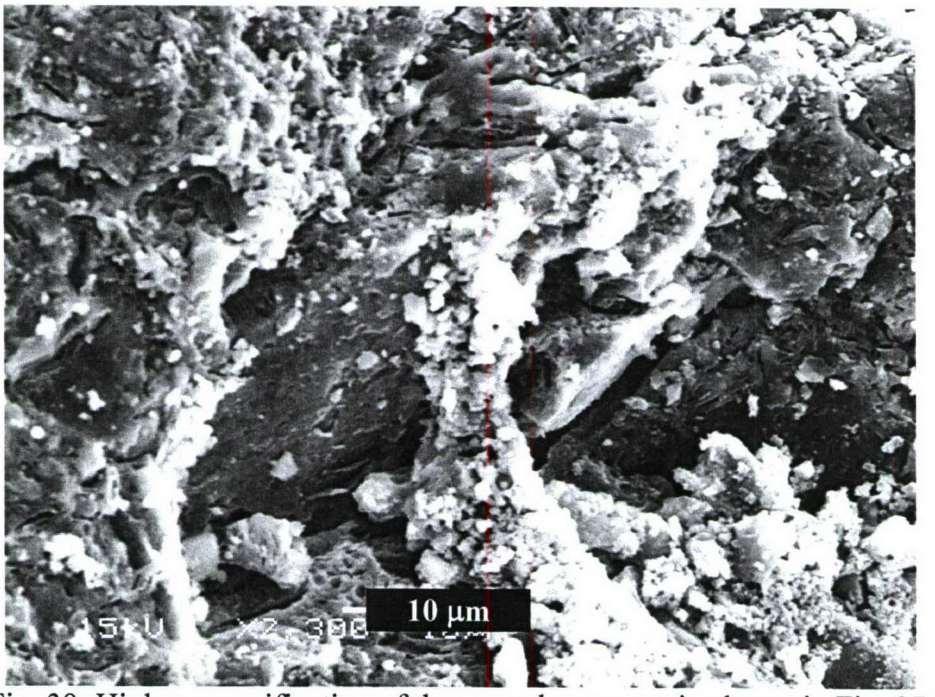

Fig. 39: Higher magnification of the geopolymer matrix shown in Fig. 37.

Fig. 40: Top view of the damaged pouring area for the graphite-fiber reinforced geopolymer composite plate with 10 volume % filler Al_2O_3 particles.

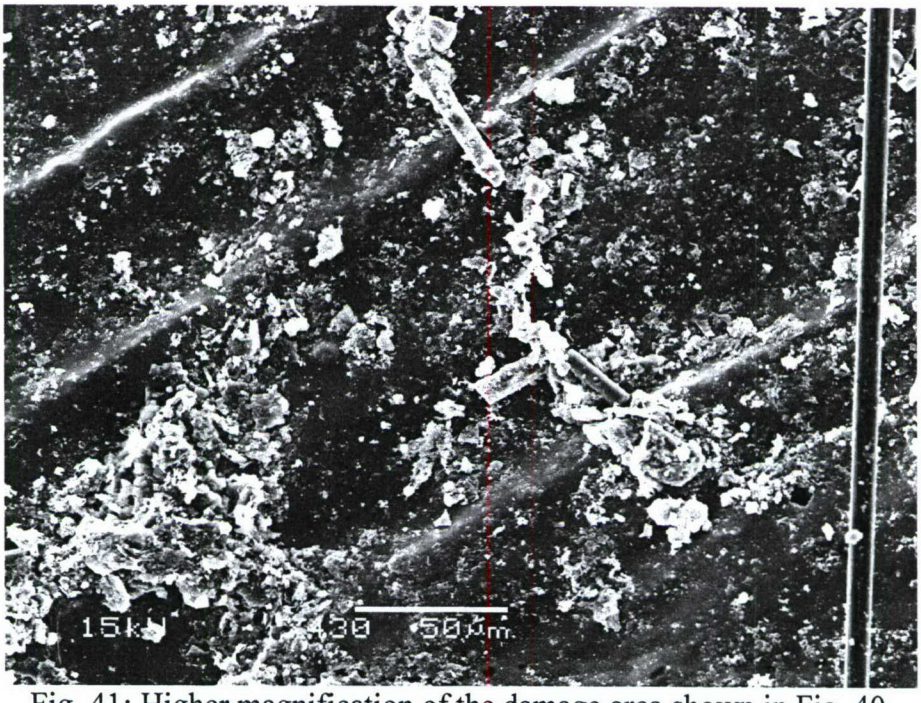

Fig. 41: Higher magnification of the damage area shown in Fig. 40.

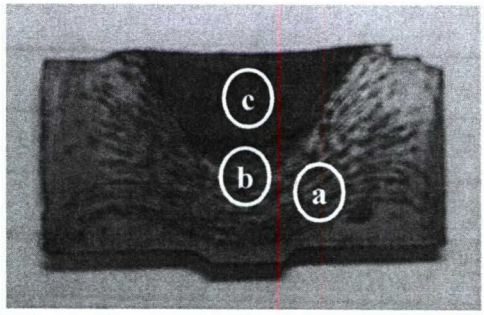

Fig. 42: Cross-sectional view of graphite-fiber reinforced geopolymer pressure cured mold reinforced with 15 vol% 1 – 5 μm molybdenum. The labels correspond to a) a cross section away from the damage surface, b) cross section near the damage surface and c) top view of the damage surface. The SEM results for analysis of these areas are shown in Fig. 43 – Fig. 51.

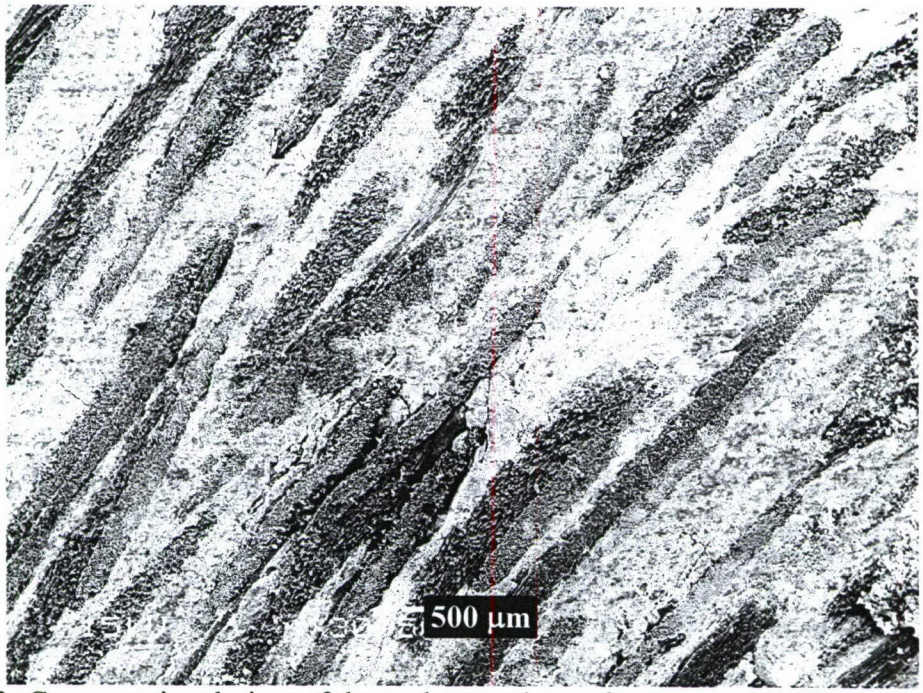

Fig. 43: Cross sectional view of the undamaged area for the graphite-fiber reinforced geopolymer pressure cured mold reinforced with 15 vol% 1 – 5 μm diameter particles of molybdenum.

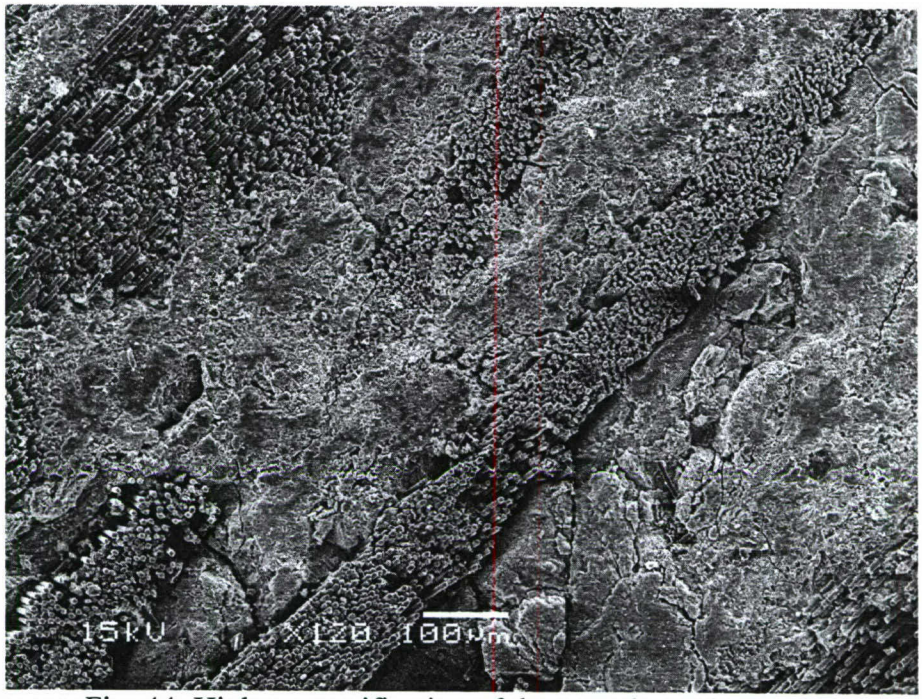

Fig. 44: Higher magnification of the area shown in Fig. 43.

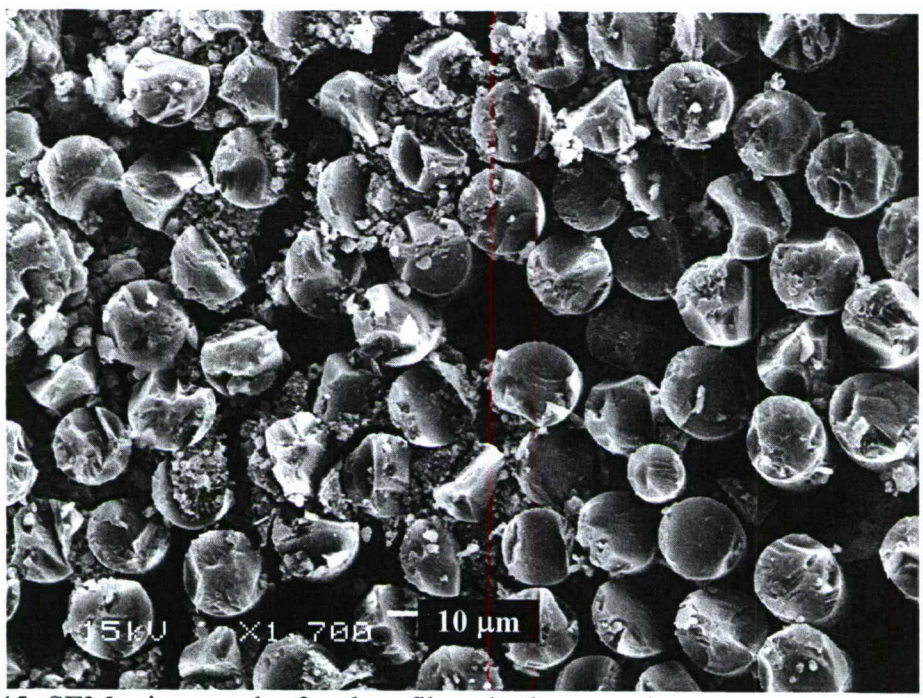

Fig. 45: SEM micrograph of carbon fibers in the geopolymer pressure cured mold reinforced with 15 vol% 1 – 5 µm diameter particles of molybdenum. Some infiltration of the matrix is present between the fibers.

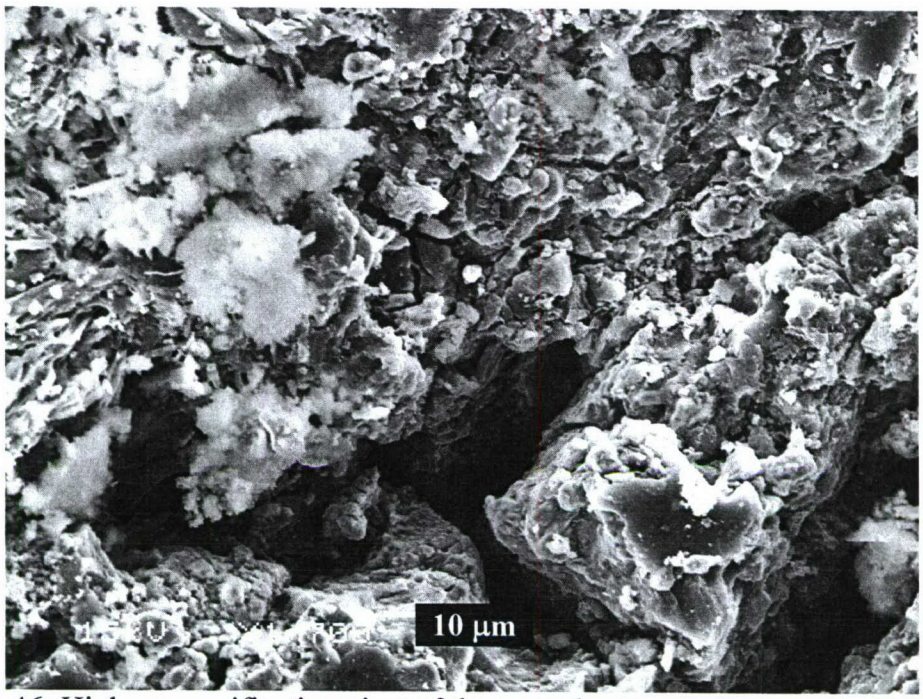

Fig. 46: Higher magnification view of the geopolymer matrix shown in Fig. 44.

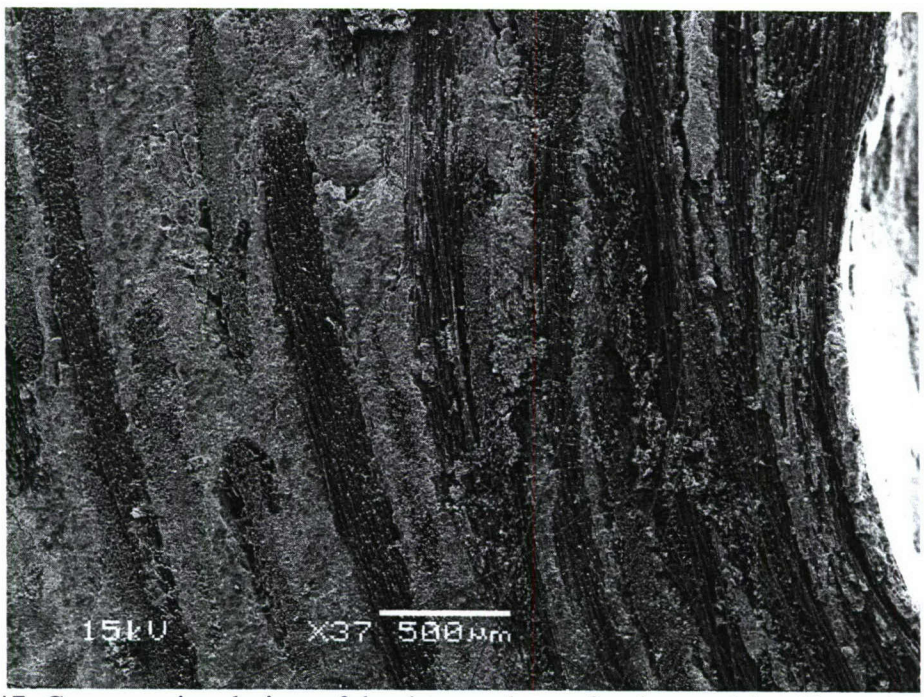

Fig. 47: Cross sectional view of the damaged area for the graphite-fiber reinforced geopolymer pressure cured mold reinforced with 15 vol% 1 – 5 μm molybdenum. The pour region is located on the right side of the micrograph.

Fig. 48: Higher magnification of damaged region shown in Fig. 47.

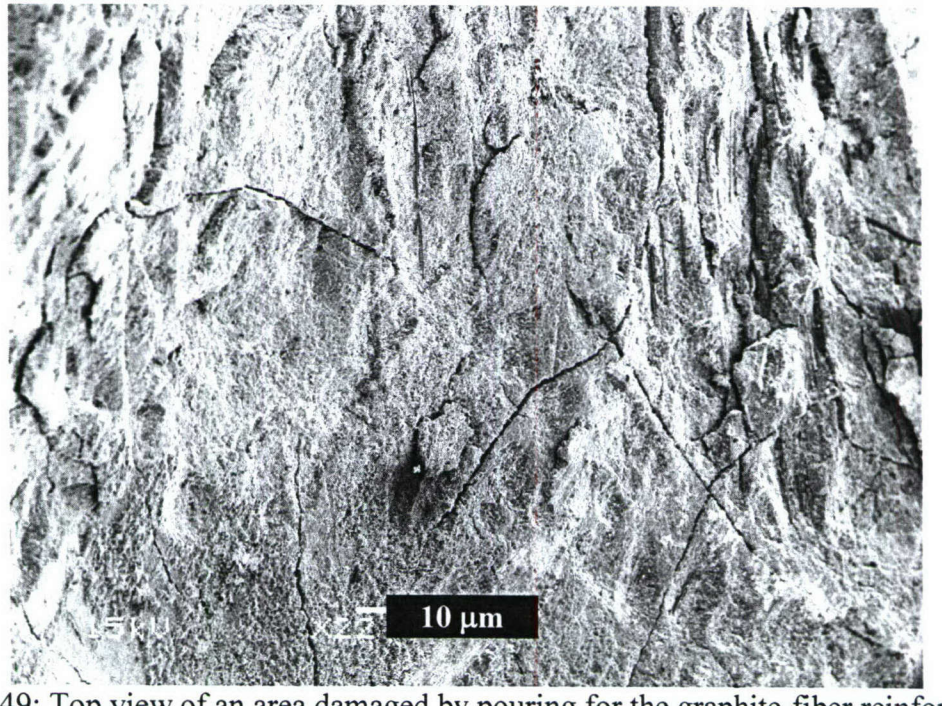

Fig. 49: Top view of an area damaged by pouring for the graphite-fiber reinforced geopolymer pressure cured mold reinforced with 15 vol% 1 – 5 µm molybdenum.

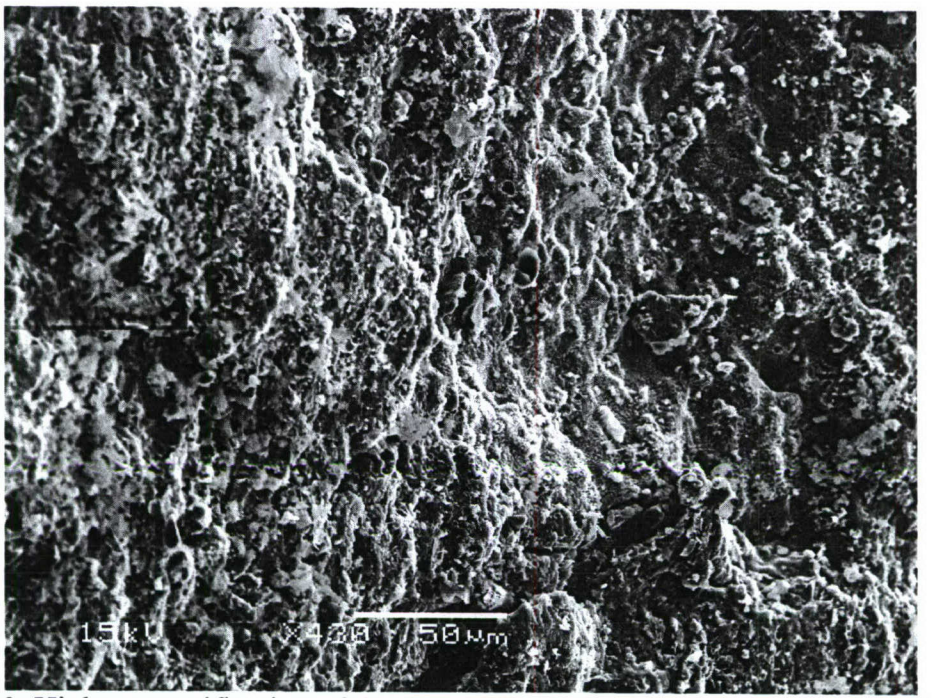

Fig. 50: Higher magnification of the damaged geopolymer region shown in Fig. 49.

Fig. 51: Higher magnification of the damaged geopolymer region shown in Fig. 49. The microstructure suggests melting of the geopolymer matrix.

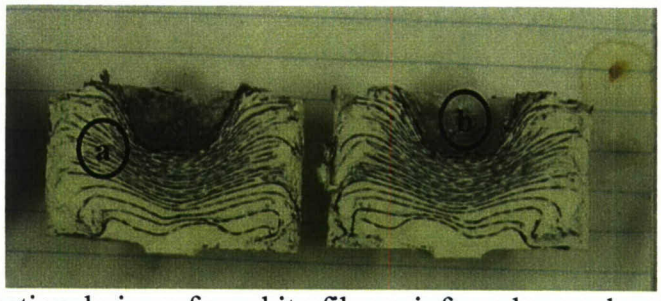

Fig. 52: Cross-sectional view of graphite-fiber reinforced geopolymer pressure cured mold reinforced with 15 vol% Al_2O_3. The labels correspond to a) a cross section away from the damage surface and b) top view of the damage surface. The SEM results for analysis of this area are shown in Fig. 53 – Fig. 57.

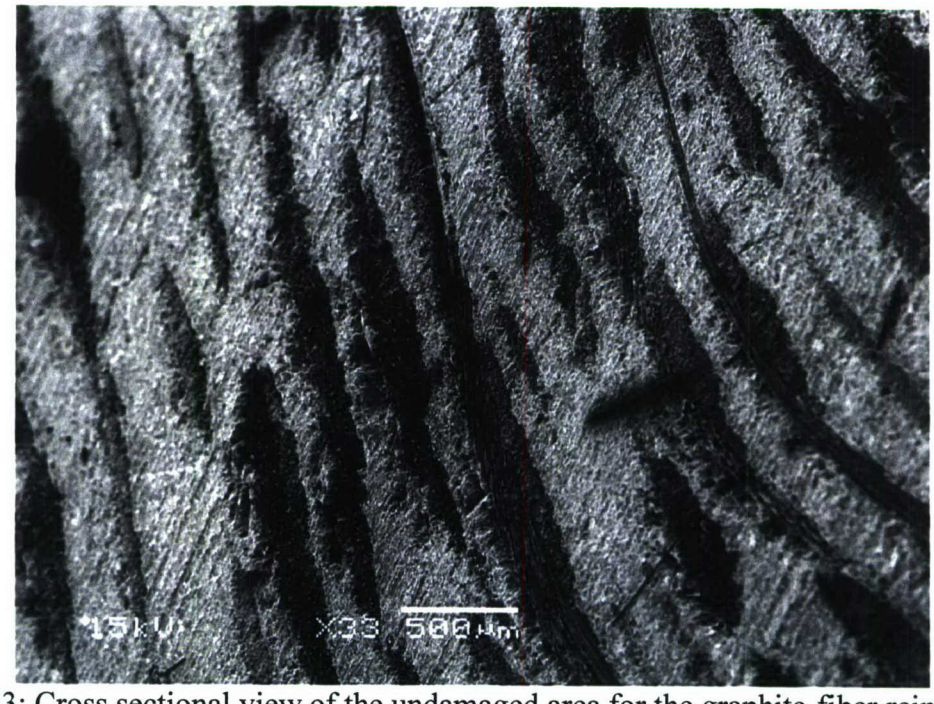

Fig. 53: Cross sectional view of the undamaged area for the graphite-fiber reinforced geopolymer pressure cured mold reinforced with 15 vol% Al_2O_3.

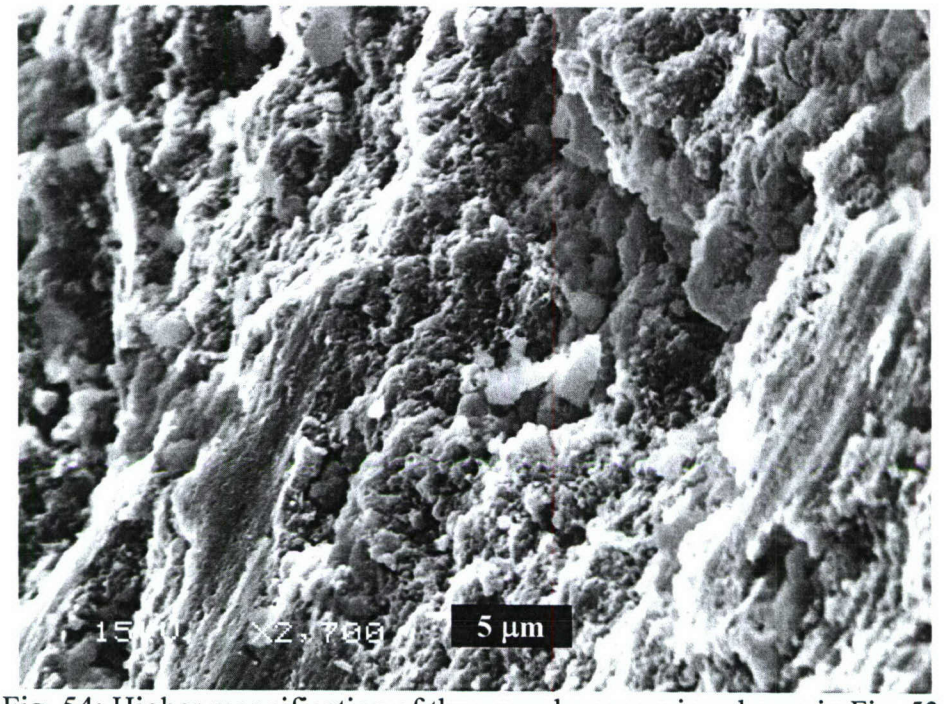

Fig. 54: Higher magnification of the geopolymer region shown in Fig. 53.

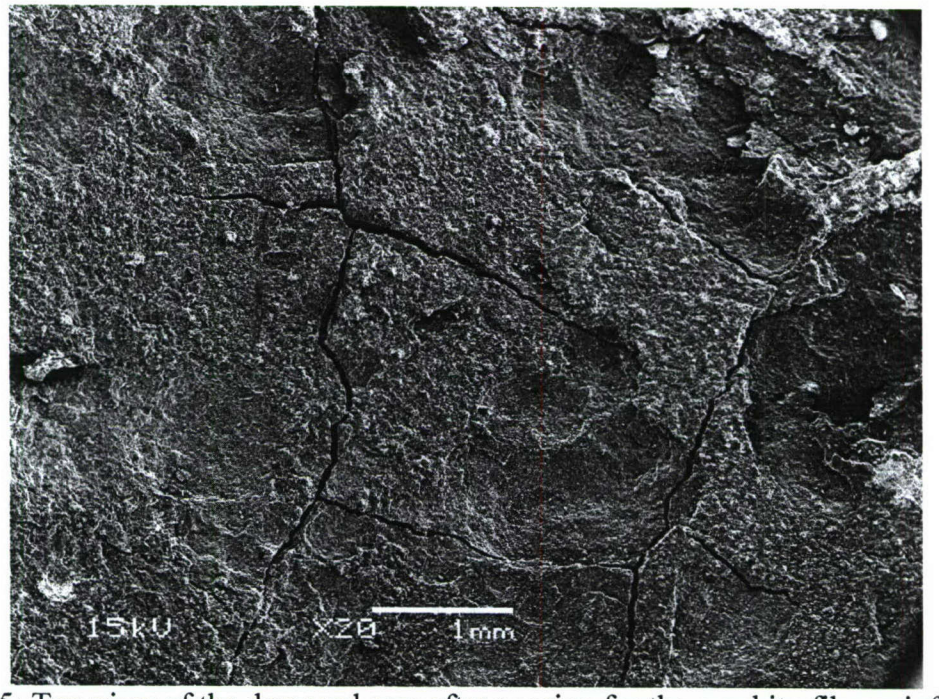

Fig. 55: Top view of the damaged area after pouring for the graphite-fiber reinforced geopolymer pressure cured mold reinforced with 15 vol% Al_2O_3.

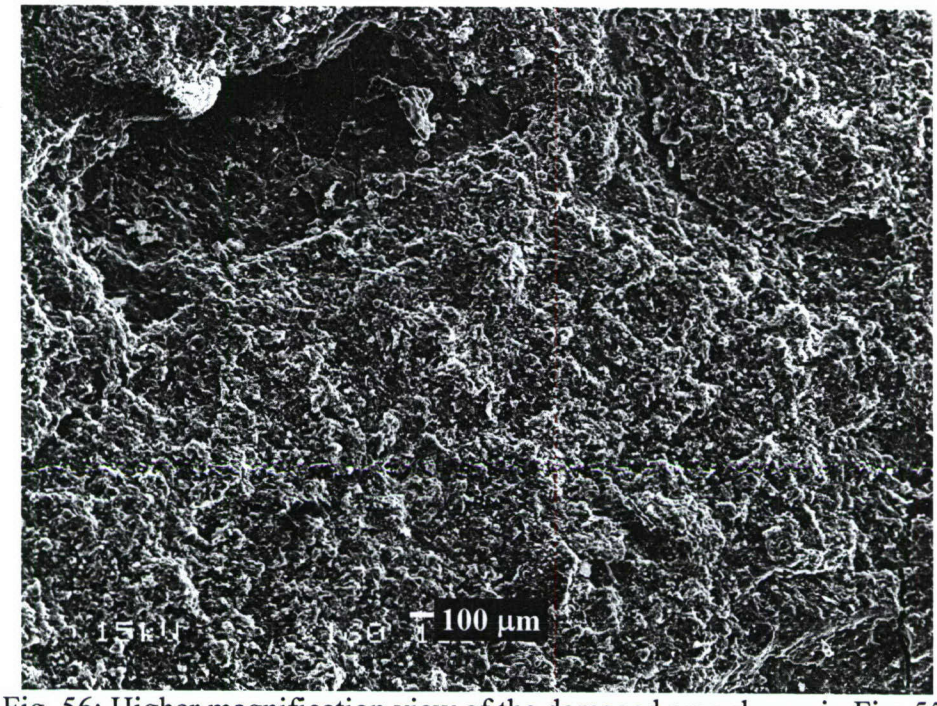

Fig. 56: Higher magnification view of the damaged area shown in Fig. 55.

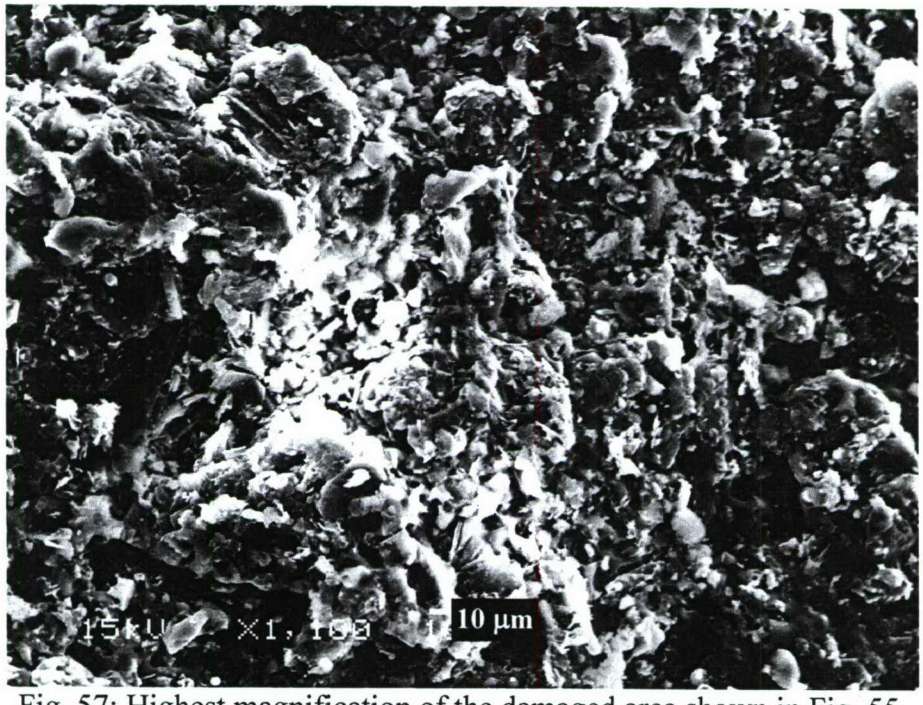

Fig. 57: Highest magnification of the damaged area shown in Fig. 55.

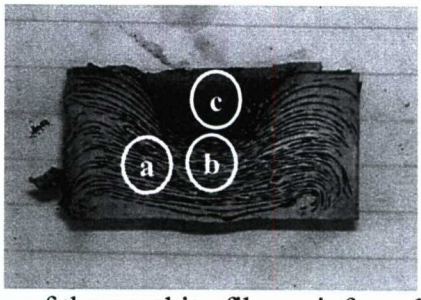

Fig. 58: Cross-sectional view of the graphite-fiber reinforced geopolymer pressure cured mold reinforced with 15 vol% SiC. The labels correspond to a) a cross section away from the damage surface, b) cross section near the damage surface and c) top view of the damage surface. The SEM results for analysis of these areas are shown in Fig. 59 – Fig. 66.

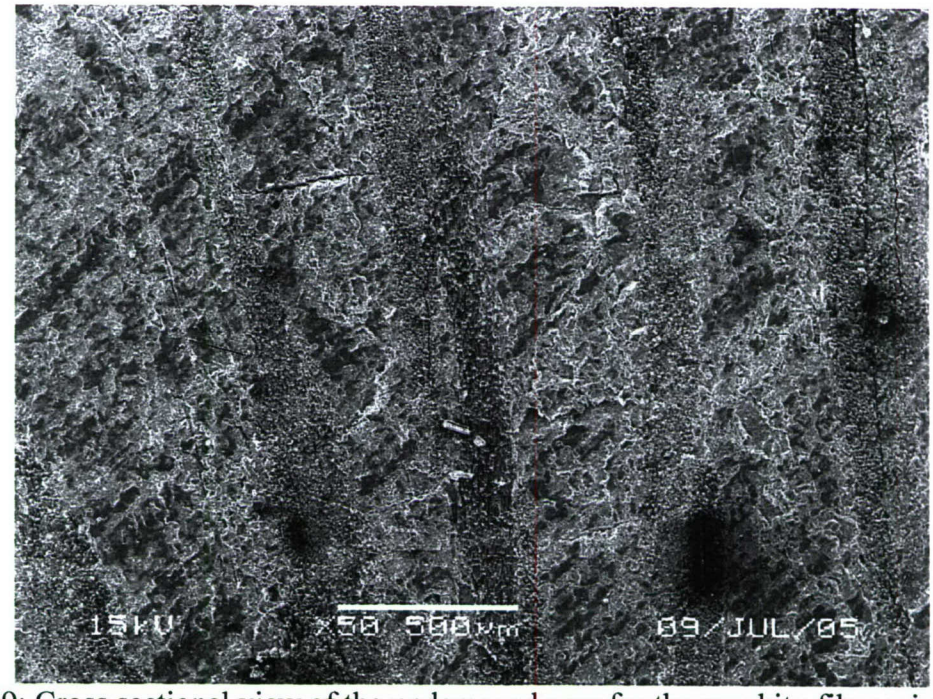

Fig. 59: Cross sectional view of the undamaged area for the graphite-fiber reinforced geopolymer pressure cured mold reinforced with 15 vol% SiC.

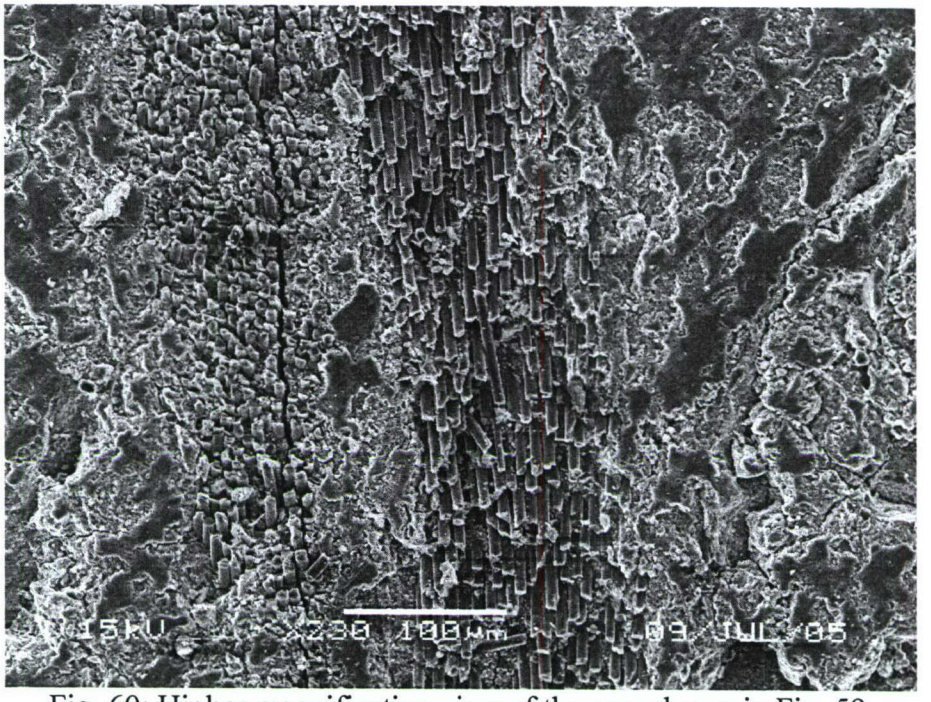

Fig. 60: Higher magnification view of the area shown in Fig. 59.

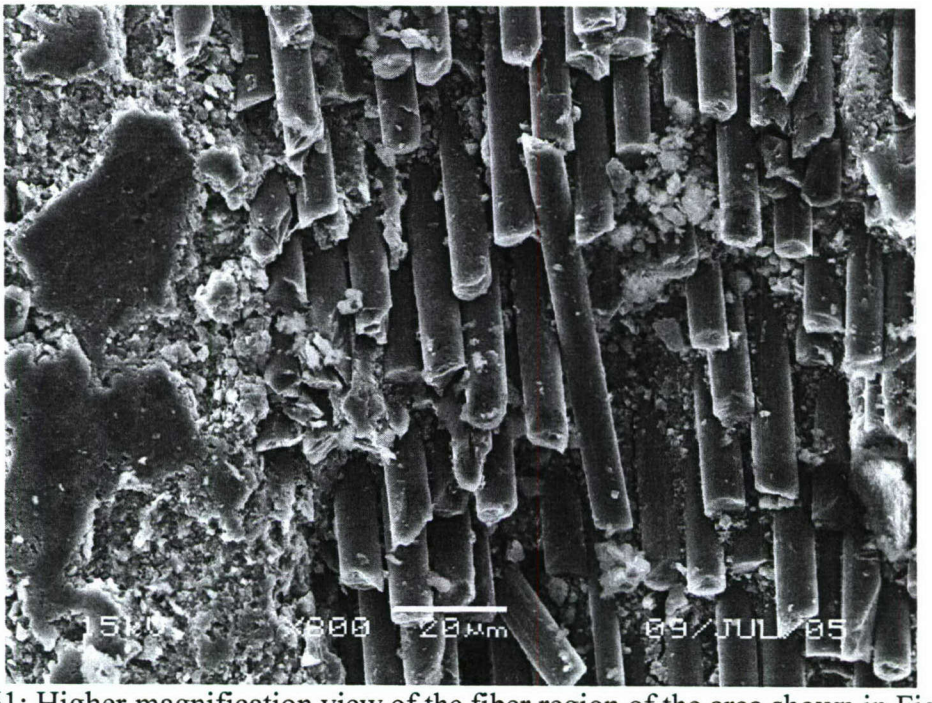

Fig. 61: Higher magnification view of the fiber region of the area shown in Fig. 60, showing matrix infiltration between the graphite fibers.

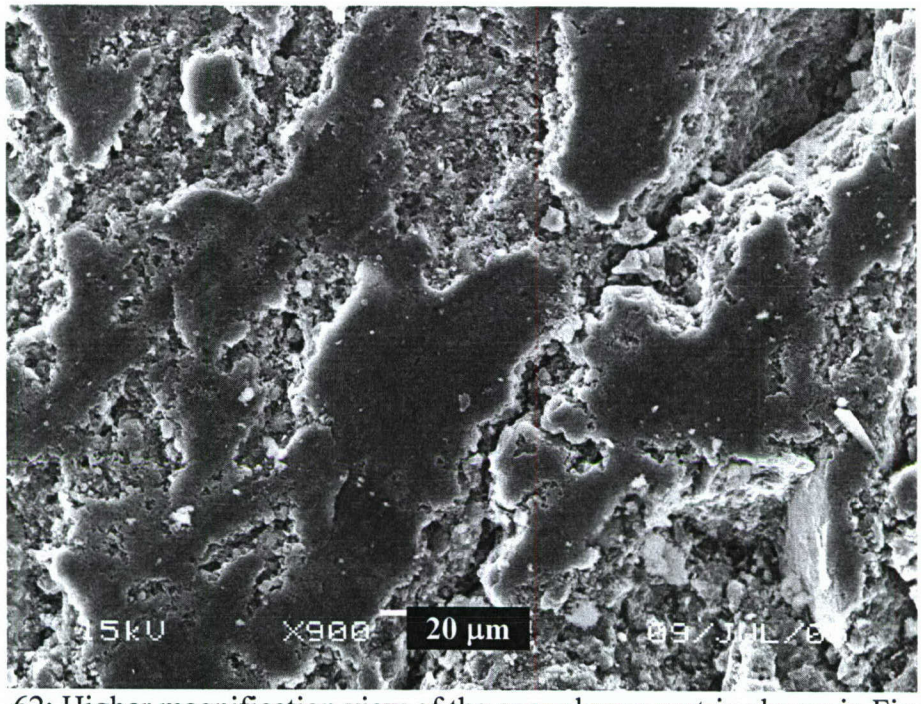

Fig. 62: Higher magnification view of the geopolymer matrix shown in Fig. 60.

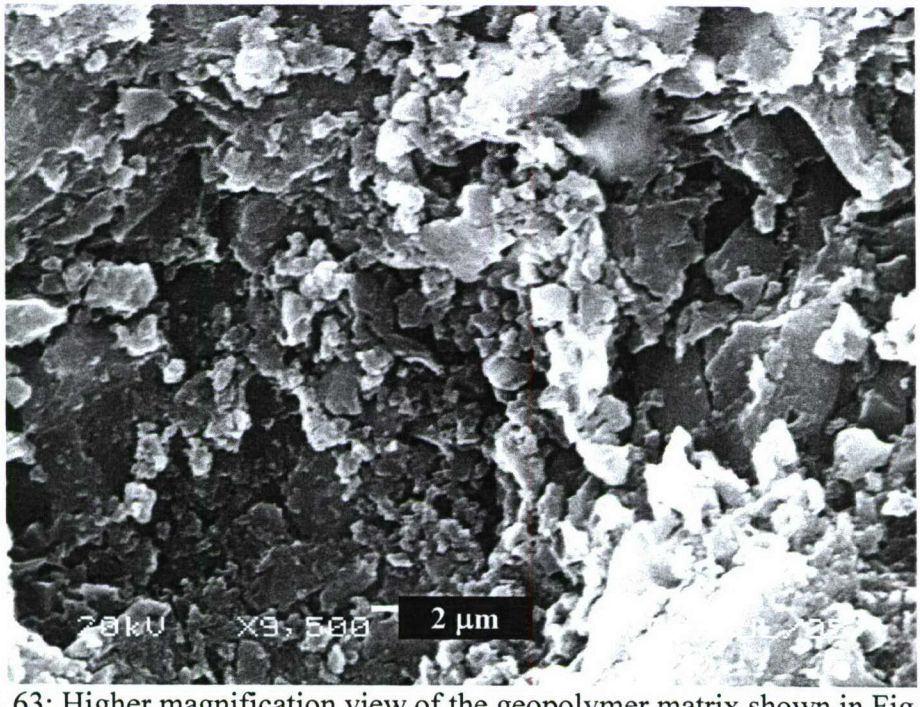

Fig. 63: Higher magnification view of the geopolymer matrix shown in Fig. 60.

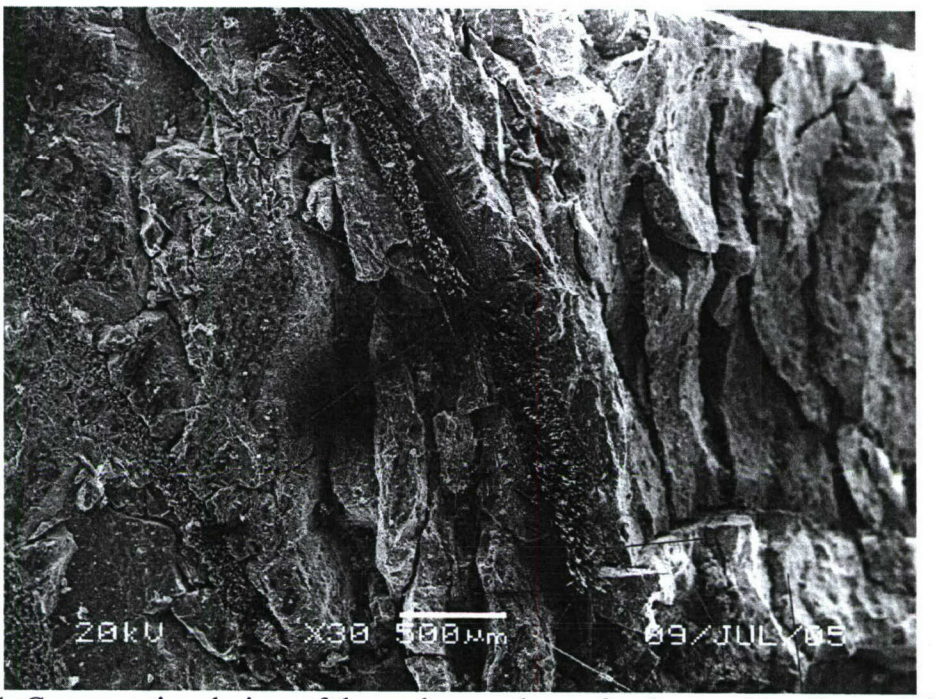

Fig. 64: Cross sectional view of the undamaged area for the graphite-fiber reinforced geopolymer pressure cured mold reinforced with 15 vol% SiC. Significant cracking can be observed in the pour region (right side of the micrograph).

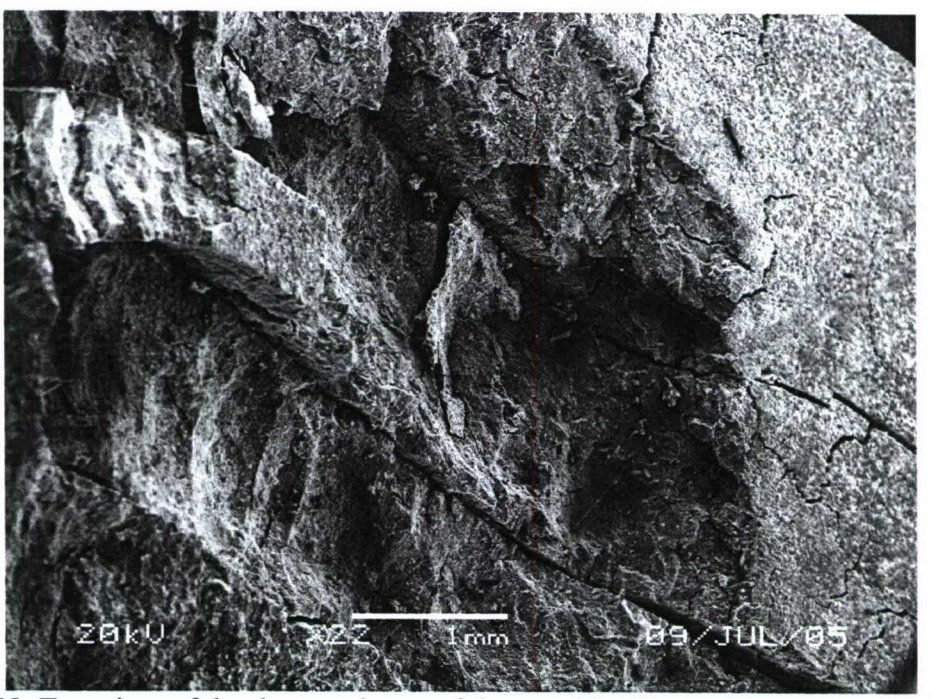

Fig. 65: Top view of the damaged area of the graphite-fiber reinforced geopolymer pressure cured mold reinforced with 15 vol% SiC.

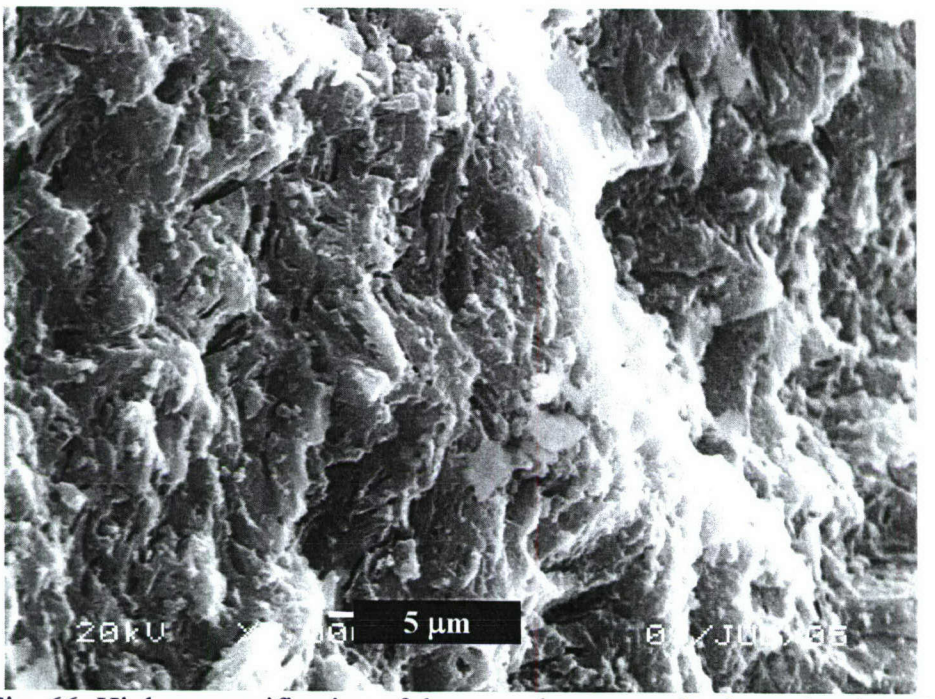

Fig. 66: Higher magnification of the geopolymer matrix shown in Fig. 65.

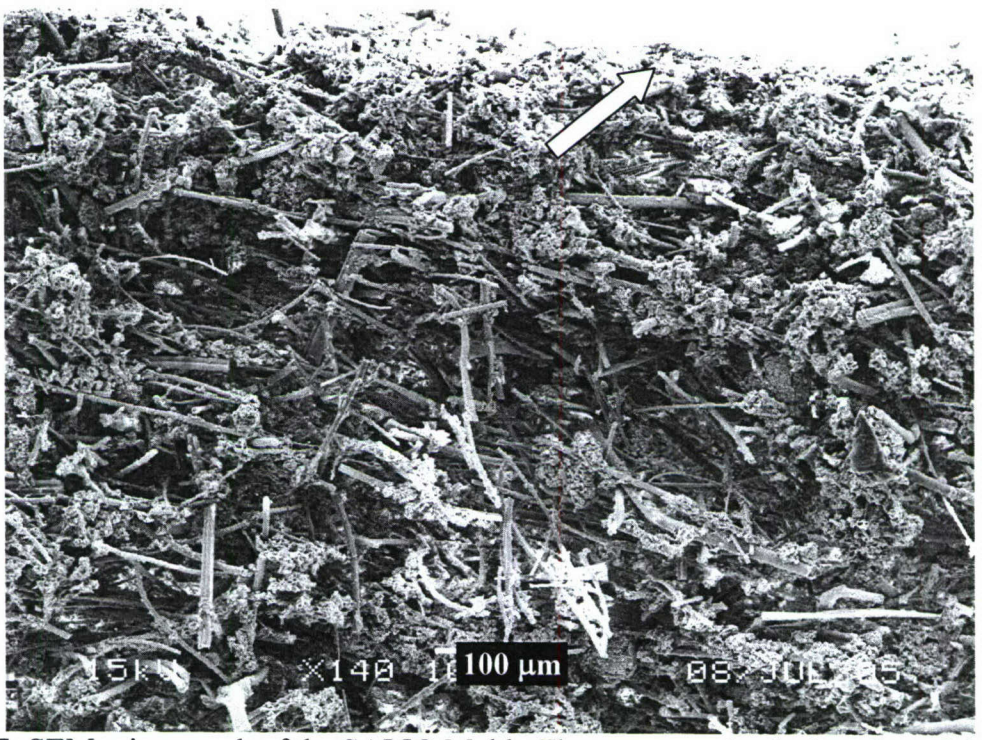

Fig. 67: SEM micrograph of the SALI® Mold. The arrow marks the location of the pour region.

Discussion

It has already been demonstrated that geopolymer composites reinforced with fibrous weaves have a work of fracture three orders of magnitude greater than the constituent geopolymer alone.[2] The combination of graphite-fiber reinforcement with the intrinsic porosity ~ 40% and low modulus (~ 2 GPa) of geopolymers resulted in a composite with exceptional thermal shock capability. After testing, representatives of CMMA expressed interest in large-scale durability testing of the geopolymer molds.

On the macro level it appeared that the more conductive fillers, SiC and molybdenum cooled faster than the Al_2O_3 fillers, but SEM results show essentially no microstructural difference between the filler types. The geopolymer matrix is formed by the dissolution of aluminosilicates; it was expected that the sub-micron Al_2O_3 may also be integrated into the geopolymer matrix, dissolving in the caustic alkali-silicate activating solution. The dissolution of the Al_2O_3 filler would explain why the filler was not visible in the SEM. Both the molybdenum and SiC fillers were also not observed under SEM. It is unclear if the molybdenum and SiC fillers were weakly bound to the geopolymer matrix and were pulled out when the samples were sectioned or if these fillers and the Al_2O_3 fillers were sufficiently coated with geopolymer and small enough to avoid being noticed under the SEM. In either event, if SiC or molybdenum fillers oxidize and integrate into the geopolymer matrix under repeated castings, they would result in a greatly reduced melting point of the final ceramic compound.

In the fabrication of polymer matrix composites, typical resin systems have viscosities between 1 – 10 cP. Although not quantitatively determined, the geopolymer slurries used in this study had viscosities approximately 4 – 5 orders of magnitude higher. As a result, the degree of infiltration of the geopolymer matrices between individual carbon fibers is extremely limited. The application of pressure, however, did lead to better infiltration of the geopolymer into the graphite fibers as shown in Fig. 45 and Fig. 60 and a denser matrix.

Leucite based glass-ceramics are known to have relatively high coefficients of thermal expansion.[3, 4] Prior to testing, there was a concern that geopolymers, having a composition similar to leucite may also have a very high coefficient of the thermal expansion ($> 10^{-5}/^{o}C$ which could lead to failure under thermal shock. Testing revealed, however, that this concern was unwarranted. The formation of needle-like crystallites (presumably leucite) was observed in areas near the pouring zone but only on the plate-shaped molds which were allowed to air cool after pouring of the Fe_2Si. The morphology of the crystallites, is similar to dendrite sheaves or spherulites found in glass-ceramics [3]. The crystallization of ceramics from a glass is a kinetically controlled event. In the case of the pressure cured molds which were water quenched, there was insufficient time for crystallization to occur. The melt point of $K_2O \bullet Al_2O_3 \bullet 4\ SiO_2$ is 1698°C, less than 300°C higher than the pour temperature of the Fe_2Si (1428°C). Since geopolymer is essentially as amorphous material, it must posses a glass transition point, T_g. The signs of melting of the geopolymer matrix (Fig. 21, Fig. 31, and Fig. 41) are likely the result of operating above T_g (typically two-thirds of T_{melt}) which would resulting in soften and viscous flow of the geopolymer matrix.

Despite being mechanically weak, the SALI® mold also made a thermally shock resistant mold. The microstructure is a porous Al_2O_3 foam reinforced with 150 – 200 μm long chopped Al_2O_3 fibers. Due to this microstructure, crack running was minimal and thermal shock properties were maximized. The performance of the SALI® suggests that a high volume fraction of chopped graphite-fibers may be sufficient or even preferable to reinforcing geopolymer molds with graphite-fiber weaves.

The shape of the pour zone was the strongest factor in ejection of Fe_2Si. The wider, shallower, pour zone of the plate-shaped molds allowed for easy ejection, while the solidified Fe_2Si could not eject from crucibles. The pour zone of future molds will imitate the low depth-to-diameter of the plate-shaped molds.

Conclusions

Graphite fiber-reinforced geopolymers are have exceptional thermal shock resistance and are viable candidates as casting molds for molten Fe_2Si. When the Fe_2Si was allowed to solidify by air cooling, needle-like crystals (presumably leucite) were found in areas close to the pour zone. None of the filler phases (Al_2O_3, SiC, and molybdenum) were distinguishable from the geopolymer matrix. There appeared to be minimal infiltration between the individual carbon fibers in plate-shaped geopolymer molds. Pressure cured molds were significantly denser than the other geopolymer molds and had a greater degree of geopolymer infiltration of between individual carbon fibers. Solidified Fe_2Si could not be ejected from the crucible-shaped molds and detrimental cracking was present on the outside of the crucibles following testing. For all of the tested geopolymer molds', cracking of the geopolymer matrix was observed near the pour zone. SALI® fibrous ceramic insulation also performed well as a casting mold for Fe_2Si but may lack the mechanically durability for repeated castings. Concerns regarding rapid spalling of the geopolymer matrix during thermal shock testing and the success of the SALI® - based mold lead to the development of a chopped-fiber based geopolymer composite.

References

[1]R. W. Hertzberg, *Deformation and Fracture Mechanics of Engineering Materials, 4th ed.* , Edited, John Wiley and Sons Inc. , New York, NY, 1996.

[2]W. M. Kriven, J. Bell and M. Gordon, "Microstructure and Microchemistry of Fully-Reacted Geopolymers and Geopolymer Matrix Composites"; pp. 227-250 in Ceramic Transactions, Vol. 153, *Better Ceramics*. Edited by J. Green, American Ceramic Society, Westerville, OH, 2003.

[3]W. Höland and G. Beall, *Glass-Ceramic Technology*, Edited, The American Ceramic Society, Westerville, OH, 2002.

[4]R. L. Bedard, R. W. Broach and E. M. Flanigen, "Leucite-pollucite glass ceramics: A new family of refractory materials with adjustable thermal-expansion"; pp. 581-587 in Materials Research Society Symposium Proceedings, Vol. 271, *Better Ceramics Through Chemistry V* Edited by M. J. Hampden–Smith, W. G. Klemperer and C. J. Brinker, 1992.

Section C - Chopped Fiber-Reinforced Composites

Introduction

Despite the use of external pressure (21.5 – 43 MPa) during the fabrication of graphite-weave reinforced geopolymer molds (Section B), infiltration between individual graphite fibers with geopolymer paste was severely limited. The poor degree of infiltration led to severe spalling of the geopolymer matrix after thermal shock testing. SEM analysis indicated that approximately ≥ 600 μm of composite material was damaged after one exposure to molten Fe_2Si (~ 1428°C). It was expected that repeated thermal shocking of graphite-weave reinforced geopolymer composites would rapidly result in failure. Based on the thermal shock testing of a commercially available aluminosilicate foam reinforced with chopped oxide fibers (SALI®, Zircar Ceramics, Florida, NY), it was decided that the thermal shock resistance and mechanical integrity of the geopolymer composites could be improved by replacing continuous weaves of fibers with chopped fibers.

The substitution of continuous fibers with chopped fibers could also have led to added processing versatility. Currently, sheet-molding compounds are compromised of randomly orientated fiber reinforcements in an organic pre-preg resin that can be shaped (under pressure) to conform to 2-dimensional dies. An uncured geopolymer-based composite material, however, could act as an inorganic pre-preg material suitable for shaping and subsequent high-temperature use. In principle, reinforced geopolymer pastes could be processed at a commercial laboratory, then refrigerated to prevent premature curing and shipped to an end-user to mold and cure into shape.

Experimental Procedure

Geopolymer composites made with varying water contents, fiber fractions and curing temperatures were prepared following the given process flow diagram (Figure 1). Alkali-silicate solutions were prepared by dissolving Cab-O-Sil fumed silica (Cabot Corp.) into solutions of potassium hydroxide and deionized water. Alkali-silicate solutions were refrigeration prior to mixing with metakaolin to prevent premature curing of the geopolymer composites during mixing. MetaMax® metakaolin powder (Engelhard

Corporation, Iselin, NJ) was mixed with the alkali-silicate solutions using a dispersion mixer to form geopolymers with molar ratios of K_2O - Al_2O_3 – 4 SiO_2. It was assumed that the metakaolin had a stoichiometric composition of Al_2O_3 – 2 SiO_2. The geopolymer paste was then mixed with 0.25 inch chopped graphite fibers (Zoltek Corp., St Louis) using a Hobart paddle mixer. The resulting dough was homogenized using a Ross 3-roll mixer (Charles Ross & Son Company, St. Charles, IL) and pressed into panels between Mylar® sheets. The pressure applied to the geopolymer panel was dependent on the viscosity of the geopolymer dough but was estimated to be approximately 1.5 MPa.

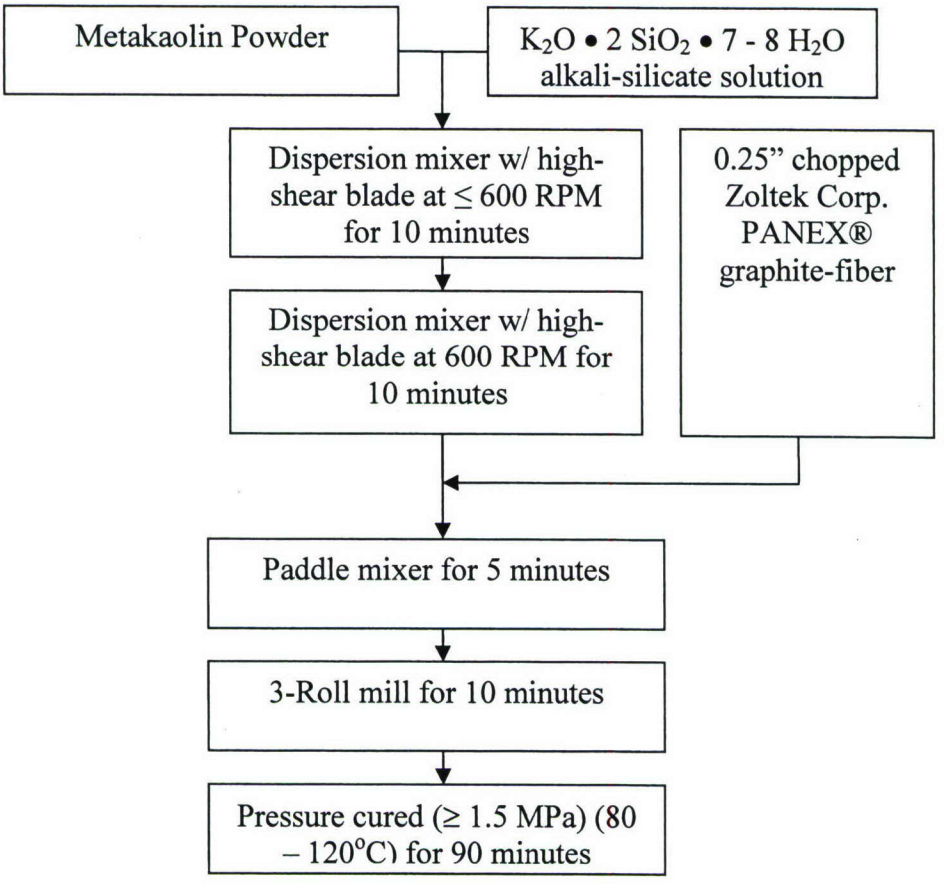

Figure 1: Process flow diagram for chopped graphite-fiber reinforced geopolymer composite

The maximum fiber chopped fiber content was 25 w%, however the viscosity was generally unsuitable for proper mixing. A fiber content of 20 – 25 w% yielded desirable rheological characteristics. Composite materials were also machined, and were cut into simple geometric shapes (e.g. discs, rectangles). Machined samples of the chopped fiber reinforced composites ($K_2O \bullet Al_2O_3 \bullet 4\ SiO_2 \bullet 7\ H_2O$, pressed at 120°C, 25 w% fiber) were heated to 1100°C for approximately 25 hours under vacuum in an effort to crystallize the geopolymer matrix into a glass-ceramic. Sections of the heated and unheated geopolymer composites were sputter-coated with a gold-palladium alloy and examined with a JEOL 6060LV scanning electron microscopy (SEM) (JEOL USA, Inc. Peabody, MA).

Results

Pressed geopolymer composites were smooth; no pores were visible to the naked eye (Fig.2). SEM analysis of the composites, however, showed poor fiber dispersion and substantial porosity near the fiber-matrix interface Figure 3 - Figure 4. Thermally treated samples remained intact; no macro-cracks were visible. The mechanical strength of the thermally treated composite was extremely low, however. A test coupon was accidentally broken before mechanical testing could be performed. Analysis by the thermally treated samples by SEM showed a heavily cracked microstructure, consisting of irregularly shaped "islands" of matrix bridged by graphite fibers (Figure 5 and Figure 6).

Figure 2: Photograph of 20 w% chopped graphite-fiber reinforced geopolymer composite plate.

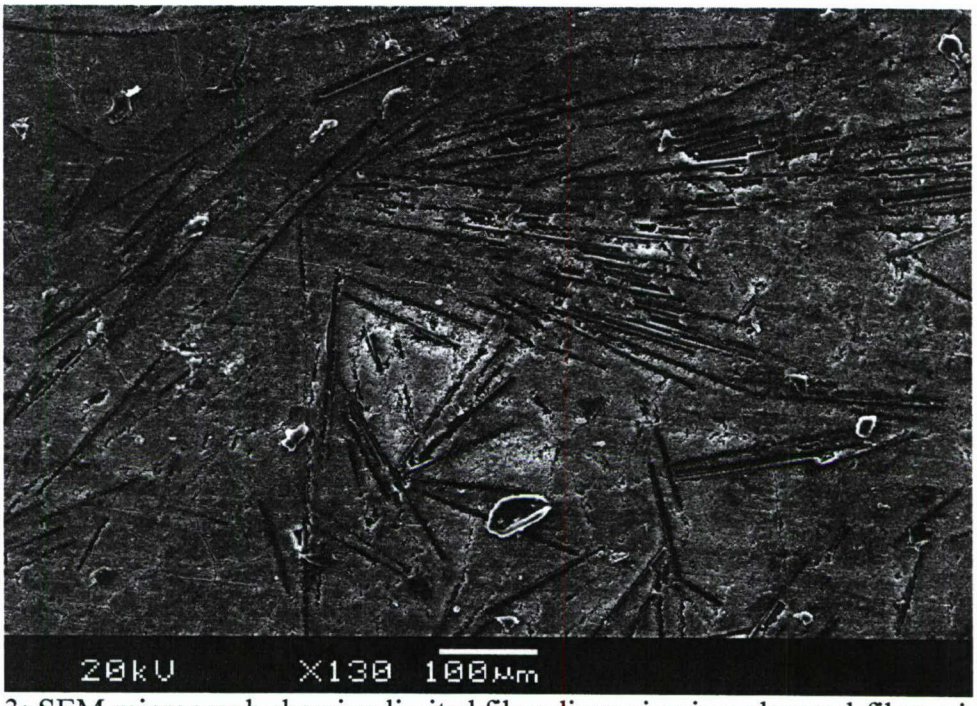

Figure 3: SEM micrograph showing limited fiber dispersion in a chopped-fiber reinforced geopolymer composite.

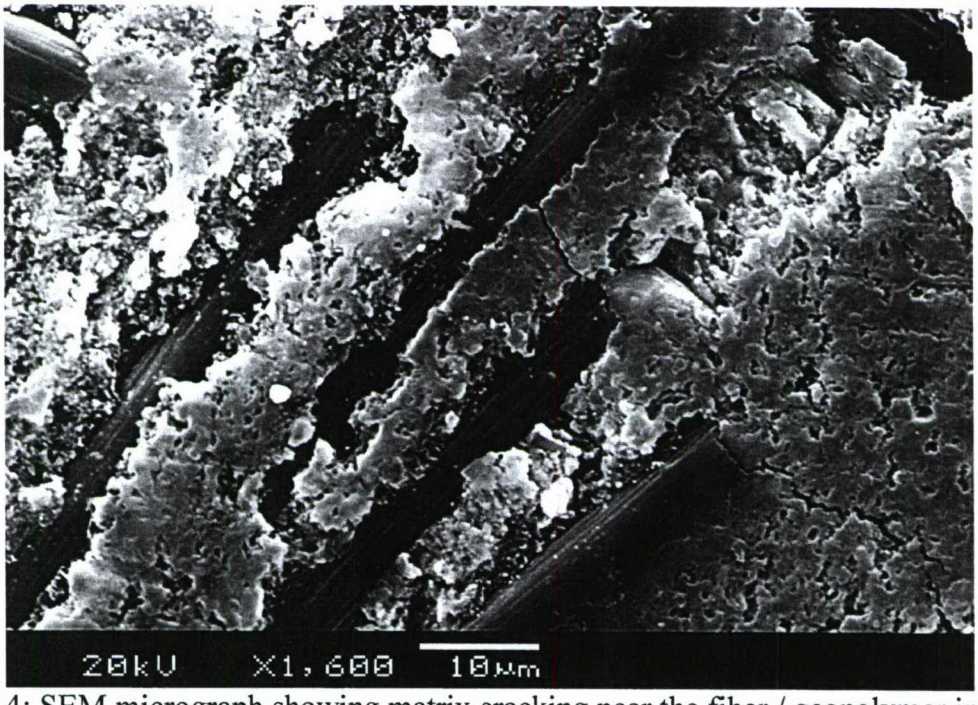

Figure 4: SEM micrograph showing matrix cracking near the fiber / geopolymer interface.

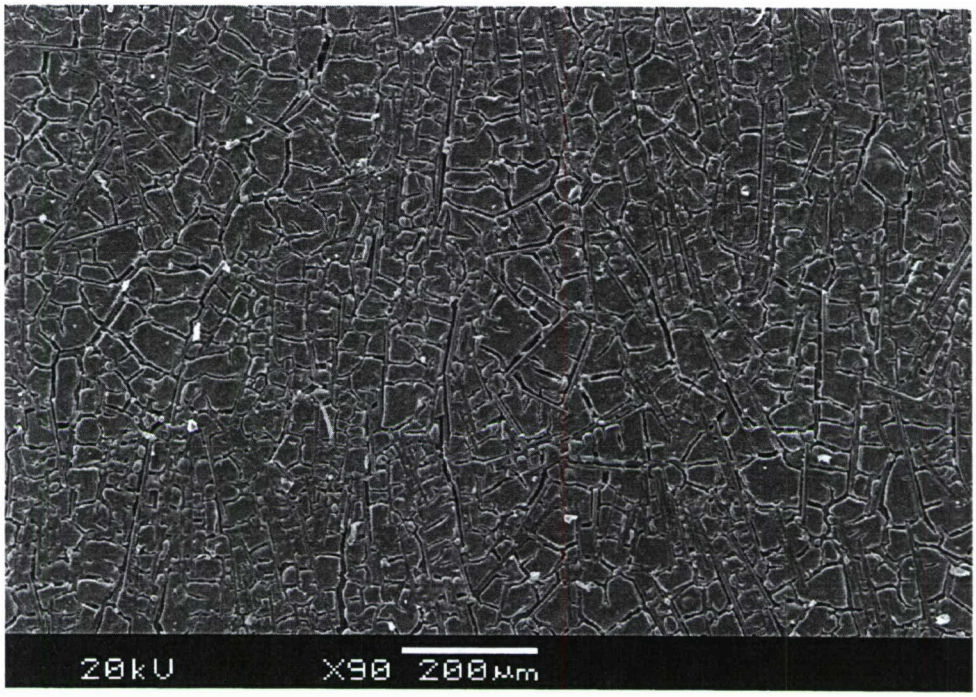

Figure 5: SEM micrograph showing matrix cracking of graphite-fiber reinforced thermally treated potassium-based geopolymer

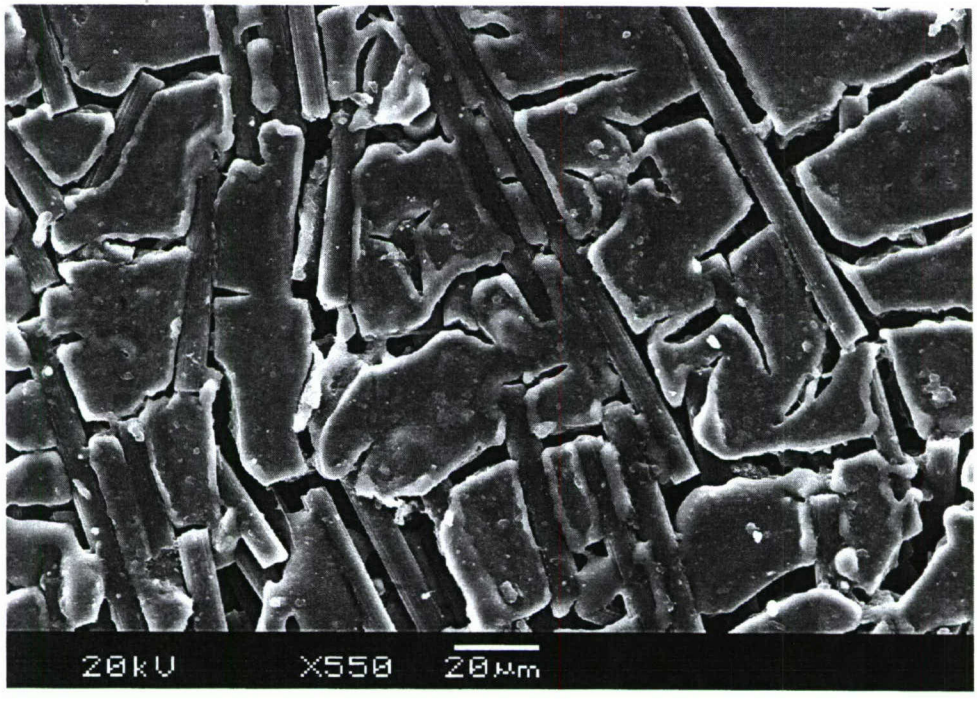

Figure 6: SEM micrograph showing matrix cracking of graphite-fiber reinforced thermally treated potassium-based geopolymer.

Discussion

Chopped fiber-reinforced composites were successfully produced using the described method. Although the lowest achievable alkali-to-water ratio was seven (K_2O: 7 H_2O) a higher alkali to water ratio (7.61 - 8.00) is preferred. (Commercially available KOH solutions are limited to a maximum concentration of 45 w%, K_2O:7.61 H_2O). Thermally treatment of the resulting composite material, however, resulted in failure of the resulting composite. Despite the limited amount of water present in the final composite, severe microcracking occurred. Macro cracking of the heated composite was avoided by fiber bridging.

The current approach (reducing water content and increasing the volume fraction of inert filler) could be extended further by substituting metakaolin with fly ash. Geopolymer cements made from fly ash require substantially less water than metakaolin-based geopolymers, due to the lower specific surface area of fly ash particles [1, 2]. Unlike metakaolin, only the surfaces of fly ash particles react during geopolymerization. The interiors of fly ash particles act as inert fillers in geopolymers, improving resistance to cracking during heating. The drawback to substituting fly ash for metakaolin, however, is increased levels of chemical impurities. Additionally, the large size of fly ash particles (dia $\approx$ 45 μm) would result in large chemical heterogeneities. After being mixed with an alkali-activating solution, the core of each fly ash particle would be alkali-poor, while the reacted surfaces of fly ash particles would be alkali-rich. As a result, geopolymers produced from fly ash would form multiple (and perhaps undesirable) ceramic phases at high temperatures.

Conclusion

Due to the high amount of water required to properly mix metakaolin-based geopolymers, it is highly unlikely that any metakaolin-based geopolymer will be able to survive thermal conversion into a bulk ceramic. The use of fly ash particles may be a simple, cheap and viable alternative to producing geopolymer materials that can be subsequently converted into useful ceramic bodies.

References

[1]A. Fernandez-Jimenez and A. Palomo, "Characterization of fly ashes. Potential reactivity as alkaline cements," *Fuel*, **82**[18] 2259-2265 (2003).

[2]J. G. S. van Jaarsveld, J. S. J. van Deventer and G. C. Lukey, "The characterization of source materials in fly ash-based geopolymers," *Materials Letters*, **57**[7] 1272-1280 (2003).

Section D - Thermal Conversion of Bulk Geopolymers

Introduction

Geopolymers can be produced over a wide range of compositions, centered on the molar ratios of $M_2O - Al_2O_3 - SiO_2 - H_2O$ (where M is an alkali metal cation, typically Na^+, or K^+).[1-4] Most important to this study is the geopolymer composition of $K_2O \bullet Al_2O_3 \bullet 4\ SiO_2 \bullet x\ H_2O$, where x = 7.5 – 10). Upon removal of water, the composition $K_2O \bullet Al_2O_3 \bullet 4\ SiO_2$ corresponds to the ceramic leucite, often used in glass ceramics for dental purposes.[5] The thermal conversion of amorphous geopolymer powder into a crystalline phase has been demonstrated in literature and is not a difficult technical challenge (i.e. simply heating the material to approximately 1000°C will induce crystallization). The conversion of a bulk geopolymer into a useful ceramic body is problematic, however, due to water loss, cracking and shrinkage. The amount of cracking and shrinkage can be minimized by the addition of a filler-phase or reducing the water content in the geopolymer. This work covers the thermal conversion of bulk potassium-based geopolymers into leucite and an investigation into the resulting microstructure of subsequent ceramic materials. Chemical homogeneity of the resulting ceramic microstructure was key goal in this study.

Experimental Procedures

SiO_2 reinforced sample

A concentrated solution of potassium hydroxide was mixed using deionized water and potassium hydroxide pellets (Fisher Scientific Inc., Pittsburgh, PA). It was assumed that 12.5 weight percent of each potassium hydroxide pellet was water. Cab-O-Sil EH-5® fumed silica (Cabot Corp., Wheaton, IL) was dissolved into the potassium hydroxide solution to form a potassium silicate solution with a molar ratio of $K_2O \bullet SiO_2 \bullet 7.5\ H_2O$. After complete dissolution of the fumed silica, the potassium silicate solution was a transparent yellow liquid. The aluminosilicate source used for forming the geopolymer came from metakaolin, derived from Hydrite PXN® kaolin (Imerys, Dry Branch, GA). The kaolin was converted into metakaolin by calcining at 700°C for one hour using a heating and cooling ramp rate of 5°C/min. Amorphous silica spheres, 500 nm in diameter (Fiber Optic Center Inc., New

Bedford, MA) were sieved through a 200 mesh sieve, in preparation for mixing. Using an ice bath, the potassium silicate solution, metakaolin, and SiO_2 spheres were mixed together in a dispersion mixer with a high-shear blade. The molar ratios of the final geopolymer were $K_2O \cdot Al_2O_3 \cdot 4\ SiO_2 \cdot 7.5\ H_2O$. The resulting paste was then applied to the surface of an untreated glass microscope slides as a thin (~ 1 mm thick) layer. The slides were placed onto a perforated stainless steel plate, suspended above water in a sealed plastic container and allowed to cure at 50°C for 50 days. It was assumed that the SiO_2 spheres would be incorporated into the geopolymer matrix upon heating to produce a chemically homogenous microstructure. After curing a sample was heated to 700°C for one hour at 0.5°C/min. The sample was intact after the initial heating to 700°C. The sample was then heated to 1400°C for one hour using a heating and cooling ramp rate of 5°C/min. After firing, the sample was still intact; however, several major cracks had developed on the sample surface. Some warping near the sample's edges was also observed.

Samples of the SiO_2 reinforced geopolymer were ground using a mortar and pestle. The powder was then heated to 900°, 1100° and 1400°C for one hour at 5°C/min. A section of the geopolymer, heated to 1400°C, was polished and sputter-coated with a gold-palladium alloy for scanning electron microscopy (SEM Model S-4700, Hitachi, Osaka, Japan). XRD patterns of the powdered geopolymer were taken using a step size of 0.02 at a rate of 0.5° 2θ/min at an operating voltage of 45 kV and 20 mA from 5° to 75° 2θ using Cu Kα radiation (Rigaku D/Max, Tokyo, Japan). Analysis of the XRD data was done with JADE PC software (Minerals Data Inc., Livermore, CA).

Powder pressed sample

MetaMax EF® metakaolin (Engelhard Corp., Iselin, NJ) was added to a potassium silicate solution pre-prepared with a molar ratio of $K_2O \cdot 2\ SiO_2 \cdot 10\ H_2O$ and mixed to form an geopolymer having a nominal molar ratio of $K_2O \cdot Al_2O_3 \cdot 4\ SiO_2 \cdot 10\ H_2O$. The geopolymer gel was then poured into an airtight plastic container and allowed to cure at 50°C for two days, followed by air drying at 50°C for two days. After drying, the geopolymer was ground and sieved through a 200 mesh sieve, to eliminate particles > 75 μm. Using poly-vinyl alcohol as a binder, 1.5 inch diameter pellets of the sieved powder were pressed at 500

psi (3.45 MPa). The pressed pellets were heated to 1200°C for ten hours at a heating and cooling rate of 5°C/min. One of the pellets was further annealed at 1400°C for five hours. The sintered pellets showed no signs of cracking. After heating, the pellets were prepared for either XRD or SEM analysis in a manner similar to the preparation of the SiO_2 sphere-reinforced samples. TEM preparation of the samples was done using standard ion milling preparation techniques. The samples were then carbon coated and examined by TEM at an operating voltage of 120 kV using a Phillips CM12 TEM (Phillips, Tokyo, Japan).

Results

SiO_2 reinforced sample

The geopolymer remained amorphous or semi-crystalline between room temperature and 900°C (Fig. 1). Above 900°C, however the geopolymer crystallized into single-phase, low temperature, tetragonal leucite ($KAlSi_2O_6$). Ceramic grains are visibly absent from the SEM micrographs of the heated and polished geopolymer sample and large spherical voids, on the order of 50 microns, covered the surface of the sample (Fig. 2).

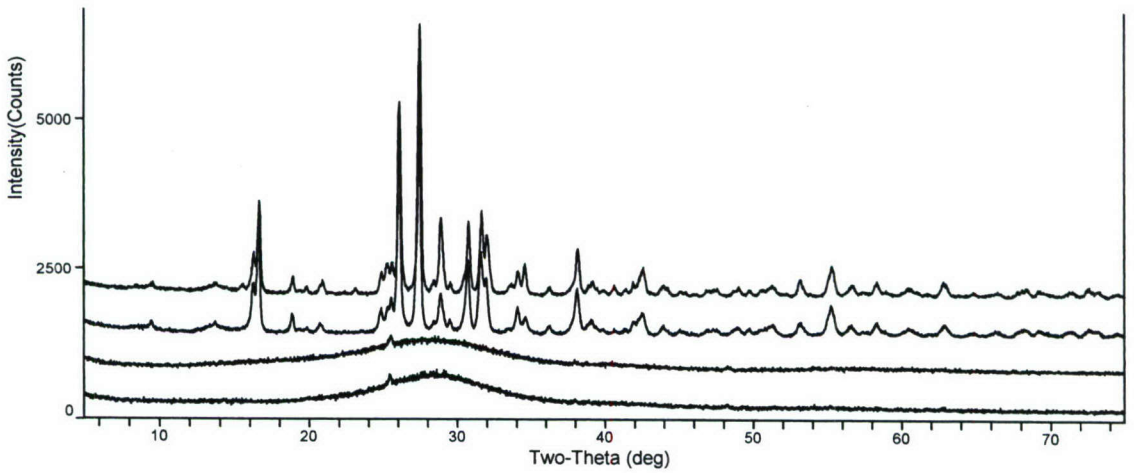

Fig. 1: Ex-situ XRD patterns of geopolymer with a composition of $K_2O \cdot Al_2O_3 \cdot 4\ SiO_2 \cdot 7.5\ H_2O$, incorporating amorphous 500 nm SiO_2 spheres after being heated to 25°C (bottom pattern), 900°C, 1100°C and 1400°C (top pattern).

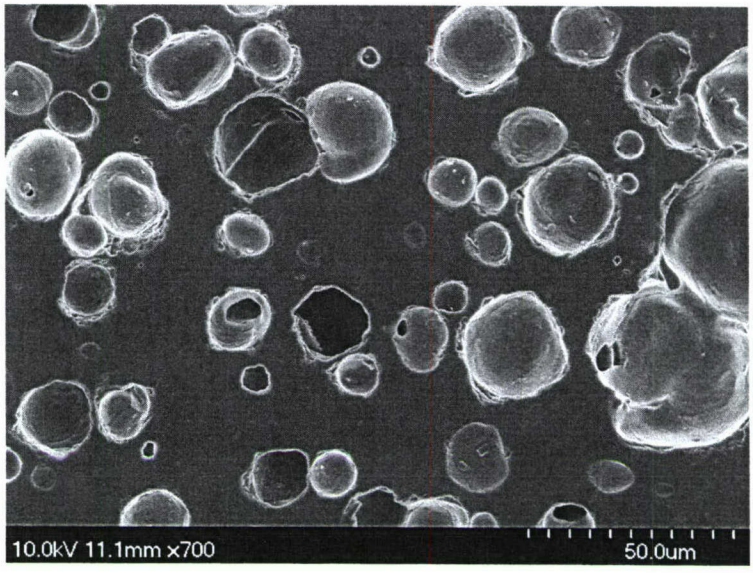

Fig. 2: SEM image of geopolymer with a composition 4 SiO_2 - 7.5 H_2O, incorporating amorphous 500 nm SiO_2 spheres after being heated 1400°C for one hour.

Powder Pressed Sample

The diffraction pattern of the geopolymer heated to 1200°C (Fig. 3) indicated that the geopolymer crystallized into leucite ($K_2O \bullet Al_2O_3 \bullet 4\ SiO_2$). As seen through large pores on the surface (Fig. 4), the internal microstructure of converted geopolymer consisted of fused agglomerates, approximately three microns in diameter (Fig. 5). SEM analysis, of the pressed powder sample, first heated to 1200°C/10hr and then further annealed at 1400°C/5h showed no distinct ceramic grains, although there was a suggestion of a facetted phase dispersed in a continuous glassy matrix phase (Fig. 3– Fig. 6).

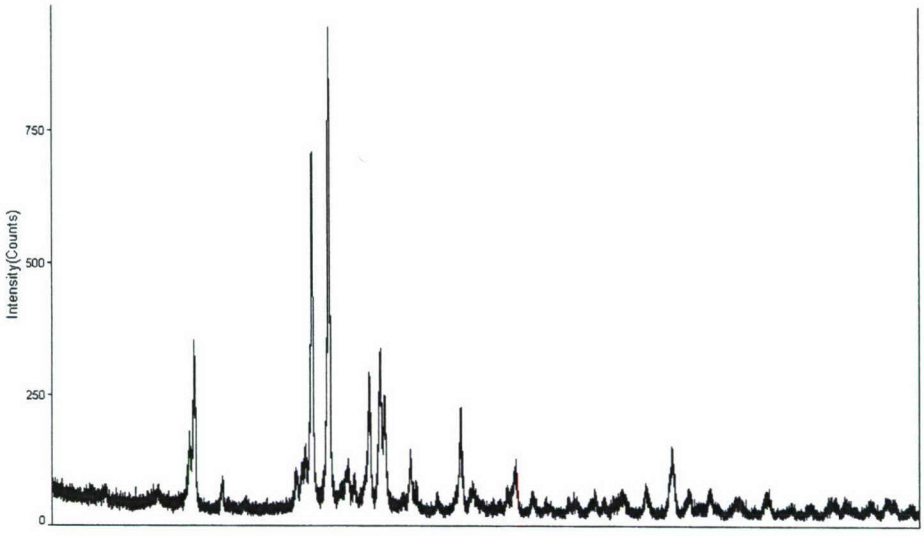

Fig. 3: Ex-situ XRD patterns of geopolymer with a composition of $K_2O \bullet Al_2O_3 \bullet 4\ SiO_2 \bullet 10\ H_2O$ after being heated to 1200°C/10h.

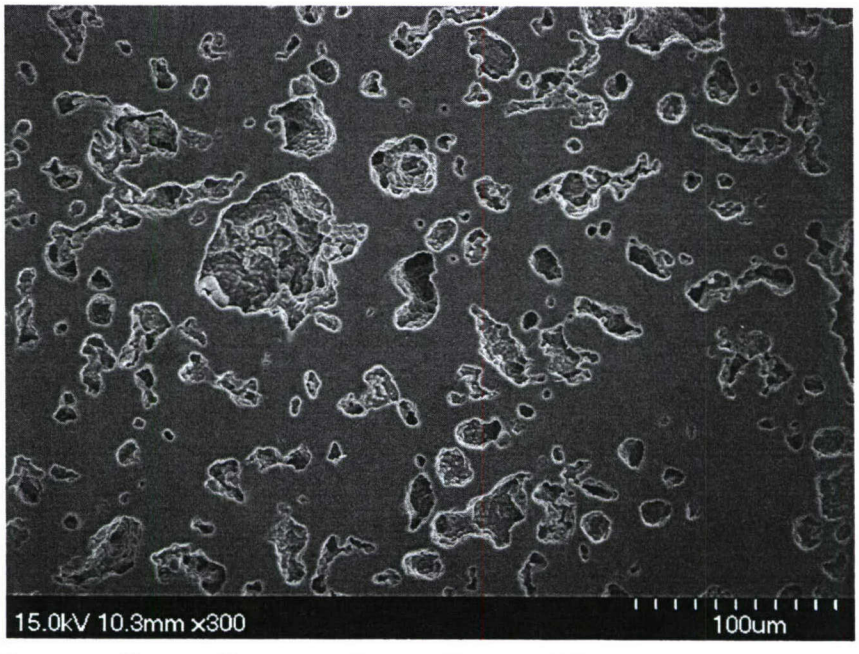

Fig. 4: SEM images of a powder-pressed geopolymer with a composition of $K_2O \bullet Al_2O_3 \bullet 4\ SiO_2 \bullet 10\ H_2O$ after being heated to 1200°C/10 h.

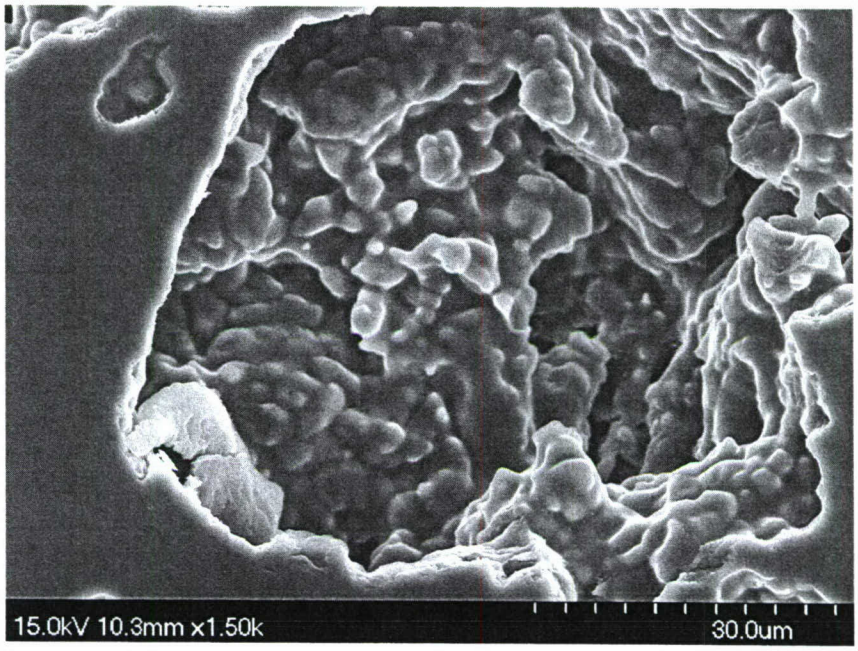

Fig. 5: SEM micrograph of geopolymer heated to 1200°C/12h viewed through a surface pore showing 3 μm agglomerates in the interior of the sample.

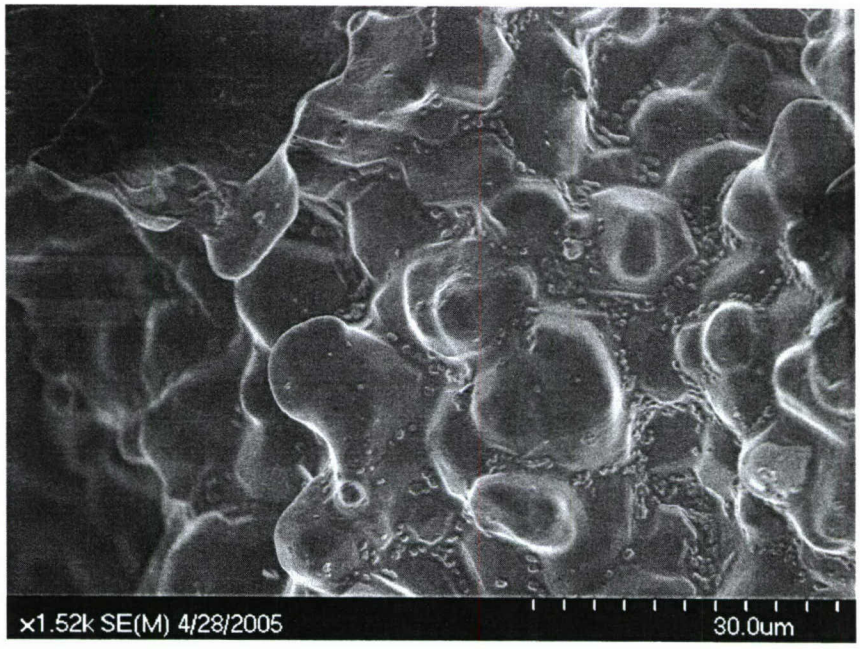

Fig. 6: Fracture surface SEM micrograph of geopolymer heated to 1200°C/12h and further annealed to 1400°C/5h sowing a facetted phase dispersed in the matrix.

TEM and SAD of the geopolymer sample hearted to 1200°C confirmed the presence of leucite crystals (Fig. 7). Micrographs of the continuous phase were taken, and are illustrated (Fig. 8 - Fig. 11). TEM and SAD micrographs indicated that the continuous matrix phase was amorphous, with possibly some incipient nanocrystals of leucite forming. The microstructure consisted of a lighter continuous matrix phase surrounding a few darker inclusions ~5 nm in diameter. Increased micrograph exposure times in SAD mode showed faint diffraction spots in addition to amorphous diffuse diffraction (Fig. 9).

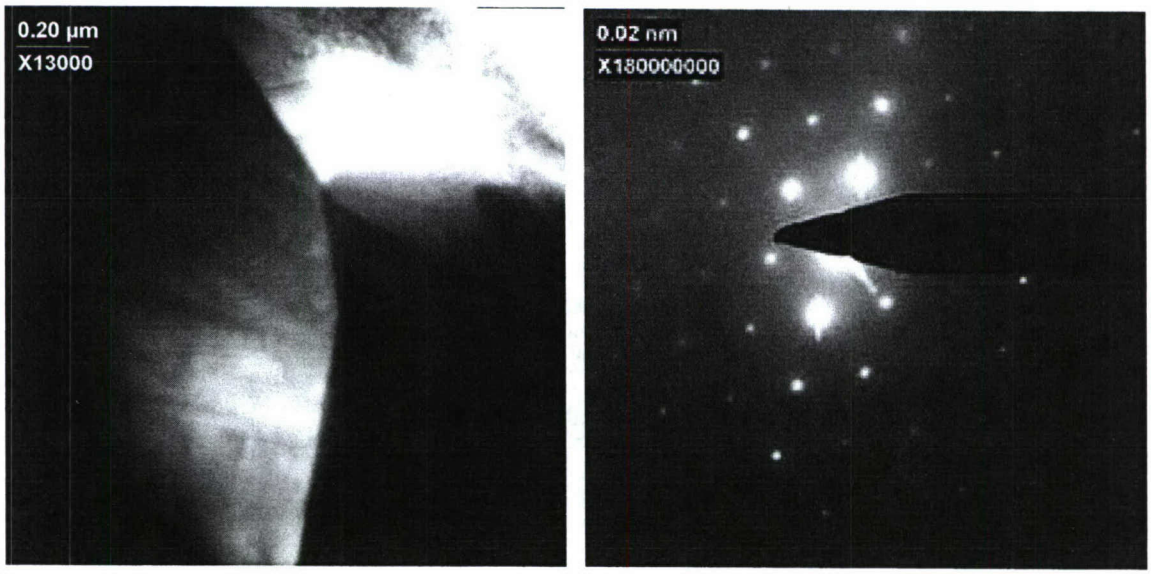

Fig. 7:: TEM micrographs of a geopolymer with a composition of $K_2O \cdot Al_2O_3 \cdot 4\ SiO_2 \cdot 10\ H_2O$ after being heated to 1200°C for one hour (left). Selected area diffraction (SAD) of the region (right).

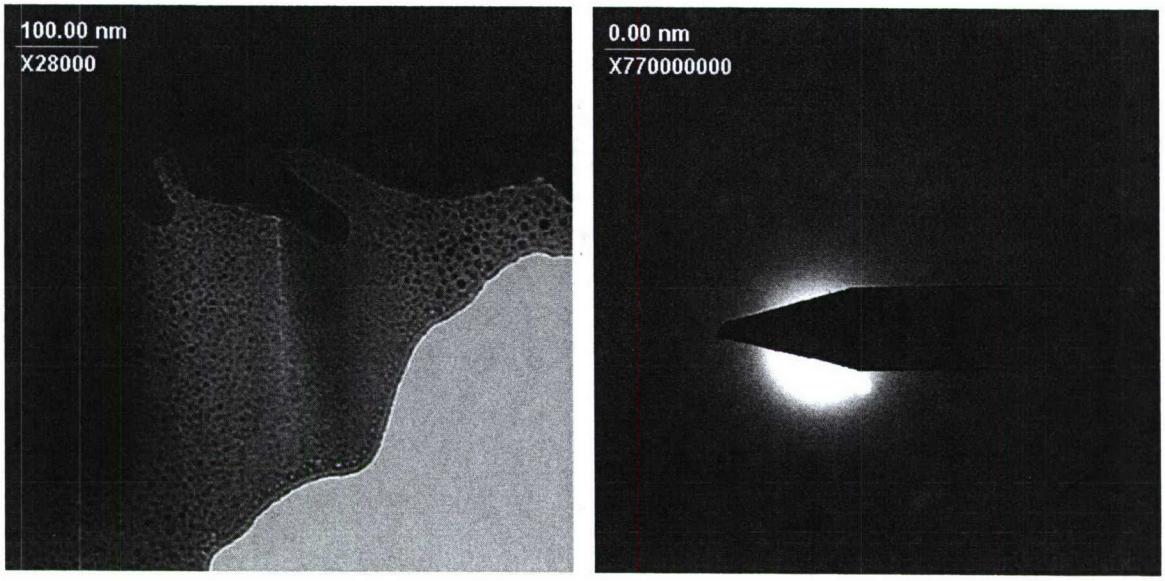

Fig. 8: Bright-Field TEM micrograph of geopolymer with a composition of $K_2O \bullet Al_2O_3 \bullet 4\ SiO_2 \bullet 10\ H_2O$ after being heated to 1200°C for one hour (left). Corresponding selected area diffraction (SAD) of the region (right).

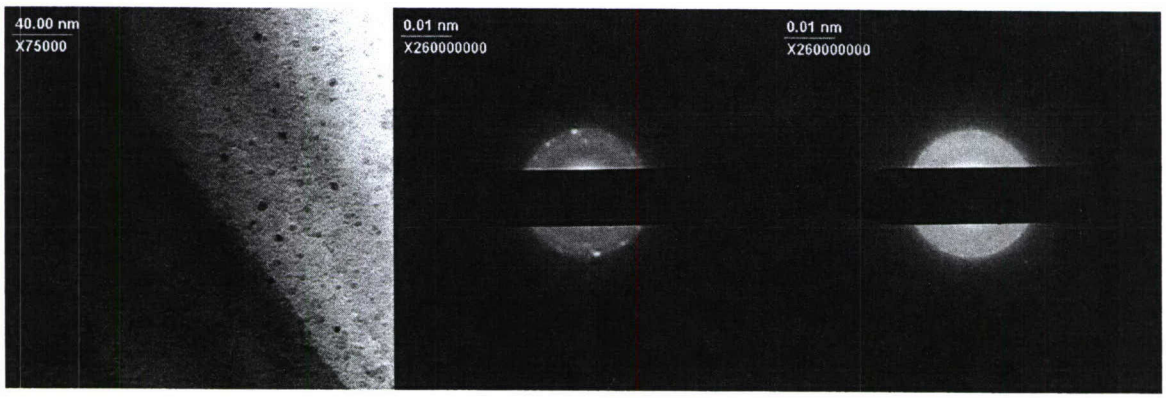

Fig. 9: Bright-Field TEM image of a geopolymer with a composition of $K_2O \bullet Al_2O_3 \bullet 4\ SiO_2 \bullet 10\ H_2O$ after being heated to 1200°C (left). Selected area diffraction of the region with one second exposure time (center), 30 second exposure time (right).

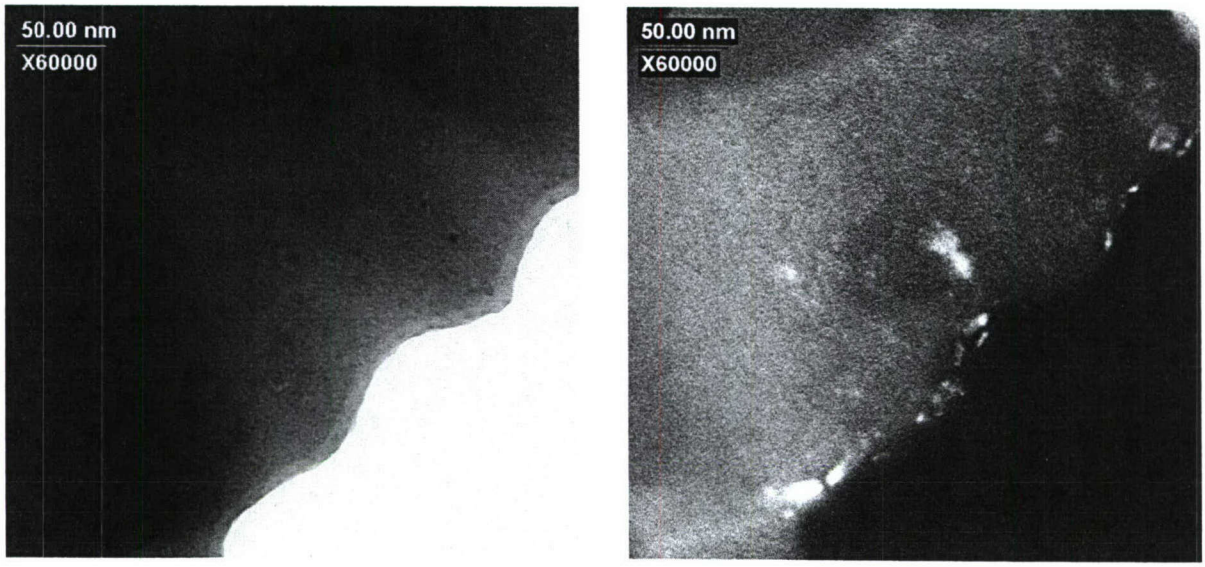

Fig. 10: TEM micrographs taken in bright field (BF) (left) and corresponding dark field (DF) (right) conditions, confirming the presence of incipient nanocrystallites, thought to be leucite.

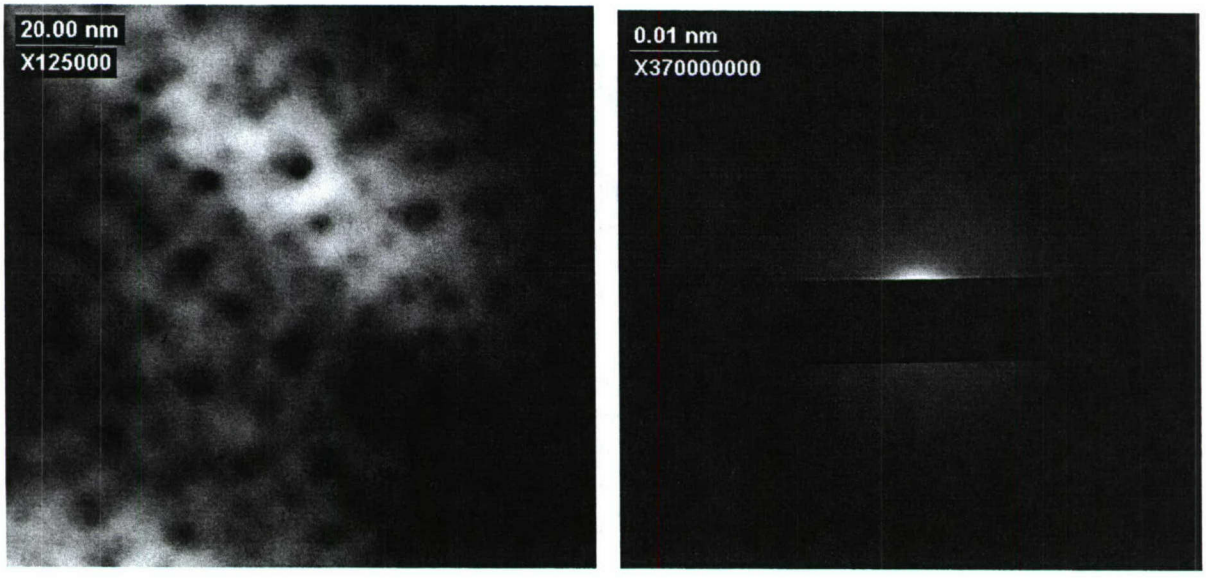

Fig. 11: TEM micrographs of a geopolymer with a composition of $K_2O \bullet Al_2O_3 \bullet 4\ SiO_2 \bullet 10\ H_2O$ after being heated to 1200°C for one hour (left). Selected area diffraction (SAD) of the region (right).

Discussion

SiO_2 reinforced sample

The added silica spheres were successfully incorporated into the geopolymer paste, such that upon heating the final geopolymer crystallized into leucite. The presence of spherical pores, two orders of magnitude larger than the added SiO_2 spheres, were the result air entrapped in the geopolymer paste. The lack of easily definable grains in the microstructure in conjunction with the XRD pattern of heated the geopolymers is an indication that geopolymers, which are amorphous materials, convert into glass-ceramics upon heating. Despite the low amount of water used to fabricate the geopolymer and the reinforcement with SiO_2 spheres, cracking of the geopolymer samples still occurred upon heating. Without significant alterations to the processing of geopolymers (e.g. pressure curing, further reduction of water, increasing the volume fraction of a second phase) it is unlikely that monolithic geopolymers can not be converted into ceramics without catastrophic cracking.

Powder pressed sample

As in the SiO_2 reinforced sample, no ceramic grains were visible on the surface of the sample. This is due to the surface being covered with an amorphous glass-like phase. The agglomerations in the interior of the sample are thought to be the crystalline leucite grains indicated by XRD, covered with an intergranular amorphous phase. This type of microstructure is reminiscent of glass-ceramics.

TEM and SAD of the continuous matrix phase (Fig. 8– Fig. 11) suggested that it was generally amorphous, with incipient nanocrystals of leucite forming. This structure is similar to the structure of glass ceramics with cellular membrane microstructures.[5] The lack of diffraction in Fig. 11, however, may indicate that the darker regions are pores, not crystallites. This hypothesis is supported by previous gas phase porosimetry results that indicated that the average pore radius of unheated geopolymers was approximately three nanometers.

The process of forming geopolymers can be utilized to hydro thermally synthesize amorphous glass-like phases at low temperatures, which can subsequently be crystallized into

leucite. Depending on the choice of alkali and the amount of silica present, the geopolymer processing route could be extended to forming amorphous precursors to nepheline ($NaAlSiO_4$), kalsilite ($KAlSiO_4$) and pollucite ($CsAlSi_2O_6$) at low temperatures.

Conclusions

Crystallization of potassium-based geopolymers into leucite ($K_2O \cdot Al_2O_3 \cdot 4\ SiO_2$) occurs between 900 and 1000°C. Crystallized geopolymers have microstructures similar to glass ceramics. TEM and SAD of the geopolymer heated to 1200°C indicate the presence of leucite grains and an amorphous, matrix phase of a geopolymer heated to 1200°C shows a two-phase microstructure, reminiscent of a spinodal decomposition product or a glass-ceramic. SAD of the amorphous phase of the leucite-based geopolymer showed diffuse scattering characteristic of amorphous phase, as well as some reflections due to incipient nanocrystals, as confirmed by TEM DF imaging. Powders derived from geopolymers can be used in traditional ceramic processing techniques to produce crack-free ceramics.

References

[1]V. F. F. Barbosa and K. J. D. MacKenzie, "Thermal behaviour of inorganic geopolymers and composites derived from sodium polysialate," *Materials Research Bulletin*, **38**[2] 319-331 (2003).

[2]V. F. F. Barbosa and K. J. D. MacKenzie, "Synthesis and thermal behaviour of potassium sialate geopolymers," *Materials Letters*, **57**[9-10] 1477-1482 (2003).

[3]V. F. F. Barbosa, K. J. D. MacKenzie and C. Thaumaturgo, "Synthesis and characterization of materials based on inorganic polymers of alumina and silica: sodium polysialate polymers," *International Journal of Inorganic Materials*, **2**[4] 309-317 (2000).

[4]J. Davidovits, "Geopolymers - inorganic polymeric new materials," *Journal of Thermal Analysis*, **37**[8] 1633-1656 (1991).

[5]W. Höland and G. Beall, *Glass-Ceramic Technology*, Edited, The American Ceramic Society, Westerville, OH, 2002.

Section E – Thermal Conversion of Geopolymer Foams

Introduction

Pressure gradients develop within geopolymers during drying that give rise to capillary forces. These forces are sufficient to induce both microscopic and macroscopic cracking in geopolymers. One method of preventing cracking during drying and thermal conversion of a geopolymer into a glass-ceramic is to limit the diffusion distance that water must travel from the interior of the geopolymer to the solid/vapor interface. By engineering porosity into a geopolymer (i.e. making a geopolymer foam), the diffusion distance can be sufficiently limited, such that the geopolymers will not fail upon drying and thermal conversion. Figure 1 is a cartoon showing, d_{min}, the minimum distance that entrapped water must travel from the interior of the geopolymer to the solid/vapor interface for both a solid (A) and foamed material (B).

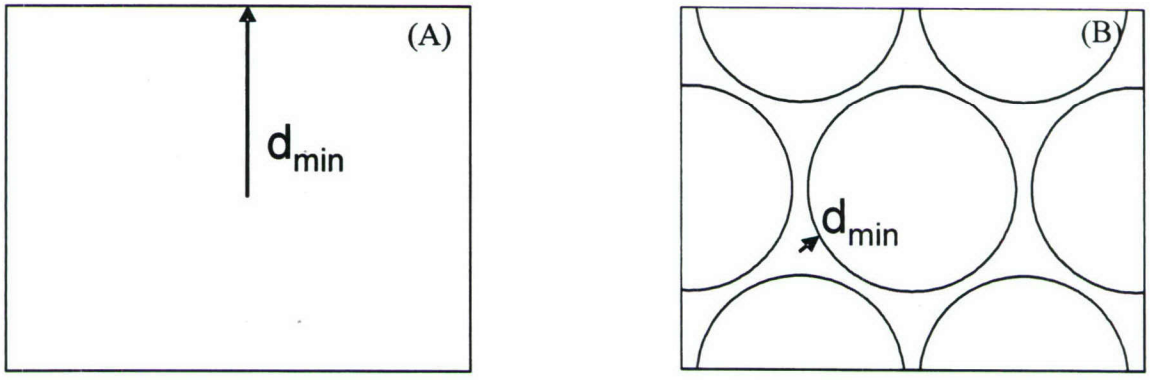

Figure 1: Cartoon showing the minimum distance that entrapped water must diffuse to leave the interior of the geopolymer for a solid sample (A), foam (B).

Conventionally, porous or aerated cements are produced by the addition of zinc or aluminum to a cement paste, which react to evolve hydrogen gas. Careful control of the curing conditions is required to create desirable pore morphologies. Porous cements can also be produced by generating foam separately from the cement paste using foaming agents in a pressurized vessel.[1] The pre-made foam is then mixed with the cement paste and cast into shape.

In principle, geopolymer foam could also be produced by the addition of hydrogen peroxide (H_2O_2) to a geopolymer paste and allowing the H_2O_2 to decompose in a sealed vessel. As the H_2O_2 decomposes into water and oxygen gas, unfilled volume within the container and air entrapped within the geopolymer paste will become pressurized. The pressure within the pores will stabilize the pores during the curing of the geopolymer paste. The size of the resulting pores will be inversely proportional to the pressure following the Young-Laplace Equation (Equation 1).

Equation 1 $\Delta P = 2 \gamma / \text{radius}$

It assumed that the surface tension of the geopolymer paste, aqueous slurry, is on the order of 7.29×10^{-2} J/m^2, the surface tension of water. By adjusting the pressure and free volume within the container, both the pore size and total porosity within the geopolymer foam could be controlled.

Another approach to creating geopolymer foams had been incorporating wax spheres in geopolymers. The wax spheres were removed from the geopolymers by boiling the geopolymer in water. The resulting geopolymer foam was then thermally converted into a glass ceramic (Figure 2).

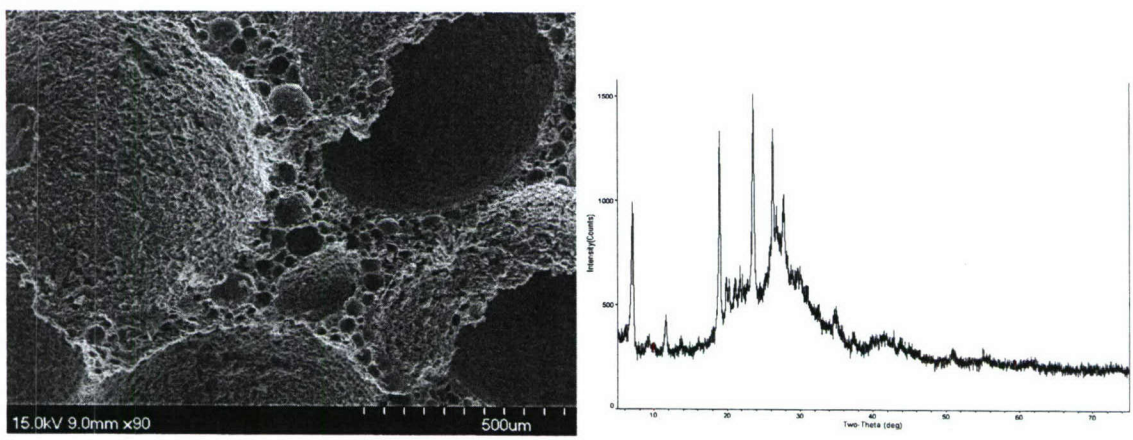

Figure 2: SEM micrograph of a potassium-based geopolymer foam after being heated to 1000°C for 18 hours (left) and the accompanying X-ray diffraction plot (right) indicating partial crystallinity. Wax spheres had been embedded in the initial geopolymer and boiled out prior to heating to 1000°C.

Experimental Procedures

Internal Pressure

Alkali-silicate solutions were prepared by dissolving Cab-O-Sil fumed silica (Cabot Corp.) into solutions of potassium hydroxide and deionized water. MetaMax® metakaolin powder (Engelhard Corporation, Iselin, NJ) was mixed with the alkali-silicate solutions using a dispersion mixer to form geopolymers with molar ratios of $K_2O \bullet Al_2O_3 \bullet 4\ SiO_2$. It was assumed that the metakaolin had a stoichiometric composition of $Al_2O_3 \bullet 2\ SiO_2$. Hydrogen peroxide solution (30 w %) was added to geopolymer slurry during mixing. The slurry was poured into a steel tube, sealed and cured at 50°C for three days. The free volume in the cylinder was approximately 1% of the total volume of the cylinder. The pressure resulting from the decomposition of the H_2O_2 within the steel container was estimated to be 3.5 MPa. The resulting geopolymer filled the steel container and bonded strongly to the container walls. The force required to extract the geopolymer from the steel vessel broke the geopolymer into fragments. Analysis of the fragments was performed using a JEOL 6060LV scanning electron microscope (SEM).

A second experiment replaced the steel tube with 4-inch long, 1-inch I.D. cylinders of polypropylene (McMaster-Carr, Chicago, IL). The interior surfaces of the tubes were machined to produce a smooth to facilitate the extraction of the geopolymer from the containers. The free volume within polypropylene containers was varied from 15 – 50 vol% and the samples were cured at 50°C for 72 hours. The internal pressure caused by decomposition of the H_2O_2 within the vessels was limited to 0.5 MPa due to the lower strength of the polypropylene (compared to steel) containers. Similar to results with the steel vessel, the geopolymer sample could not be extracted from the vessel without breaking the geopolymer into small fragments.

External Pressure

Geopolymer paste was loaded with approximately 55 w% aluminum powder. The composite paste was then forced into a 12.7 x 4.1 x 3.1 cm steel die using a hydraulic press. A heating strip was wrapped around the die and operated at 50% power (~ 150°C).

The initial pressure on the sample was 4 MPa but increased to 12 MPa after curing for 24 hours. The increasing pressure was caused by aluminum powder reacting with the caustic paste and evolving hydrogen gas. The resulting geopolymer appeared to be dense to the naked eye; no pores were visible. Microscopy of the sample was performed using a Hitachi S-4700 SEM. A second section the pressed geopolymer was broken off and heated to 1000°C at 5°C/min after initial heating ramps of 0.1C/min to 300°C and 0.5°C to 600°C. Each set temperature, 300, 600; 1000°C was followed by a 1 hour soak. The sample failed catastrophically after heating. Macro cracks throughout the sample were filled with a solidified melt of ceramic material.

Lost Wax / Combined Additives

Forty cylinders (1 inch diameter, 4.5 inches long) and a prototype mold of for casting molten metal were made using a potassium-based geopolymer and wax powder, E-Z Wax Release (Yaley Enterprises, Redding, CA). The wax powders had a melting point of 98°C and a spherical morphology. Large agglomerates were removed from the wax powder by sieving through a 20-mesh sieve (841 μm). The addition of 30 w% wax significantly reduced the mechanical integrity of the geopolymer samples. Only one geopolymer / wax composite did not fail during boiling. Residual wax within the interior of the successful sample resulted in failure upon further heating. Additional samples were made from a second, lower melting wax, (T_{melt} = 60°C), KKW 4043, (Paramold MFG Ltd. Inc., Sayville, NY) but these samples also failed during boiling.

Numerous attempts were made to form geopolymer foams using combinations of hydrogen peroxide, aluminum powder and Daravair, an air-entrapment agent used in cement mixtures (Grace Construction Products). Additionally, geopolymer slurry was filtered through hydrophobic and hydroscopic polymer foams (E.N. Murray Co., Denver, CO) in the expectation that the geopolymer slurry would coat the underlying foam, after which the foam could be burned out. (Infiltration followed by burn out is the conventional method of producing ceramic foams.)

Results

Internal Pressure

SEM analysis of the geopolymer fragment formed inside the steel container at 3.5 MPa showed a microstructure with spherical pores randomly dispersed in a matrix of geopolymer (Figure 3). The characteristic pore size was approximately 50 μm. Geopolymers formed with greater than 15 vol % free space within the plastic containers had inhomogeneous microstructures; pore sizes were variable along the length of the containers and sometimes exceeded 5 mm in diameter.

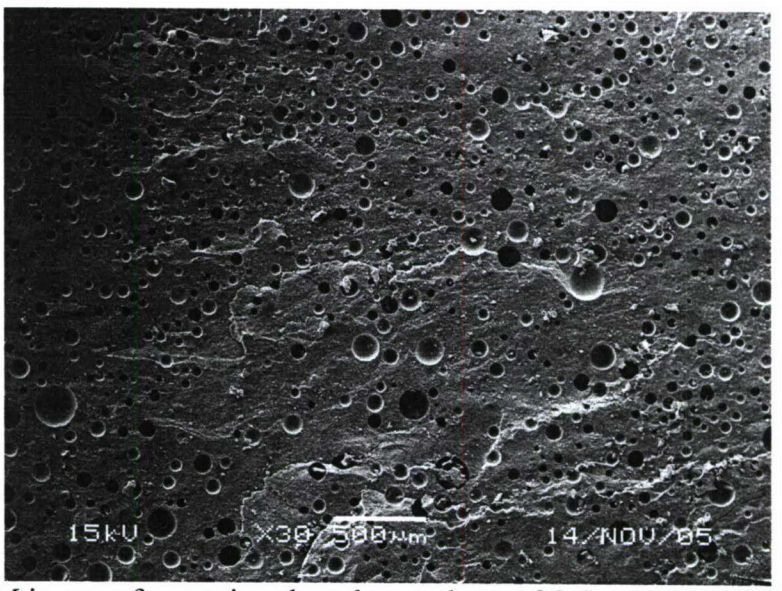

Figure 3: SEM image of potassium-based geopolymer fabricated at 3.5 MPa of pressure using H_2O_2 to intentionally produce macro porosity.

External Pressure

Although the geopolymer sample cured under external pressure appeared too solid and defect free to the naked eye. SEM analysis of showed a highly porous microstructure, however, with a characteristic pore size of approximately 20 μm (Figure 4 - Figure 6).

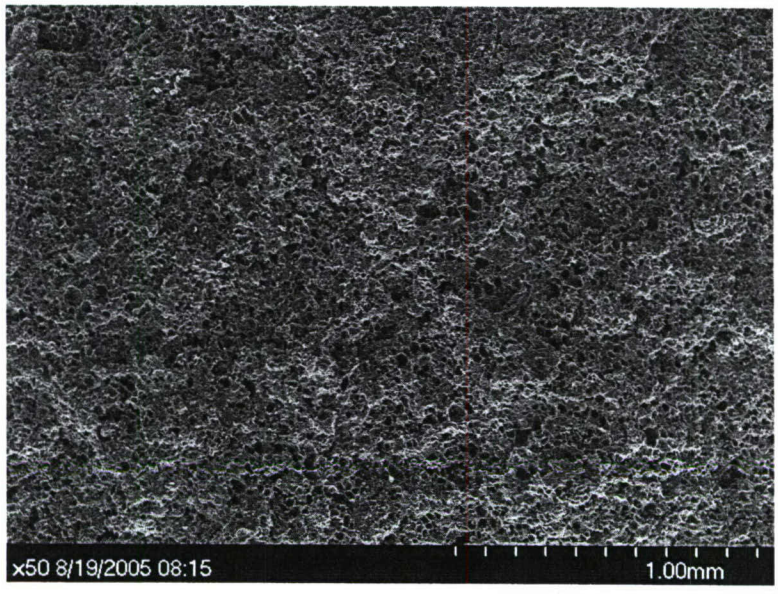

Figure 4. SEM micrograph of an aluminum-reinforced geopolymer fabricated under pressure.

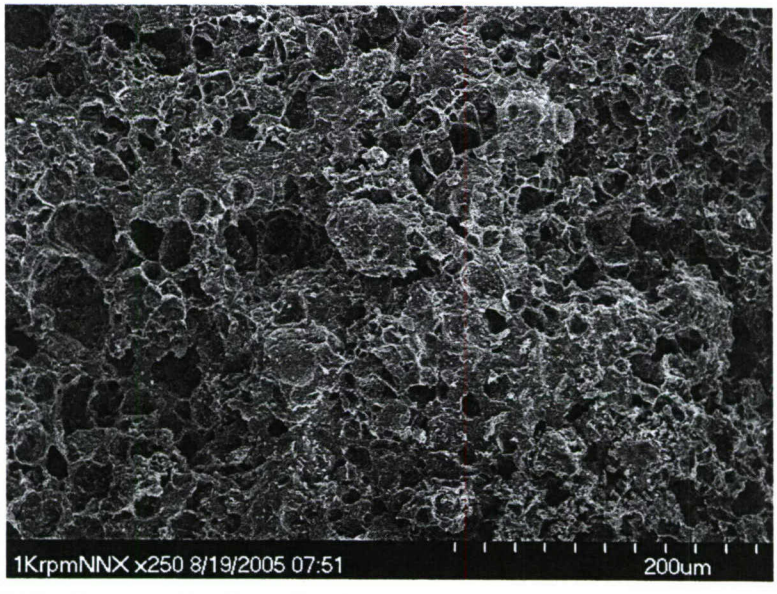

Figure 5. SEM micrograph of an aluminum-reinforced geopolymer fabricated under pressure.

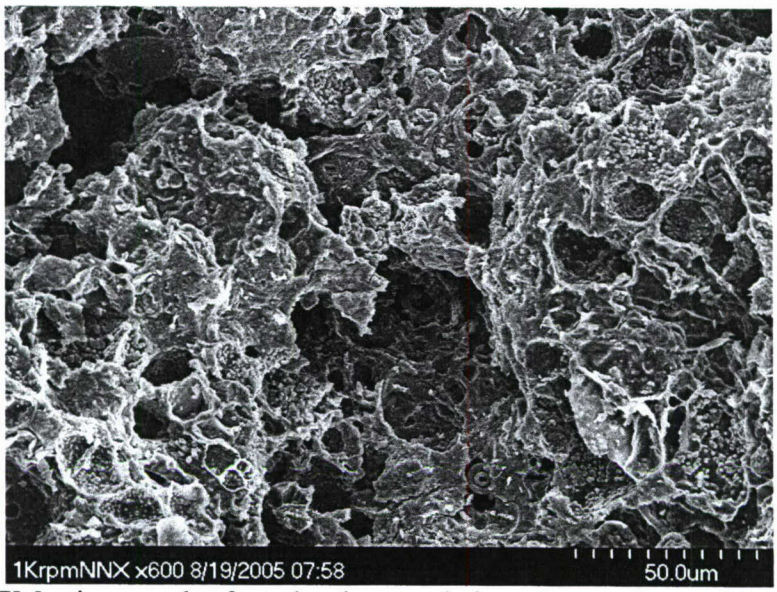

Figure 6. SEM micrograph of an aluminum-reinforced geopolymer fabricated under pressure.

Lost Wax / Combined Additives

Boiling of the wax geopolymer composites resulted in failure of the samples. Attempts to form porosity through the combined or singular action of aluminum, H_2O_2 and air-entrapment agents resulted in either the formation of uncontrolled macro pores ~ 5 mm diameter or no additional porosity being formed. Geopolymer slurry failed to coat the hydroscopic foam continuously, however. The hydroscopic foam was destroyed by the high pH of the geopolymer slurry.

Discussion

Internal Pressure

In principle, the approach of using H_2O_2 to form pores of a controlled size in a pressurized container is feasible. The extraction, however, of the resulting geopolymer is problematic. If the ratio of pressure / free volume is too low, pores within the geopolymer paste coalesced and a useful engineering microstructure could not be generated. It is doubtful that geopolymers produced using this method can be extracted from pressure vessels (metal or plastic) without destroying the produced geopolymer.

External Pressure

External pressure did produce an open-pore microstructure that would have facilitated the thermal conversion of a geopolymer into a ceramic material. Residual, un-reacted aluminum however was present within the geopolymer. Upon heating, then aluminum melted and then oxidized, fracturing the geopolymer.

Lost Wax / Combined Additives

Despite the previous success of using wax to produce geopolymer foams, the process of boiling embedded wax out of cast geopolymers to create porous microstructures did not produce geopolymer foams in a reliable manner. The incorporation of wax into the geopolymers led to lower mechanical strengths, resulting in failure during wax removal. Without the addition of external pressure or inducing a significant build-up of internal pressure, controlled porosity could not be produced in geopolymers using aluminum powder, H_2O_2 and/or air entrapment agents

Conclusion

None of the tested methods (utilizing a build-up of internal pressure, applying external pressure, addition of foaming agents or removal of embedded wax) proved to be practical route for producing geopolymers capable of undergoing thermal conversion into porous glass-ceramics. The most effective method for preparing geopolymer foams is most likely by a more conventional route, mixing pre-prepared foams into the geopolymer slurry.

References

[1]T. D. Tonyan and L. J. Gibson, "Structure and Mechanics of Cement Foams," *Journal of Materials Science*, **27**[23] 6371-6378 (1992).

Section F - Laser Scanning Confocal Microscopy

Introduction

A "geopolymer" is an aluminosilicate binder formed by mixing aluminosilicate materials (e.g. metakaolin, fly ash) with alkali or alkali-silicate solutions.[1] The set time and resultant properties are dependant on the processing conditions, materials used, and the $M_2O:SiO_2:Al_2O_3:H_2O$ molar ratios ($M = Li^+$, Na^+, K^+, Rb^+ or Cs^+). Typically Na^+ or K^+ is used as the alkali source due to cost and performance concerns. After mixing the metakaolin and the alkali-silicate solution, the resultant gel is typically sealed to prevent dehydration and allow proper chemical setting while being cured between 40 – 80°C. Setting times are rapid, 1 – 3 hours; however maturation time may take days or weeks, depending on conditions. The aluminosilicate source material must be sufficiently reactive in the alkali-silicate solution to promote leaching of dissolution and release of aluminum. For this reason, crystalline kaolin is typically dehydroxylated via calcination into amorphous metakaolin to ensure proper reactivity.[2] Although dependent on composition and processing conditions, metakaolin-based geopolymers are heterogeneous in nature. In addition to the formed geopolymer phase, metakaolin-based geopolymers contain porosity, unreacted metakaolin, chemical impurities, and weakly and strongly bound water.[3] Geopolymers consist of four coordinated (IV) interlinked Si and Al, although metakaolin contains Al(IV), Al(V), and Al(VI).[1, 4] The relative degree of reaction between alkali-silicate solutions and metakaolin precursors was explored by Duxson *et. al.* using MAS NMR. Duxson et al. compared the amount of Al(VI) (attributed to residual metakaolin) present in geopolymers synthesized with varying silica contents and alkali chemistries.[4] Duxson et al. concluded that the degree of reaction between metakaolin and alkali-silicate solutions decreased as the ratio of Si/Al and the ratio of Na/K in the alkali-silicate solutions increased.[4] SEM analysis of geopolymers made with metakaolin and sodium silicate solutions indicated that the geopolymer microstructure became more homogenous with increasing silica content.[5]

The majority of the work done to visually study the geopolymer structure has been based on electron and conventionally optical-light microscopy. Although useful, these techniques observe only the surface of a material; the former operates in low

vacuum, which can damage the microstructure of hydrated systems (e.g. cements and geopolymers). Confocal microscopy has been used to generate three-dimensional topographic maps of cement fracture surfaces to generate fractal dimensions and roughness parameters which were then related to porosity, compressive strength, and fracture properties.[6-9] Laser scanning confocal microscopy (LSCM) has several advantages over traditional confocal microscopy. Laser light can be transmitted through thin sections of a sample to capture 2-dimensional images of the sample interior. The focal planes are adjusted by computer controlled stepping motors, allowing for high resolution images higher (~ 0.2 μm horizontal and ~ 0.5 μm vertical).[10] The individual slices can then be processed using imaging software to generate a three-dimensional representation of the sample. Starting materials can be dyed with appropriate fluorescing agents to enhance visualization of the sample interior. LSCM has been used to perform wet-chemistry studies and surface characterization of cements and *in-situ* monitoring of the alkali/silicate reaction near the cement/aggregate interface.[11, 12] LSCM can be used to collect a variety of information: reaction products at the interface, three-dimensional representations of the aggregate, the development of cracks, and quantitative measurements of the gel ring thickness around aggregate particles. The ability to collect three-dimensional information *in-situ* without disruption of the hydration process separates LSCM from conventional microscopy methods.

In this study, metakaolin-based geopolymers were studied LSCM. Attempts were made to correlate the distribution of the fluorescing dyes to the final geopolymer microstructure and the nature of the alkali-silicate/metakaolin reaction as function of silica content and alkali chemistry.

Experimental

Nine alkali-silicate solutions (Table 1) were prepared by dissolving Cab-O-Sil fumed silica (Cabot Corp.) into solutions of potassium hydroxide (KOH), sodium hydroxide (NaOH) and mixed alkali (NaOH/KOH) solutions. When fumed silica was dissolved into the alkali solutions, the resultant alkali-silicate solutions were allowed to mature for at least 24 hours to ensure complete silica dissolution.

Table 1: Composition of alkali-silicate solutions.

Composition (Molar Oxide Ratio)			
Na_2O	K_2O	SiO_2	H_2O
1			11
1		1	11
1		2	11
	1		11
	1	1	11
	1	2	11
0.5	0.5		11
0.5	0.5	1	11
0.5	0.5	2	11

Fluorescein isocyanate (FI) solutions were prepared by adding 1 g/L of FI powder to pre-made 1 N alkaline solutions. Alkali-silicate solutions (Table 1) were made fluorescent by mixing with pre-made solutions of FI dye in volume ratios of 95:5 (alkali-silicate, FI solution). It was found that FI was degraded by the alkali solutions when no silica was present; the initial yellow color of the solutions became light blue after two days. Metakaolin powder for the experiment was also dyed by mixing the metakaolin with a dyeing solution of rhodamine-B (RB) in a ratio of 10 mL of RB solution per 1 g of metakaolin. The RB solution was prepared by mixing 10 mg of RB powder per liter of de-ionized water. After mixing, the dyed metakaolin slurry was centrifuged at 1300 RPM. The ssupernatant was discarded. The dyed metakaolin was collected and dried at 40°C for 3 days. Geopolymers were made by hand mixing the dyed metakaolin and alkali-silicate solutions. The molar ratios of all the geopolymers were $1M_2O$:1 Al_2O_3. (It was assumed that the metakaolin had a stoichiometric composition of A_2lO_3:2 SiO_2.) Geopolymer slurry was placed between two glass slide cover slips and cured at 40°C for

36 hours. Slurry viscosity increased with increasing sodium content; slurry viscosity also increased with decreasing silica content. The geopolymers samples were 2 – 8 μm thick; however no attempt was made to control the thickness of the samples.

The geopolymer samples were analyzed using a laser scanning confocal microscope (LSCM) equipped with an argon laser (Leica Microsystems Pty Ltd., Gladesville, NSW Australia). Both reflected and transmitted pictures were taken simultaneously. At the beginning of each run, the photomultiplier tube gain value was adjusted in scanning mode to minimize image saturation. The step size in the z (thickness) direction was 0.5 μm. 3D representations of the geopolymer samples were constructed using image analysis software. Attempts were made to observe the evolution of the geopolymer microstructure during curing, however useful data could not extracted due to rearrangement of metakaolin particles and flow of the alkali solutions. Samples were removed from the glass cover slips sputter coated with a gold-palladium alloy and examined using a scanning electron microscope (Hitachi S-4700 SEM).

Results

Three-dimensional reconstructions of the analyzed geopolymers were produced are given in Fig. 1 - Fig. 3. Regions rich in RB are shown as red, green regions indicate the presence of FI. The intensity of the color (bright or dark) is proportional to the concentration of dye in the geopolymer; bright red or green indicates a higher concentration of respective dyes. No color indicates a region completely devoid of dye.

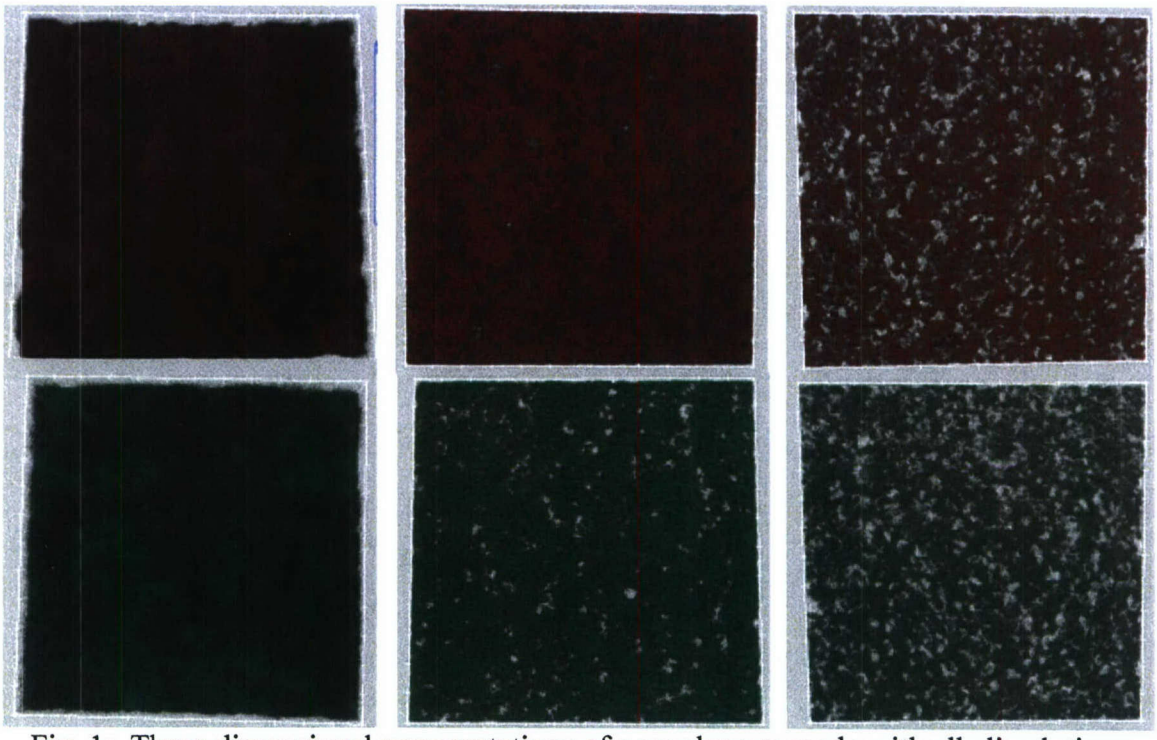

Fig. 1: Three-dimensional representations of geopolymers made with alkali solutions (M_2O : 0 SiO_2), showing the fluorescing signal from rhodamine-B (top) and fluorescein isocyanate (bottom). Na^+ based geopolymers (left), Na^+/K^+ geopolymers (center), K^+ geopolymers (right). All of the above pictures are 60 μm x 60 μm with varying thickness.

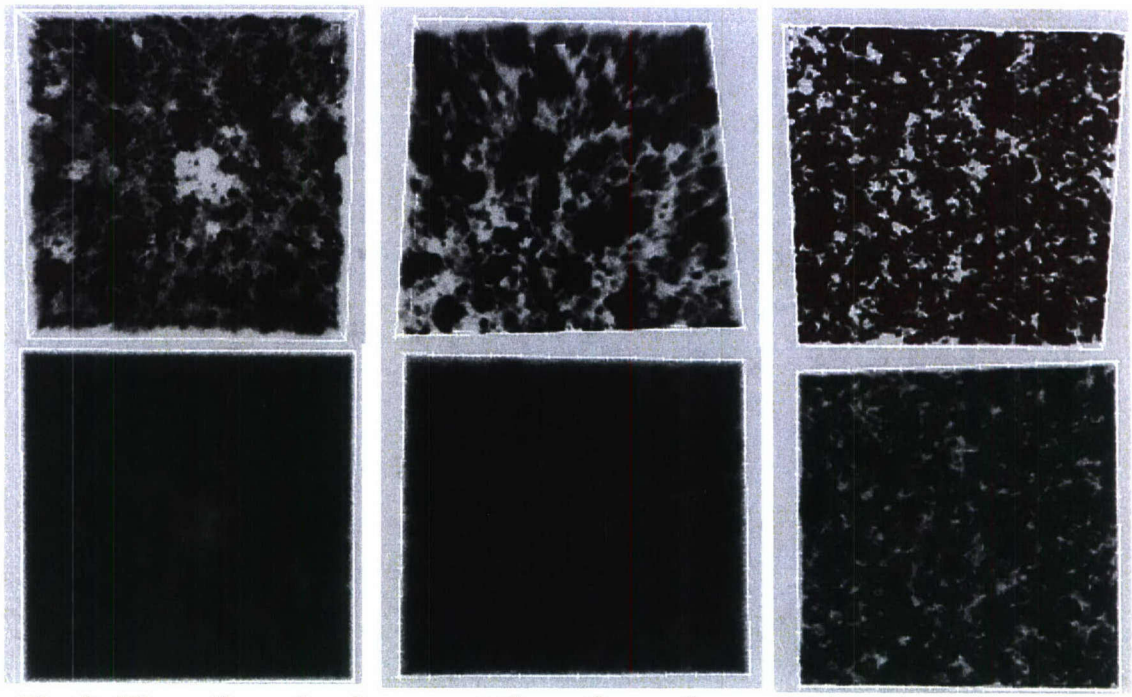

Fig. 2: Three-dimensional representations of geopolymers made with alkali solutions (M_2O : 1 SiO_2), showing the fluorescing signal from rhodamine-B (top) and fluorescein isocyanate (bottom). Na^+ based geopolymers (left), Na^+/K^+ geopolymers (center), K^+ geopolymers (right). All of the above pictures are 60 μm x 60 μm with varying thickness.

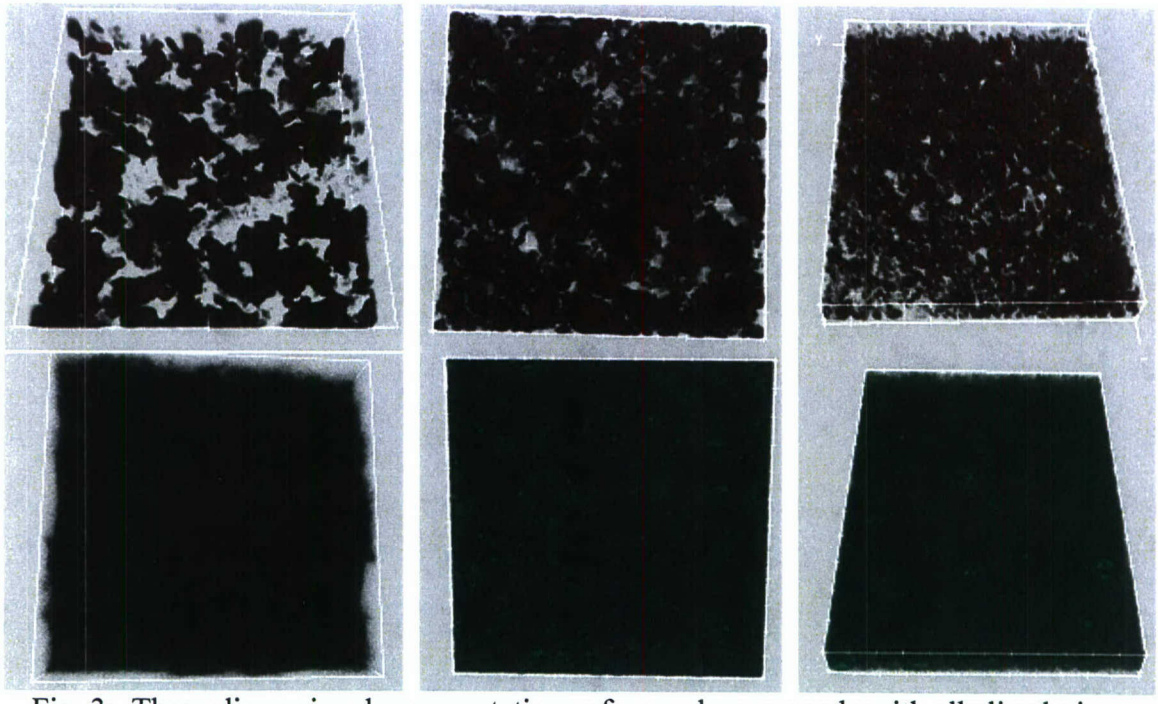

Fig. 3: Three-dimensional representations of geopolymers made with alkali solutions (M_2O : 2 SiO_2), showing the fluorescing signal from rhodamine-B (top) and fluorescein isocyanate (bottom). Na^+ based geopolymers (left), Na^+/K^+ geopolymers (center), K^+ geopolymers (right). All of the above pictures are 60 μm x 60 μm with varying thickness.

SEM analysis showed geopolymers made with alkali solutions without dissolved silica (Fig. 4) were significantly more porous than geopolymers formed from alkali-silicate solutions (Fig. 5 and Fig. 6). Increasing the dissolved silica content in the activating alkali-silicate solutions did not appeared to alter the surface of the geopolymer samples significantly (Fig. 5 and Fig. 6). Alkali chemistry (e.g. Na^+ or K^+) appeared to have no affect on the microstructure of higher silica geopolymers (Fig. 5 and Fig. 6) but did have a pronounced affect on the low silica geopolymers (Fig. 4). Low-silica sodium based geopolymers were comprised of equiaxed precipitates, approximately 0.5 μm in diameter (Fig. 4). The morphology of the precipitates became plate-like as sodium was replaced with potassium (Fig. 4).

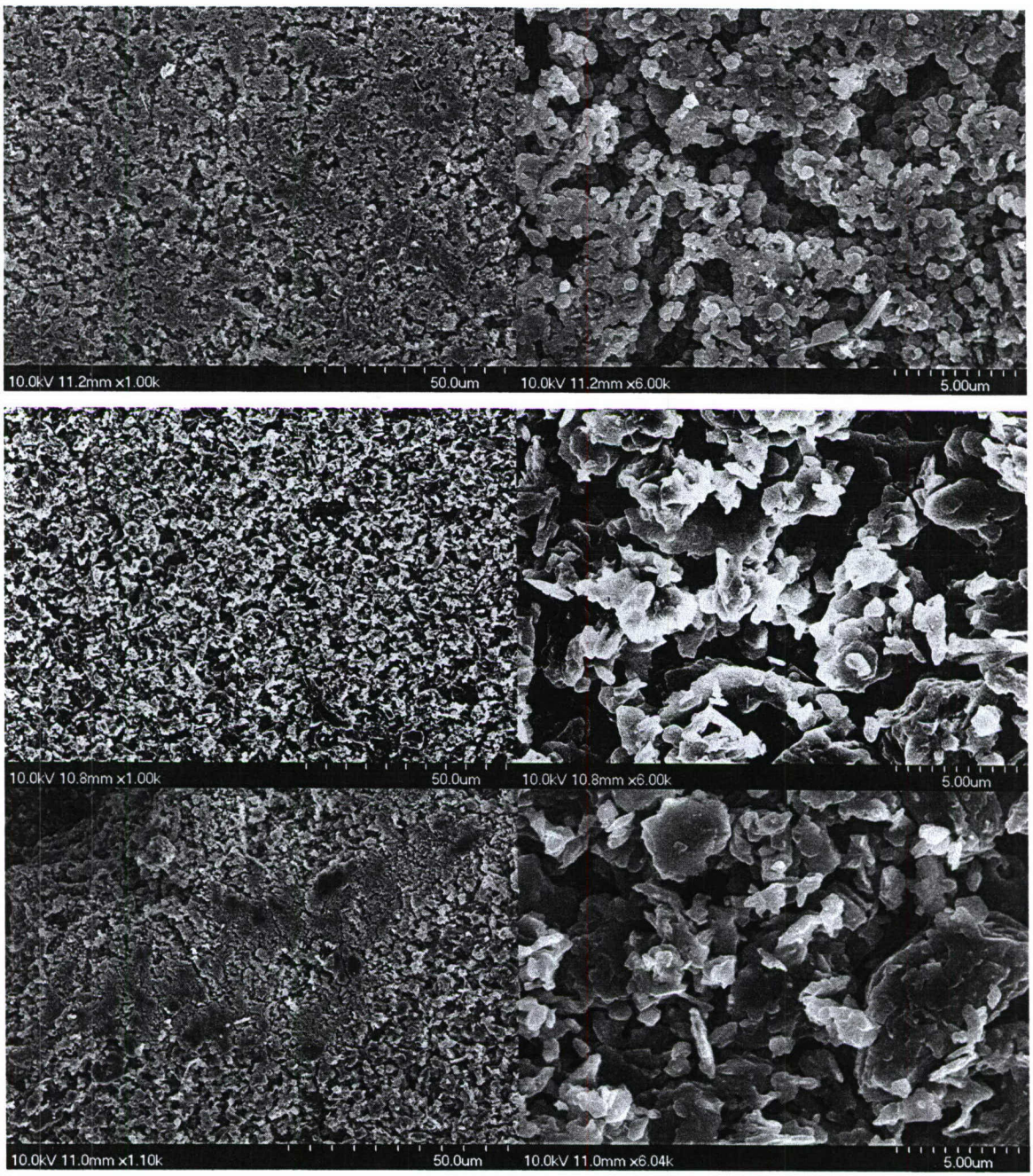

Fig. 4: High and low magnification SEM images of geopolymers produced with alkali-silicate solutions (M_2O : 0 SiO_2), varying the alkali chemistries. Na^+ based geopolymers (top), Na^+/K^+ geopolymers (center line), K^+ geopolymers (bottom line).

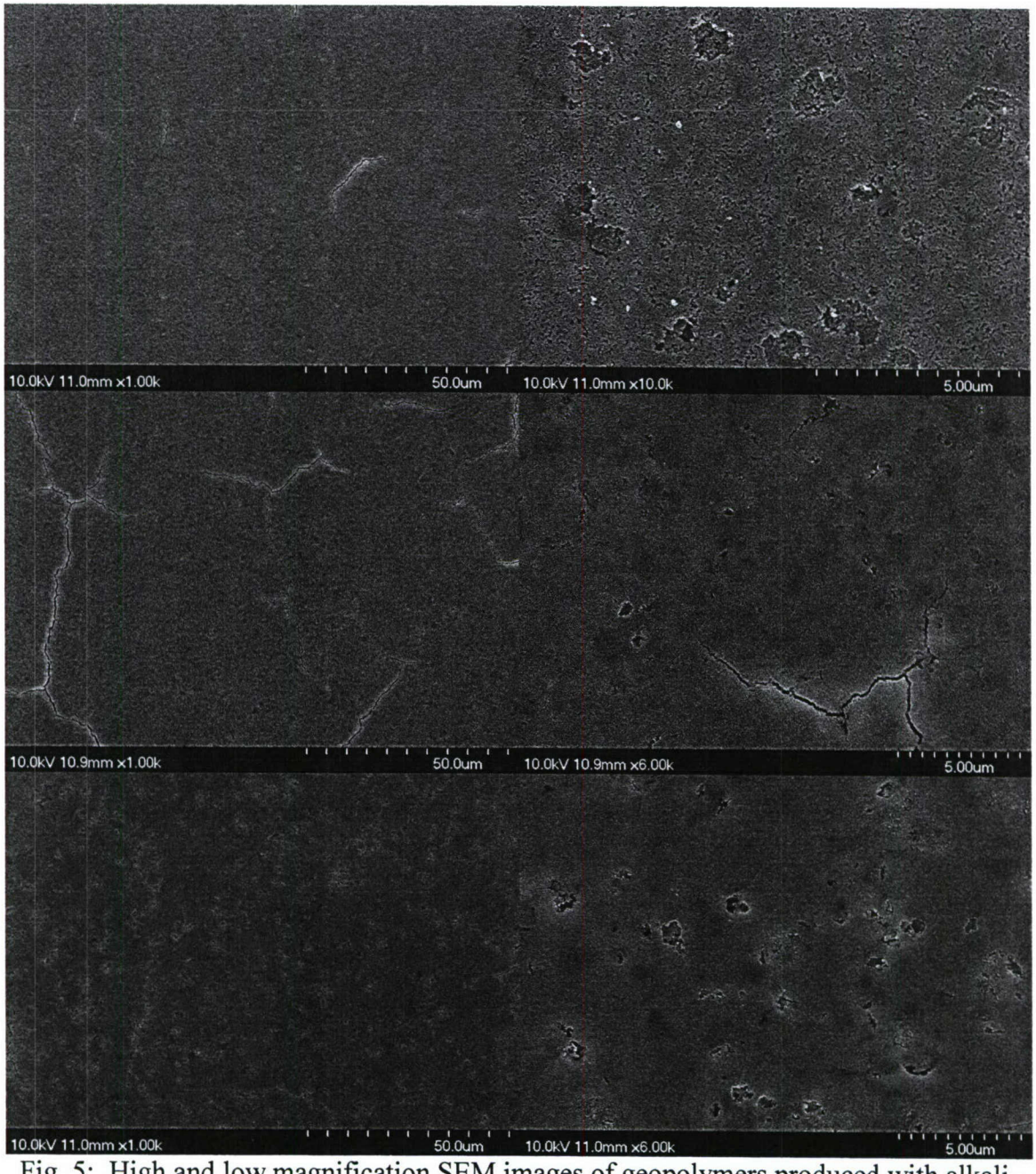

Fig. 5: High and low magnification SEM images of geopolymers produced with alkali-silicate solutions (M_2O : 1 SiO_2), varying the alkali chemistries. Na^+ based geopolymers (top), Na^+/K^+ geopolymers (center line), K^+ geopolymers (bottom line).

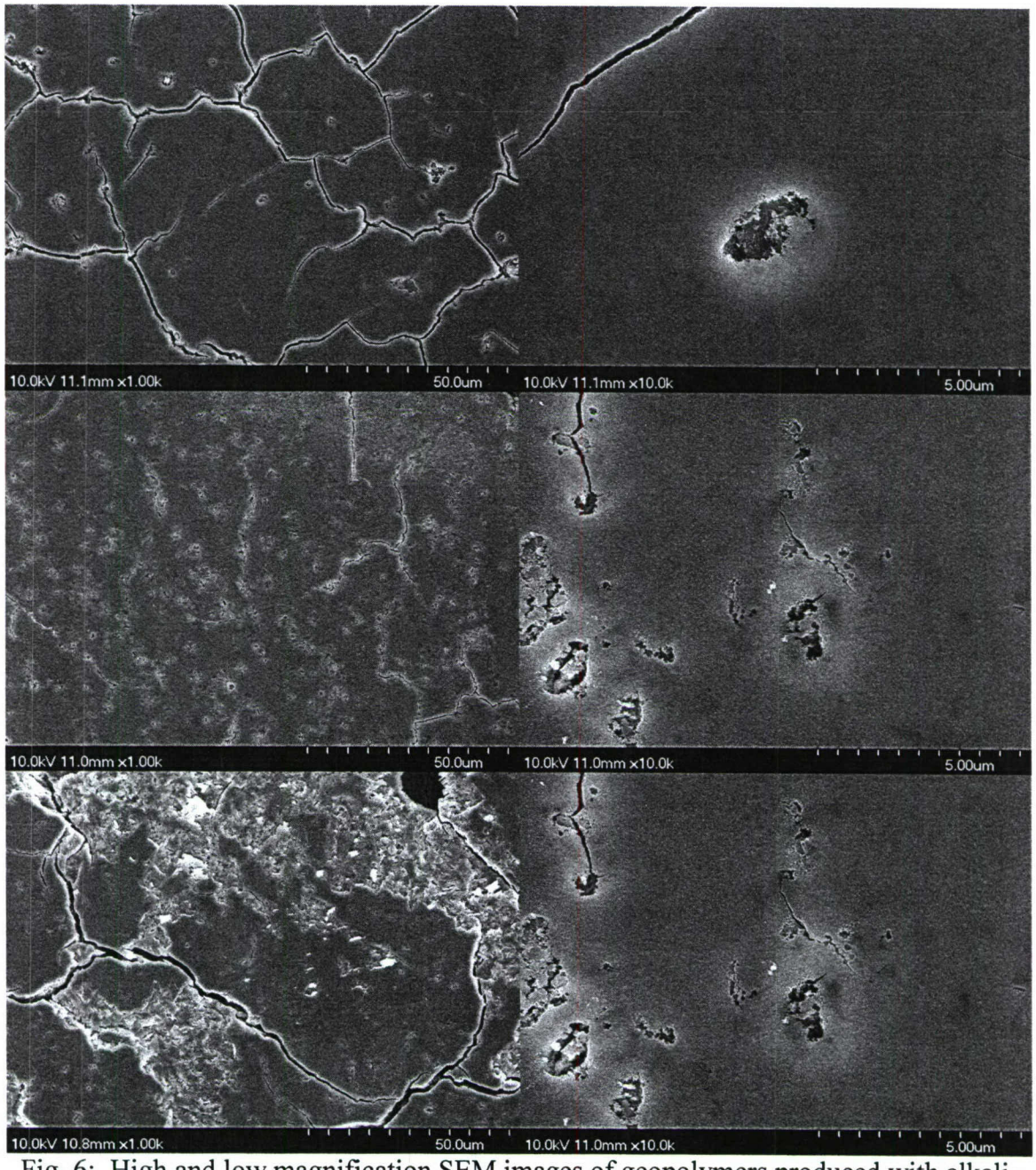

Fig. 6: High and low magnification SEM images of geopolymers produced with alkali-silicate solutions (M_2O : 2 SiO_2), varying the alkali chemistries. Na^+ based geopolymers (top), Na^+/K^+ geopolymers (center line), K^+ geopolymers (bottom line).

Discussion

Large clusters of RB dye in the LSCM data were representative of unreacted metakaolin particles. Conversely, increased levels of reaction between metakaolin and alkali-silicate solutions were characterized by RB dye being distributed throughout the geopolymers. Results from LSCM images indicated that as the silica content was increased, the amount of unreacted metakaolin increased in geopolymers made from sodium and mixed alkali-silicate solutions. LSCM images also indicated that potassium-silicate solutions reacted more readily than sodium or mixed alkali-silicate solutions. Both trends, the affect of silica content and alkali chemistry, are consistent with MAS NMR results in literature.[4]

Overlapping of the LSCM scans showed that void regions in low silica geopolymers, where the alkali to silica ratio (M_2O:SiO_2) within the activating solution was ≤ 1 had neither dye present, indicating pore space. In the highest silica (M_2O : 2 SiO_2) geopolymer sample, however, it was apparent that FI dye was distributed throughout the microstructure, even in regions that were poor in metakaolin (no RB dye was present). These regions were presumably pores as well, however in the case of higher silica systems, the pores are filled with fluid (or silica gel) carrying the FI dye. SEM analysis showed the microstructures of the geopolymers became homogenous when silica was added to the alkali solution, agreeing with the findings of Duxson *et al.*[5]

Conclusion

LSCM has the potential for being a powerful tool to measure the degree of reaction between the constituent aluminosilicate powders and the activating alkali-silicate solutions. LSCM results agree with findings in literature; reactivity between alkali-silicate solutions and metakaolin particles was decreased when higher amounts of dissolved silica were present in the alkali-silicate solutions and when the ratio of potassium to sodium in solution was increased.

References

[1]J. Davidovits, "Geopolymers and Geopolymeric Materials," *Journal of Thermal Analysis*, **35**[2] 429-441 (1989).

[2]H. Rahier, B. Wullaert and B. Van Mele, "Influence of the degree of dehydroxylation of kaolinite on the properties of aluminosilicate glasses," *Journal of Thermal Analysis and Calorimetry*, **62**[2] 417-427 (2000).

[3]I. Lecomte, M. Liegeois, A. Rulmont, R. Cloots and F. Maseri, "Synthesis and characterization of new inorganic polymeric composites based on kaolin or white clay and on ground-granulated blast furnace slag," *Journal of Materials Research*, **18**[11] 2571-2579 (2003).

[4]P. Duxson, G. C. Lukey, F. Separovic and J. S. J. van Deventer, "Effect of alkali cations on aluminum incorporation in geopolymeric gels," *Industrial & Engineering Chemistry Research*, **44**[4] 832-839 (2005).

[5]P. Duxson, J. L. Provis, G. C. Lukey, S. W. Mallicoat, W. M. Kriven and J. S. J. van Deventer, "Understanding the relationship between geopolymer composition, microstructure and mechanical properties," *Colloids and Surfaces A-Physicochemical and Engineering Aspects*, **269**[1-3] 47-58 (2005).

[6]A. B. Abell and D. A. Lange, "Fracture mechanics modeling using images of fracture surfaces," *International Journal of Solids and Structures*, **35**[31-32] 4025-4033 (1998).

[7]D. A. Lange, H. M. Jennings and S. P. Shah, "Analysis of Surface-Roughness Using Confocal Microscopy," *Journal of Materials Science*, **28**[14] 3879-3884 (1993).

[8]D. A. Lange, H. M. Jennings and S. P. Shah, "Relationship between Fracture Surface-Roughness and Fracture-Behavior of Cement Paste and Mortar," *Journal of the American Ceramic Society*, **76**[3] 589-597 (1993).

[9]D. A. Lange, C. Ouyang and S. P. Shah, "Behavior of cement based matrices reinforced by randomly dispersed micro fibers," *Advanced Cement Based Materials*, **3**[1] 20-30 (1996).

[10]S. Paddock, *Methods in Molecular Biology*. Confocal Microscopy: Methods and Protocols, Edited by J. Walker. Vol. 122, Humana Press Inc., Totowa, New Jersey, 1999.

[11]K. E. Kurtis, N. H. El-Ashkar, C. L. Collins and N. N. Nalk, "Examining cement-based materials by laser scanning confocal microscopy," *Cement & Concrete Composites*, **25**[7] 695-701 (2003).

[12]C. L. Collins, J. H. Ideker and K. E. Kurtis, "Laser scanning confocal microscopy for in situ monitoring of alkali-silica reaction," *Journal of Microscopy-Oxford*, **213** 149-157 (2004).

Section G - Crystallization of Cesium Geopolymer

Introduction

Davidovitis first coined the term "geopolymer" to describe an aluminosilicate binder formed at ambient temperatures by the reaction between alkali-silicate solutions and aluminosilicate minerals or glasses.[1] Geopolymers are X-ray amorphous (Rahier *et al.* referred to geopolymers as low-temperature synthesized aluminosilicate glasses)[2] and consist of four coordinated (IV) silica and alumina tetrahedra where the charge of the AlO_4^- tetrahedral are balanced by hydrated alkali cations.[3] The high temperature crystallization of ceramics from geopolymers was reported by Barbosa and MacKenzie, who observed the crystallization of leucite, kalsilite, quartz and cristobalite when heating potassium geopolymers to 1000°C.[4] Similarly, Barbosa and MacKenzie also reported the crystallization of nepheline, and mullite from sodium-based geopolymers.[5] Gordon *et. al.* demonstrated the crystallization of single-phase leucite from potassium-based geopolymers above ≥ 1100°C.[6] SEM and TEM analysis of the heated geopolymers showed microstructures reminiscent of glass-ceramics.[6]

Pollucite ($CsAlSi_2O_6$) is a cesium aluminosilicate with a density of 2.936 g/cm^3 and a refractive index of 1.53.[7] At room temperature pollucite adopts a cubic unit cell (Ia-3d) [8] containing 96 oxygen atoms and 48 $(Si,Al)O_4$ tetrahedra arranged in four- and six-membered rings.[9, 10] Pollucite has the highest melting temperature of any known silicate (T_{melt} > 1900°C) [11] and has exceptional creep resistance between 1400 – 1500°C, comparable to the two most creep resistant ceramic oxides, mullite and yttrium-aluminum garnet (YAG).[12] The thermal expansion of pollucite has been the subject of multiple studies.[7, 8, 10, 12-18] although individual measurements of the thermal expansion of pollucite vary; there is general agreement that the thermal expansion of pollucite is low. Yanase *et al.* reported that the coefficient of thermal expansion for pollucite was 3.3 x 10^{-6}/K (673 – 1073 K) using high-temperature X-ray diffraction (HTXRD).[18] To date, fully dense pollucite ceramics have not been successfully prepared partly due to the volitization of cesia at high temperatures.[12, 19]

Fully dense pollucite glass ceramics have been produced, however.[11, 20-22] Beall and Rittler reported a range of pollucite-based glass ceramics compositions, SiO_2 25 – 70%, Al_2O_3 20 – 50%, Cs_2O 10 – 35% (by weight).[11] The resulting glass-ceramics demonstrated high corrosion resistances and low thermal expansions ($4.03 – 4.8 \times 10^{-6}$ (0 - 1000°C). Pollucite crystallization was observed above 1000°C in cesium aluminosilicate glass ceramics without the addition of a zirconia to act as a nucleating agent. Similarly, pollucite has been crystallized from glass compacts formed from cation-ion exchanged zeolites between 1050 – 1250°C [23] and sol-gel derived cesium aluminosilicate glass powders (1026°C) [24].

The crystallization of pollucite from a room temperature synthesized glass (a geopolymer) may represent a novel approach to forming pollucite-based glass ceramics. The objective of this experiment was to observe the crystallization of pollucite from a cesium-based geopolymer (Cs-geopolymer) and record the thermal expansion of the crystallized pollucite using *in-situ* HTXRD.

Experimental Procedures

"Synthetic metakaolin" (SynMK) [25] was prepared by the organic steric entrapment method [26], as follows: A 50 wt. % solution of 98 % aluminum nitrate nonahydrate (Fisher Scientific, Pittsburgh, PA) was mixed under low heat with a 24.5 wt. % suspension of colloidal silica, Ludox SK (Grace Division, Columbia MD) in a lithium aluminosilicate glass-ceramic container. After one hour of stirring, a 5 wt. % solution of Celvol polyvinyl alcohol (PVA) (Celanese Chemicals, Dallas TX) was added to the mixture. The final molar ratio of the mixed solution was $2Al_2O_3 \cdot 4SiO_2 \cdot 7PVA$. Infrared heating lamps were set above the mixture and left operating overnight, while the mixture was simultaneously stirred and dried by a hot/stir plate. After sufficient drying (approximately 12 hours) the solution became a uniform yellow cake, which was pulverized using a mortar and pestle.

The resulting powder was then calcined at 800°C for 1 hour in a 650 Isotemp Furnace (Fisher Scientific). After calcination, the powder color changed to white. The powder was then milled with isopropyl alcohol in a Fritsch Pulverisette planetary micro mill using 8 mm ceria stabilized zirconia media (Fritsch Gmbh, Idar-Oberstein, Germany). The slurry was dried and baked at 600°C for 5 hours to remove all organics from the surface of the SynMK and sieved to -100 μm. The surface area of the SynMK was 196 m^2/g, determined from the best fit of seven datum points using the BET method with an Autosorb-1 Surface Area and Pore Size Analyzer (Quanta chrome Instruments, Boynton Beach FL). The average particle size of the powder was 1.10 μm with a standard deviation of 0.95 μm. Particle size analysis was performed with a Horiba Particle Size Distribution Analyzer CAPA-700 (Horiba International Corporation, CA) using Sedisperse A-12 (Micromeritics Instrument Corporation, Norcross, GA) as a dispersant.

The cesium silicate activating solution was derived from cesium hydroxide monohydrate (99.8%, Chemetall Chemical Products Inc., Berkeley Heights NJ), fumed silica (Cab-o-sil, Cabot, Tuscola IL), and de-ionized water. The nominal composition of the solution was $Cs_2O•2SiO_2•10\ H_2O$. Using a polypropylene container, SynMK was added incrementally to the alkali-silicate solution while mixing with a high-speed dispersion mixer. During mixing, the slurry was cooled with an ice water bath to prevent rapid setting of the geopolymer. After mixing for approximately 15 minutes, the resulting slurry was poured into chemically resistant plastic tubing, sealed using rubber stoppers, and cured at 60°C for 48 hours. The hardened geopolymer was then removed from the tubing; ground with a mortar and pestle and sieved to -45μm.

ICP elemental analysis was done using an OES Optima 2000 DV (Perkin Elmer, Norwalk CT), and showed the SynMK and geopolymer to have molar compositions of $Al_2O_3•1.96SiO_2$ and $1.23Cs_2O•Al_2O_3•3.95SiO_2$ respectively. The geopolymer was synthesized slightly rich in cesium compared to stoichiometric pollucite ($Cs_2O•Al_2O_3•4SiO_2$) to allow for some vaporization of cesium during heating, as was observed for potassium during high-temperature crystallization of leucite from oxide powders.[27] Thermal gravimetric analysis (TGA) and dynamic scanning calorimetery

(DSC) of the Cs-geopolymer was performed using a heating and cooling rate of 5°C/min (25 – 1500°C) using a Netzsch STA 409 DSC/TGA (Netzsch Instruments, Inc. Burlington, MA).

Powdered Cs-geopolymer was heated at 5°C/min to soak at set temperatures (100 – 1400°C) for 1 hour. XRD patterns of unheated and heated geopolymer powders were taken using a step size of 0.02 at a rate of 0.5° 2θ/min at an operating voltage of 45 kV and 20 mA from 5° to 75° 2θ using a Rigaku D/Max-b X-ray diffract meter with Cu Kα radiation (Rigaku D/Max, Tokyo, Japan). Analysis of the XRD data was done with JADE PC software (Minerals Data Inc., Livermore, CA).

In-situ HTXRD was performed with synchrotron radiation at the NSLS, Brookhaven National Laboratory National Photon Source (Upton, NY). Samples were heated using a quadruple, ellipsoidal, mirror heater furnace that was developed in our research laboratory (Fig. 1).[28, 29] Samples were tested using a reflection mode geometry, rocking ± 2° 2θ. The temperature of the sample was determined by the calculating the lattice parameters of the platinum that had been mixed with the ceramic powders. Lattice parameters of the ceramic phases were determined using the Pawley method with JADE crystallography software (Materials Data Inc., Livermore, California).

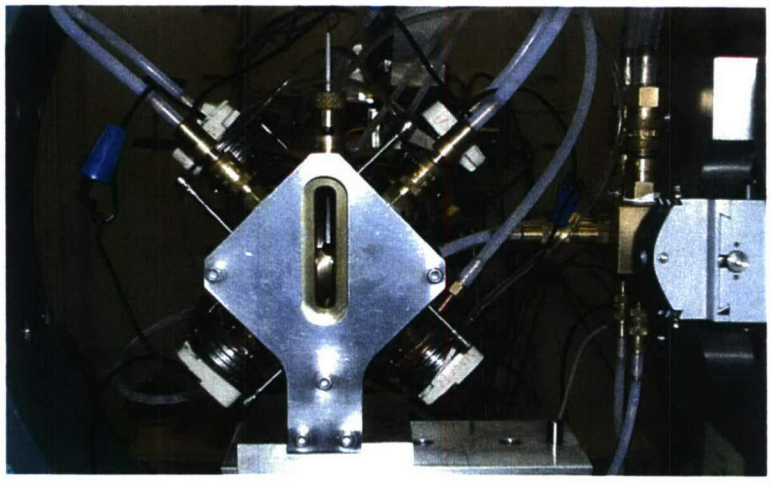

Fig. 1. Quadruple, ellipsoidal, mirror heater furnace

Results

XRD analysis of the SynMK and Cs-geopolymer showed amorphous peaks at 22° and 28° 2-theta, respectively (Fig. 2). No crystalline phases were present in either the SynMK or Cs-geopolymer.

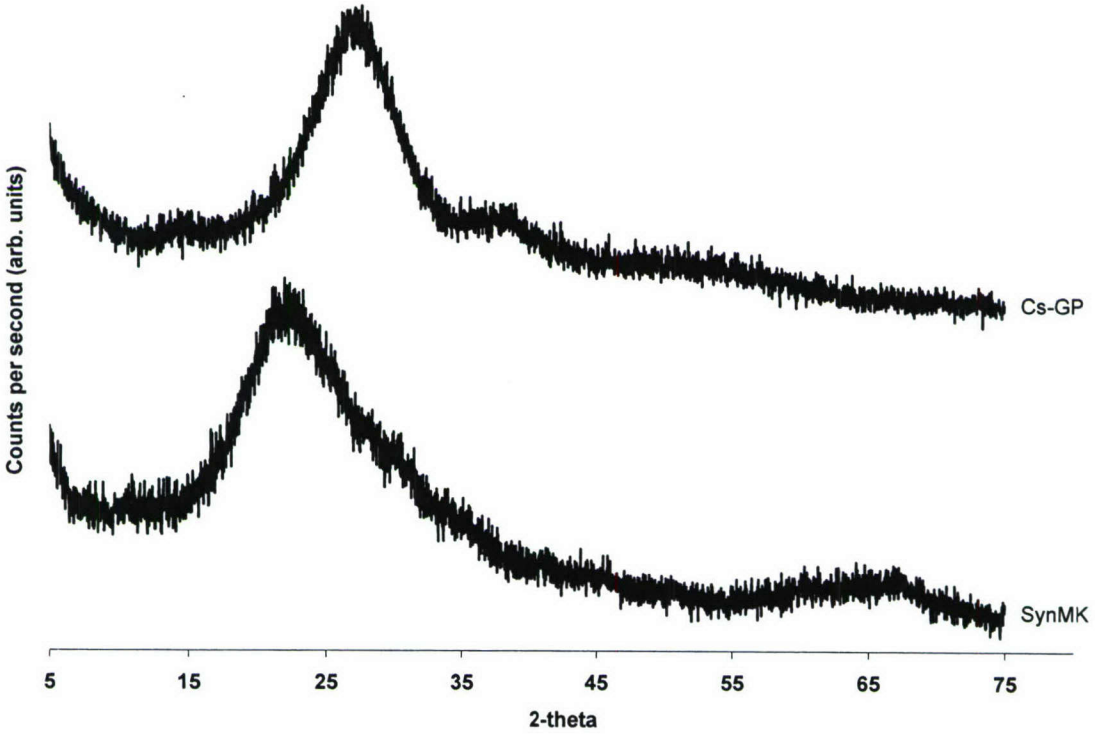

Fig. 2. Room temperature XRD scans of the aluminosilicate precursor, SynMK and the resulting cesium-based geopolymer

TGA analysis (Fig. 3) indicated a region of rapid weight loss (9.46%) below 250°C during the heating of the Cs-geopolymer powder. Continued weight loss (2.48%) was observed until the Cs-geopolymer was heated to 1000°C. A second mass loss was observed above 1250°C. DSC analysis recorded two exotherms, at approximately 1075°C and 1170°C. No appreciable weight changes or heat absorption were observed as the geopolymer was cooled.

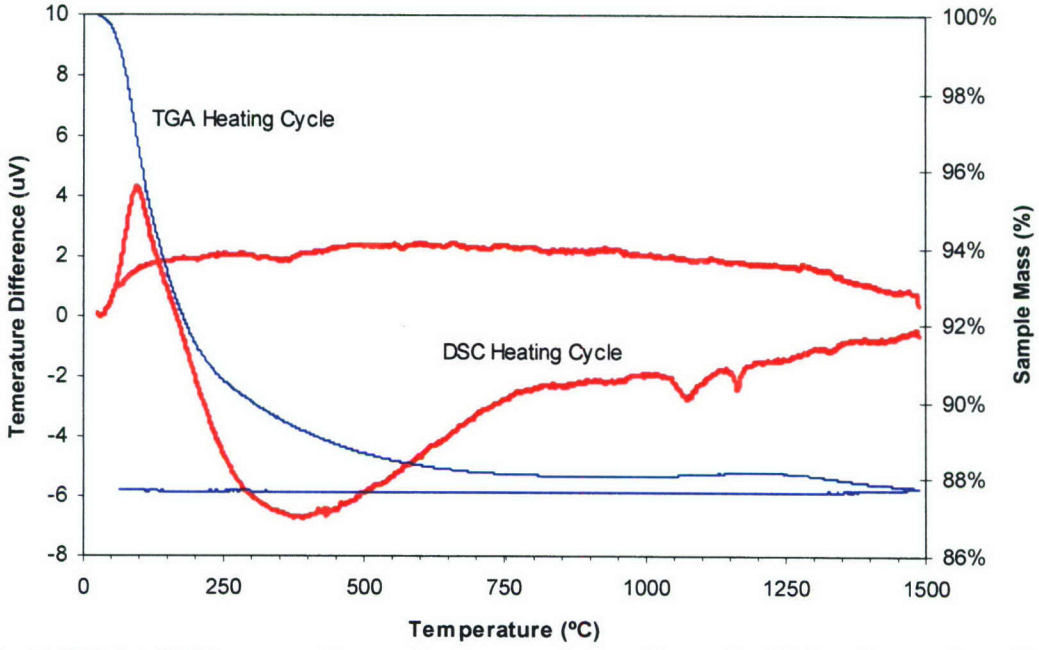

Fig. 3. TGA / DSC scans of geopolymer powder performed with heating and cooling rates of 5°C/min

Ex-situ X-ray diffraction patterns of the heated Cs-geopolymer indicated the onset of crystallinity at 900°C after heating for 1 hour. Well-formed peaks are visible after heating at 1000°C. High temperature thermal expansion measurements (Fig. 5) of the post-crystallized geopolymer, showed a low thermal expansion region, 1.8×10^{-4} $\%\Delta a/a_o$ (500 – 1180°C), followed by a region of higher thermal expansion, 6.1×10^{-4} $\%\Delta a/a_o$ (1180 – 1480°C).

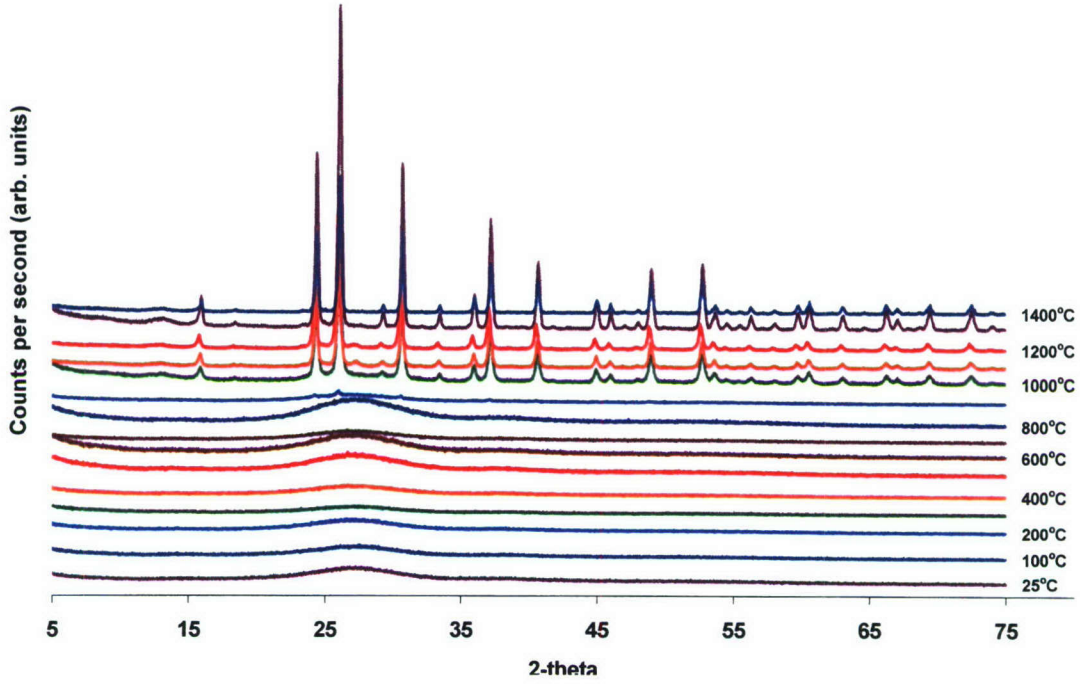

Fig. 4. Ex-situ X-ray diffraction patterns of Cs-geopolymer after heating at a set temperature for 1 hour.

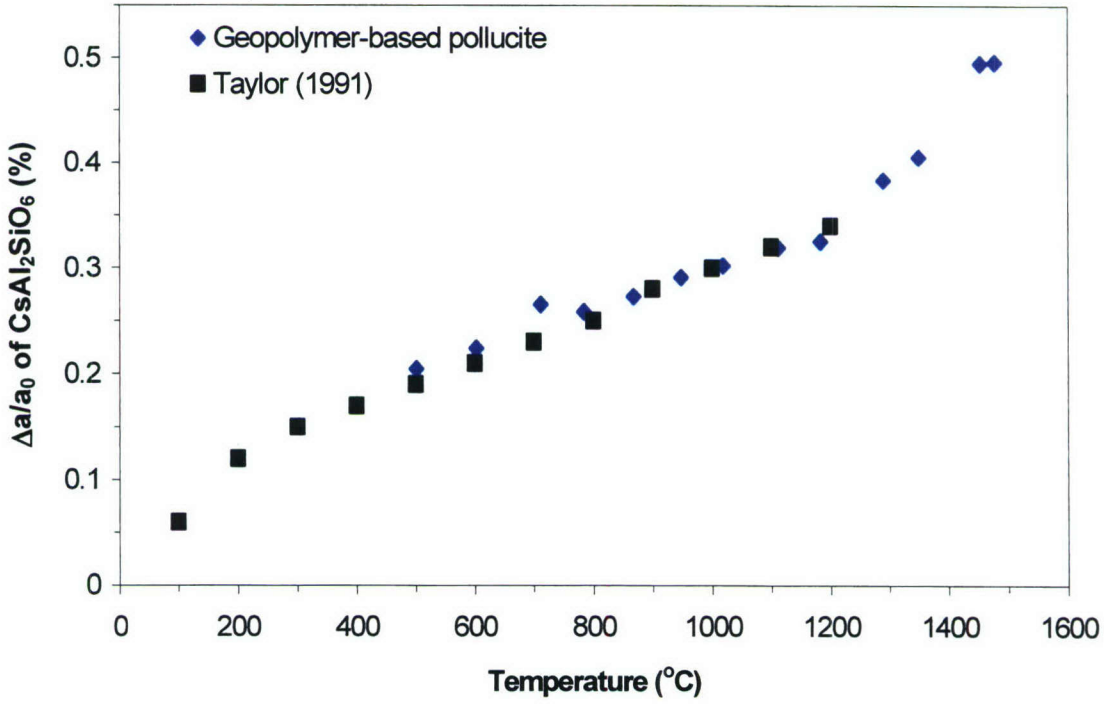

Fig. 5. Thermal expansion of pollucite crystallized from Cs-geopolymer (◆) determined from *in-situ* HTXRD plotted with data reported by Taylor(■)[16]

Discussion

The shift of the diffuse peak of SynMK at 22° 2-theta to 28° 2-theta after reaction with the cesium-silicate solution is similar to the peak shift found when natural metakaolin is converted into geopolymer by reactions with sodium or potassium alkali-silicate solutions.[3-5] The observed diffuse peak at 28° 2-theta for the Cs-geopolymer may indicate that metakaolin-based geopolymers have similar short-ranged structures, regardless of alkali-cation (e.g. Na^+, K^+, Cs^+).

The initial weight loss of the Cs-geopolymer was principally due to water loss; the second region of weight loss, which occurred above 1250°C, was the result of cesia volatilization. The observed onset of cesia loss at 1250°C is in good agreement with work by Hay *et al.* who also reported at the onset of cesia volatilization at 1250°C from pollucite powders.

The thermal expansion of the pollucite crystallized from the Cs-geopolymer was 20% lower than the thermal expansion reported by Taylor, 2.2×10^{-4} $\%\Delta a/a_o$ (500 – 1200°C). The thermal expansion of pollucite is known to be highly dependent on composition and preparation, however.[16, 18, 30] The weight loss above 1250°C corresponded to the rapid increase of the thermal expansion of pollucite. To date, thermal expansions studies conducted on pollucite have not included temperature regimes of cesia volitization. HTXRD from this study indicated that the loss of cesia from pollucite results in a >300% increase of the thermal expansion of pollucite.

DSC indicated that the crystallization temperature of the Cs-geopolymer was approximately 1075°C, which was similar to crystallization temperatures reported for pollucite in glass-ceramics.[11, 23, 24] XRD analysis of geopolymers heated for one hour showed the onset of crystallization at 900°C, although well-developed crystallites were not observed until after soaking at 1000°C for one hour. The difference between the observed crystallization temperatures corresponded to the kinetics of pollucite crystallization (1075°C no soak time, 900°C one hour soak). The presence of a second exotherm at 1170°C is more difficult to explain, however. The second exotherm may be

second crystallization event- DSC measurements showed no specific changes in heat at 1170°C during cooling, however XRD analysis showed no second phases crystallizing from the Cs-geopolymer. No well-defined endotherms were observed while heating the Cs-geopolymer, which might characterize a glass-transition temperature, T_g.

Conclusions

The reaction of cesium silicate solution with SynMK produced a Cs-geopolymer with a diffuse X-ray diffraction peak at 28° 2-theta, characteristic of metakaolin-based geopolymers formed from potassium and sodium silicate solutions. DSC indicated that the crystallization temperature of pollucite from Cs-geopolymer was 1075°C. A second, unaccounted for exotherm, was observed at 1170°C. No endotherms, indicating a T_g were observed from DSC measurements. Ex-situ XRD observed the onset of pollucite crystallization at 900°C after a one-hour soak at temperature. Well-developed crystallites of pollucite were apparent after heating the geopolymer at 1000°C for 1 hour. The thermal expansion characteristics of pollucite crystallized from Cs-geopolymer agreed well with the reported thermal expansion of pollucite. The thermal expansion of the pollucite increased from 1.8×10^{-4} $\%\Delta a/a_o$ (500 – 1180°C) to 6.1×10^{-4} $\%\Delta a/a_o$ (1180 – 1480°C) as a result of cesia volatilization.

References

[1]J. Davidovits, "Geopolymers - inorganic polymeric new materials," *Journal of Thermal Analysis*, **37**[8] 1633-1656 (1991).

[2]H. Rahier, B. VanMele, M. Biesemans, J. Wastiels and X. Wu, "Low-temperature synthesized aluminosilicate glasses .1. Low-temperature reaction stoichiometry and structure of a model compound," *Journal of Materials Science*, **31**[1] 71-79 (1996).

[3]V. F. F. Barbosa, K. J. D. MacKenzie and C. Thaumaturgo, "Synthesis and characterization of materials based on inorganic polymers of alumina and silica: sodium polysialate polymers," *International Journal of Inorganic Materials*, **2**[4] 309-317 (2000).

[4]V. F. F. Barbosa and K. J. D. MacKenzie, "Synthesis and thermal behaviour of potassium sialate geopolymers," *Materials Letters*, **57**[9-10] 1477-1482 (2003).

[5]V. F. F. Barbosa and K. J. D. MacKenzie, "Thermal behaviour of inorganic geopolymers and composites derived from sodium polysialate," *Materials Research Bulletin*, **38**[2] 319-331 (2003).

[6]M. Gordon, J. Bell and W. M. Kriven, "Thermal conversion and micro structural evaluation of geopolymers or "Alkali-bonded ceramics" (ABCs)"; pp. 215-224 in Ceramic Transactions, Vol. 175, *Advances in Ceramic Matrix Composites XI*. Edited by N. P. Bansal, J. P. Singh and W. M. Kriven, The American Ceramic Society, Westerville OH, 2005.

[7]D. W. Richerson and H. F. A., "Synthesis and thermal expansion of polycrystalline cesium minerals," *Journal of the American Ceramic Society*, **55** 269-272 (1972).

[8]I. Yanase, H. Kobayashi, Y. Shibasaki and T. Mitamura, "Tetragonal-to-cubic structural phase transition in pollucite by low-temperature X-ray powder diffraction," *Journal of the American Ceramic Society*, **80**[10] 2693-2695 (1997).

[9]B. Lawrence, G. F. Claringbull and W. H. Taylor, *Crystal Structures of Minerals*. Cornell Cornell University Press, New York, NY. 1965

[10]D. Taylor, "The thermal expansion of the leucite group of minerals," *American Mineralogist*, **53**[9-10] 1476-1488 (1968).

[11]G. H. Beall and H. L. Rittler, "Glass-ceramics based on pollucite"; pp. 301-312 in Advances in Ceramics, Vol. 4, *Nucleation and Crystallization in Glasses*. Edited by J. H. Simmons, D. R. Uhlmann and G. H. Beall, The American Ceramic Society, Columbus, OH, 1982.

[12]R. S. Hay, T. A. Parthasarathy and J. R. Welch, "Creep and stability of pollucite"; pp. 89-104 in Ceramic Transactions, Vol. 52, *Low-Expansion Materials* Edited by D. P. Stinton and S. Y. Limayme, American Ceramic Society, Westerville, OH, 1995.

[13]H. Kobayashi, T. Terasaki, T. Mori, H. Yamamura and T. Mitamura, "Thermal-expansion characteristics of Li-replaced type pollucite (Cs1-XLixAlSi2O6) powder," *Nippon Seramikkusu Kyokai Gakujutsu Ronbunshi-Journal of the Ceramic Society of Japan*, **99**[12] 1274-1276 (1991).

[14]H. Kobayashi, T. Terasaki, T. Mori, H. Yamamura and T. Mitamura, "preparation and thermal-expansion behavior of excess SiO2 pollucite powders," *Nippon Seramikkusu Kyokai Gakujutsu Ronbunshi-Journal of the Ceramic Society of Japan*, **100**[1] 91-93 (1992).

[15]H. Kobayashi, I. Yanase and T. Mitamura, "A new model for the pollucite thermal expansion mechanism," *Journal of the American Ceramic Society*, **80**[8] 2161-2164 (1997).

[16]D. Taylor, "Thermal-expansion data .15. complex oxides with the leucite structure and frameworks based on 6-membered rings of tetrahedra," *British Ceramic Transactions and Journal*, **90**[6] 197-204 (1991).

[17]I. Yanase, H. Kobayashi and T. Mitamura, "Thermal expansion property of synthetic cubic leucite-type compounds," *Journal of the Ceramic Society of Japan*, **108**[1] 26-31 (2000).

[18]I. Yanase, S. Tamai and H. Kobayashi, "Low-thermal-expansion properties of sodium- and lithium-substituted cubic cesium leucite compounds," *Journal of the American Ceramic Society*, **86**[8] 1360-1364 (2003).

[19]I. MacLaren, J. Cirre and C. B. Ponton, "Hydrothermal synthesis of pollucite (CsAlSi2O6) powders," *Journal of the American Ceramic Society*, **82**[11] 3242-3244 (1999).

[20]P. L. Bollin, "Glass formation in the system Cs2O-Al2O3-SiO2," *Journal of the American Ceramic Society*, **55**[5] 483 (1972).

[21]J. F. MacDowell, "Semicrystalline body and method of making It," U.S. Patent 3236662 (1966).

[22]N. Miyagawa, N. Shinohara and M. Okumiya, "Synthesis and fabrication of pollucite glass-ceramics by using arc melting technique," *Journal of the Ceramic Society of Japan*, **107**[8] 762-765 (1999).

[23]R. L. Bedard, R. W. Broach and E. M. Flanigen, "Leucite-pollucite glass ceramics: A new family of refractory materials with adjustable thermal-expansion"; pp. 581-587 in Materials Research Society Symposium Proceedings, Vol. 271, *Better Ceramics Through Chemistry V*. Edited by M. J. Hampden–Smith, W. G. Klemperer and C. J. Brinker, 1992.

[24]M. A. Hogan and S. H. Risbud, "Gel-derived amorphous cesium-aluminosilicate powders useful for formation of pollucite glass-ceramics," *Journal of Materials Research*, **6**[2] 217-219 (1991).

[25]M. Gordon, J. L. Bell and W. M. Kriven, "Comparison of naturally and synthetically derived, potassium-based geopolymers," *Ceram Trans*, **165** 95-106 (2004).

[26]M. A. Gulgun, M. H. Nguyen and W. M. Kriven, "Polymerized organic-inorganic synthesis of mixed oxides," *Journal of the American Ceramic Society*, **82**[3] 556-560 (1999).

[27]D. C. Palmer, M. T. Dove, R. M. Ibberson and B. M. Powell, "Structural behavior, crystal chemistry, and phase transitions in substituted leucite: High-resolution neutron powder diffraction studies," *American Mineralogist*, **82**[1-2] 16-29 (1997).

[28]L. F. Siah, W. M. Kriven and J. Schneider, "In situ, high-temperature, synchrotron, powder diffraction studies of oxide systems in air, using a thermal-image furnace," *Measurement Science & Technology*, **16**[6] 1291-1298 (2005).

[29]P. Sarin, W. Yoon, K. Jurkschat, P. Zschack and W. M. Kriven, "Quadruple Lamp Furnace for High Temperature (up to 2050K) Synchrotron Powder X-Ray Diffraction Studies in Air," *Review of Scientific Instruments*, (submitted).

[30]D. Taylor, "The thermal expansion behaviour of framework silicates," *Mineralogical Magazine*, **38**[297] 593-604 (1972).

Section H - Pair Distribution Function Analysis

Introduction

With the increasing worldwide availability of synchrotron beam lines and analytical software, the X-ray pair distribution function (PDF) method has become a significant tool in the analysis of complex or disordered materials over the past several years.[1-4] by making use of the full range of data provided by a powder diffraction experiment – diffuse scattering as well as Bragg peaks – valuable information regarding short- to medium-range ordering in amorphous or semi-crystalline materials becomes accessible. The PDF, $G(r)$, is defined as the Fourier sine transform of the structure function $S(Q)$, according to Equation (1).[2]

$$G(r) = \frac{2}{\pi}\int_0^\infty Q\left[S(Q)-1\right]\sin(Qr)\,dQ \qquad (1)$$

Here $Q = \frac{4\pi\sin\theta}{\lambda}$, with θ being the scattering angle and λ the wavelength of the incident radiation. $S(Q)$ is calculated from experimental scattering data (X-ray scattering in this case, although the use of neutrons is also popular) according to Equation (2).[1]

$$S(Q) = \frac{I_{el,coh}(Q) + \left[\left\langle f(Q)\right\rangle^2 - \left\langle f(Q)^2\right\rangle\right]}{\left\langle f(Q)\right\rangle^2} \qquad (2)$$

Here $I_{el,coh}(Q)$ is the observed elastic and quasi-elastic coherent scattering intensity, $\langle\ \rangle$ represents a compositional average, and $f(Q)$ is the atomic scattering amplitude. Calculation of $I_{el,coh}(Q)$ from X-ray scattering data requires corrections for experimental details such as detector dead-time, container background and X-ray polarization, as well as various other scattering events, in particular Compton scattering. These corrections are among those implemented by widely available software packages including PDFGETX2

[5], rendering the PDF method a relatively accessible, if complex, means of analyzing the structures of a wide range of crystalline and non-crystalline materials.

It is also possible to calculate a theoretical $G(r)$ from a known structure by Equation (3), thereby enabling real-space Rietveld refinement of an experimental data set.[6]

$$G_{calc}(r) = -4\pi r\rho_0 + \frac{1}{r}\sum_{i,j}\frac{b_i b_j}{\langle b\rangle^2}\delta(r - r_{ij}) \quad (3)$$

In this equation, ρ_0 is the average number density of the sample, b_k is the atomic form factor for X-rays, and the sum is carried out over all atom pairs i,j. The real-space Rietveld method is now being used to analyze increasingly complex structures, in particular disordered zeolites[7, 8] and poorly-crystalline nanocomposites[9], corresponding to improvements in the available software.

PDF analysis is particularly valuable in the case of amorphous materials, where structural details are inaccessible by more traditional diffraction methods due to the absence of Bragg peaks. Some geopolymers, particularly those with Si/Al ratios close to 1.0, cured at elevated temperatures, and/or containing greater than a stoichiometric amount of alkali metal cations, have been shown to contain very small zeolite crystals[10-12]. Higher Si/Al ratio materials such as those investigated here are widely observed to be amorphous on a micron length scale but relatively ordered on an atomic length scale[13, 14]. A limited PDF study of sodium silicate-metakaolin geopolymers has previously been conducted[11], however that work was focused solely on room-temperature behavior and trends across different compositions, and also only presented data up to a length scale of approximately 5Å. The current investigation therefore provides the first reported data directly relating room-temperature and high-temperature structural features of geopolymers on an atomic length scale.

Pollucite is a naturally-occurring mineral which has previously been synthesized by a variety of techniques including hydrothermal[15] or dry oxide-based[16] syntheses, high-

temperature ion exchange from leucite[17], and crystallization from sol-gel derived precursors.[18, 19] Significant industrial interest in pollucite is based around its use as an encapsulate for radioactive ^{137}Cs [16, 19, 20], or as a refractory material due to its very low coefficient of thermal expansion.[21] Here, the synthesis of pollucite from a geopolymer precursor is investigated. This has been shown to be an effective method for synthesis of phase-pure pollucite [22]. However, the primary aim of this investigation is to use this process as a means of analyzing the original geopolymer structure from which the pollucite is formed. The PDF method is ideal for this application due to its sensitivity to the short-range order known to exist in geopolymers.[14] Aspects of the transformation process will also be analyzed, using the PDF method to obtain information complementary to that obtainable by powder XRD and other methods. Hess *et al.*[20] investigated radiation damage in pollucite by the PDF method (among other techniques), but carried out experiments at 50K and with a maximum Q value of only $12Å^{-1}$. The current investigation is conducted at room temperature and with a significantly higher Q_{max} value, giving higher-resolution data and structural details that are more specifically relevant to read-world conditions.

Experimental Procedure

"Synthetic metakaolin" (SynMK) [23] was prepared by the organic steric entrapment method [24-26], as follows: A 50 wt. % solution of 98 % aluminum nitrate nonahydrate (Fisher Scientific, Pittsburgh, PA) was mixed under low heat with a 24.5 wt. % suspension of colloidal silica, Ludox SK (Grace Division, Columbia MD) in a lithium aluminosilicate glass-ceramic container. After one hour of stirring, a 5 wt. % solution of Celvol polyvinyl alcohol (PVA) (Celanese Chemicals, Dallas TX) was added to the mixture. The final molar ratio of the mixed solution was $2Al_2O_3•4SiO_2•7PVA$. Infrared heating lamps were set above the mixture and left operating overnight, while the mixture was simultaneously stirred and dried by a hot/stir plate. After sufficient drying (approximately 12 hours) the solution became a uniform yellow cake, which was pulverized using a mortar and pestle.

The resulting powder was then calcined at 800°C for 1 hour in a 650 Isotemp Furnace (Fisher Scientific). After calcination, the powder color changed to white. The powder was then milled with isopropyl alcohol in a Fritsch Pulverisette planetary micro mill using 8 mm ceria stabilized zirconia media (Fritsch Gmbh, Idar-Oberstein, Germany). The slurry was dried and baked at 600°C for 5 hours to remove all organics from the surface of the SynMK and sieved to -100 μm. The surface area of the SynMK was 196 m^2/g, determined from the best fit of seven datum points using the BET method with an Autosorb-1 Surface Area and Pore Size Analyzer (Quantachrome Instruments, Boynton Beach FL).

The cesium silicate activating solution was derived from cesium hydroxide monohydrate (99.8%, Chemetall Chemical Products Inc., Berkeley Heights NJ), fumed silica (Cab-o-sil, Cabot, Tuscola IL), and de-ionized water. The composition of the solution was $Cs_2O{\bullet}2SiO_2{\bullet}10\ H_2O$. Using a polypropylene container, SynMK was added incrementally to the alkali-silicate solution while mixing with a high speed dispersion mixer. During mixing, the slurry was cooled with an ice water bath to prevent rapid setting of the geopolymer. After mixing for approximately 15 minutes, the resulting slurry was poured into chemically resistant plastic tubing, sealed using rubber stoppers, and cured at 60°C for 48 hours. The hardened geopolymer was then removed from the tubing; ground with a mortar and pestle and sieved to -45μm.

SynMK and the geopolymer product were characterized using a Rigaku D/Max-b (Phillips) X-ray diffractometer using Cu $K_{\alpha 1}$ radiation, and both were found to be amorphous. ICP elemental analysis was done using an OES Optima 2000 DV (Perkin Elmer, Norwalk CT), and showed the SynMK and geopolymer to have molar compositions of $Al_2O_3{\bullet}1.96SiO_2$ and $1.23Cs_2O{\bullet}Al_2O_3{\bullet}3.95SiO_2$ respectively. The geopolymer was synthesized slightly rich in Cs compared to stoichiometric pollucite ($Cs_2O{\bullet}Al_2O_3{\bullet}4SiO_2$) to allow for some vaporization of Cs during heating, as was observed for K during high-temperature crystallization of leucite from oxide powders.[17] For the sake of simplicity, the composition of all geopolymer and geopolymer-derived samples will be denoted in this work as $CsAlSi_2O_6$.

Heat-treatment of crushed samples was carried out in a laboratory furnace, with a heating rate of 5°C/min, a soak time of 60 min, and a cooling rate of approximately 2°C/min. Samples were heated to 300°C, 500°C, 800°C, 900°C, 1000°C and 1400°C

X-ray scattering data were collected at Beamline X7A of the National Synchrotron Light Source (NSLS), Brookhaven National Laboratory, Upton NY, using a Kevex solid-state detector. Samples were studied in transmission geometry in a 0.5mm glass capillary. For the unheated, 500°C, 1000°C and 1400°C geopolymer samples, a wavelength of 0.4018Å was used, with a Q-range of 0.20-22.0Å^{-1}. For the 300°C, 800°C and 900°C samples, the wavelength was 0.3999Å, and scans were conducted from 0.20-25.0Å^{-1}. Each data set presented is taken as the average over two merged scans. A step size of 0.02Å^{-1} was used for amorphous (<850°C) samples, and 0.01Å^{-1} for samples showing some crystallinity (>850°C), with a 4.00s count time used in all cases. Data processing and PDF generation were conducted using PDFGETX2[5]. PDFFIT[6] was utilized for theoretical PDF calculation and real-space Rietveld refinement.

Results and Discussion

PDF calculation

Figure 1 shows the normalized X-ray scattering data for cesium aluminosilicate geopolymers heated to various selected temperatures, and Figure 2 is an expanded version of the low-Q region of the same data. The unheated and 500°C samples (Figure 1a,b) are seen to be X-ray amorphous, and essentially no change is observed upon heating from room temperature to 500°C. The 900°C sample is beginning to show signs of crystalline structure, which are particularly noticeable upon inspection of Figure 2. The 1000°C sample is significantly crystalline pollucite but also contains a discernible amorphous 'hump' underneath the Bragg peaks at around 2Å^{-1}, and the 1400°C sample appears to be essentially crystalline.

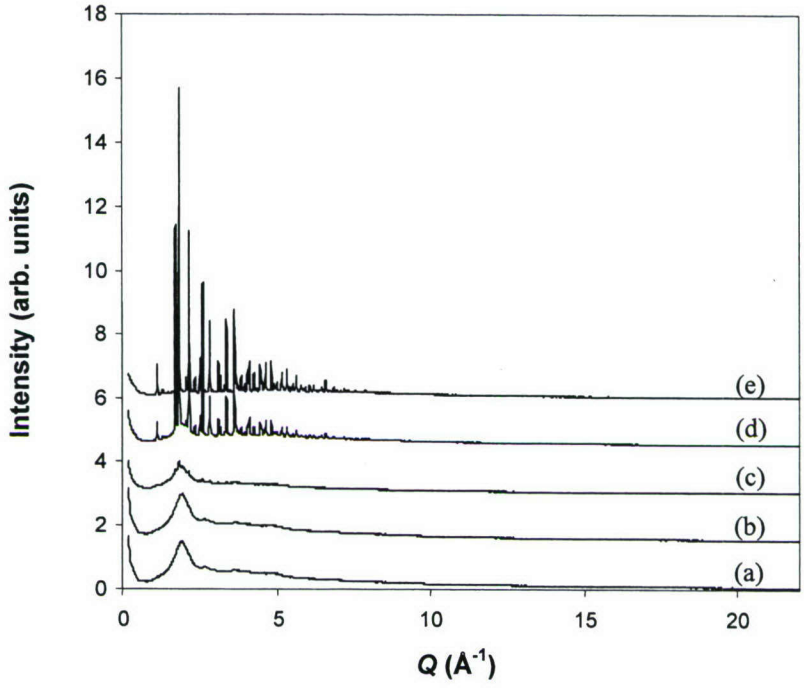

Figure 1. Synchrotron X-ray scattering results for $CsAlSi_2O_6$ geopolymers heated to: (a) unheated, (b) 500°C, (c) 900°C, (d) 1000°C, and (e) 1400°C. Each data set is the merged result of two scans following background subtraction, dead time correction and normalization by monitor counts. Successive plots are vertically offset by 1.5 units.

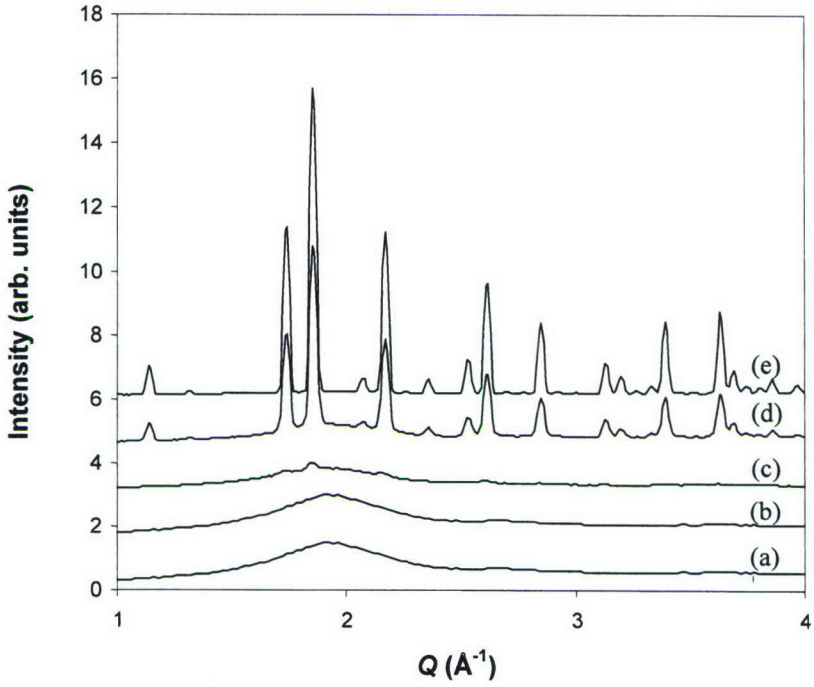

Figure 2. Expanded version of the Q = 1-4Å region of Figure 1

Using the PDFGETX2 software[5] to apply the required corrections for X-ray absorption, Compton, Laue and multiple scattering, X-ray polarization then allows $S(Q)$ to be calculated for each sample according to Equation , and converted to the PDF function $G(r)$ by taking the Fourier sine transform as shown in Equation . shows the results of this analysis for all available data sets. It must also be noted that a Gaussian damping function of width 5Å^{-1} was applied in PDFGETX2 prior to taking the Fourier transform, to remove spurious oscillations due to termination effects and other minor issues in data treatment. This damping procedure has been shown not to decrease the actual error associated with each point in the PDF, but rather to serve a largely cosmetic purpose.[27] However, as the primary aim of this investigation is to use the PDFs to observe the change in structure upon heating of the geopolymer, removal of unnecessary ripples which may vary between samples due to experimental setup effects is more important than detailed error analysis, and so damping is in fact desirable in this instance.

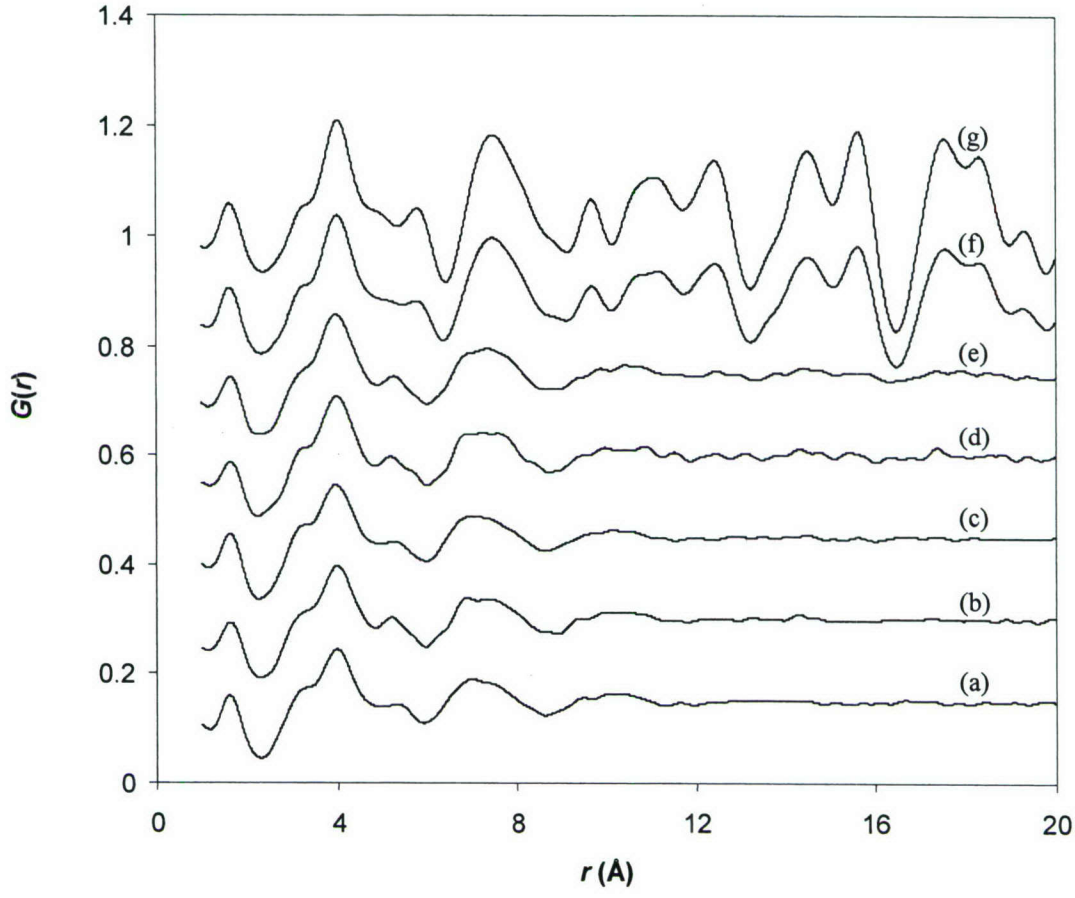

Figure 3. PDFs of $CsAlSi_2O_6$ geopolymers heated to: (a) unheated, (b) 300°C, (c) 500°C, (d) 800°C, (e) 900°C, (f) 1000°C, and (g) 1400°C. Successive plots are vertically offset by 0.15 units.

Comparison of the results presented in Figure 3 to those in Figure 1 outlines the value of the PDF method in the investigation of geopolymer structure and the effects of heating. The differences between the PDFs obtained at up to 500°C (Figure 3a-c) are less than the experimental uncertainty. At 800°C (Figure 3d), some structural changes are beginning to be observable – in particular, the peak at ~7Å appears to be beginning to move to slightly higher *r*, matching its position in the crystalline pollucite structure (Figure 3g). Also, the increased amplitude of the oscillations in $G(r)$ above 10Å shows that these small peaks do in fact match many of the peak positions in the crystalline structure – in particular, the 'ripples' at 14.6, 15.7, 17.5 and 19.5 match peaks in Figure 3g quite closely. The fact that these small peaks are also present in the 900°C sample (Figure 3e) corresponds to the

observation of small Bragg peaks for the same sample in Figure 2c. However, the PDF method is particularly valuable in identifying the changes in structure on an even shorter length scale than this. Figure 4 is an expanded view of the region around $r = 4$Å, with the vertical offset removed from all data sets to enable direct comparison.

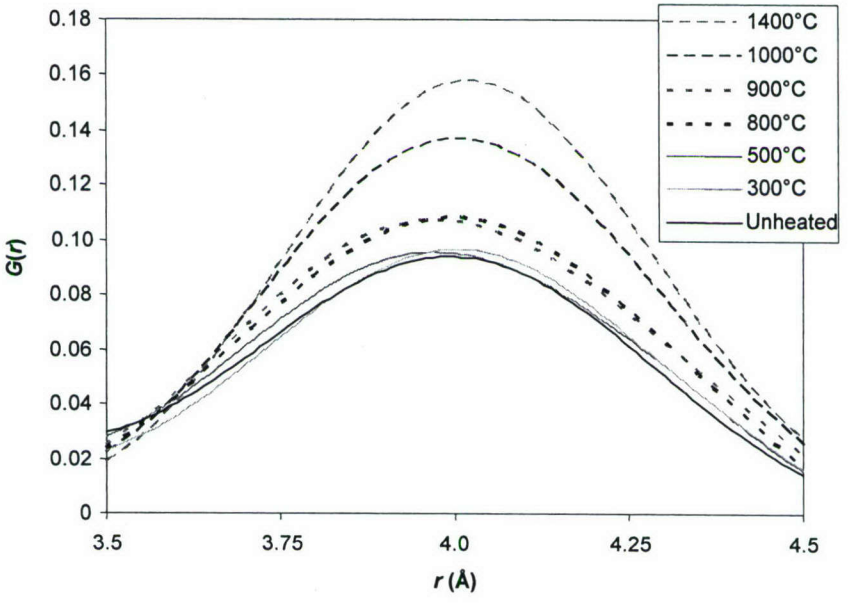

Figure 4. Expanded view of PDFs around $r = 4.0$Å.

From Figure 4, it is clear that the very short-range ordering within the geopolymer structure behaves somewhat differently to the longer-range crystallinity. The peak at ~4.0Å, in the region corresponding to Cs-T and next-nearest-neighbor T-O correlations (T: tetrahedral Si or Al) as will be discussed in more detail later in this paper, shows a distinct change from 500°C to 800°C, growing larger and having its 'center of mass' shifting to higher r. The shift in the center of mass is most clearly observable in a direct comparison between the 800°C and 900°C data sets, which have approximately the same amplitude but significantly different peak shapes. With the progressive increase in crystallinity upon heating to 1000°C then to 1400°C this peak becomes relatively sharper and more intense, corresponding to the increased order in the more highly crystalline structure. The observation of crystallization of the amorphous powder primarily occurring at or around 1000°C is in agreement with previous results on the crystallization

temperature of pollucite from gel-phase or clay precursors [16], and from sol-gel derived powders [28].

PDF refinement

Over the past 70 years, structural assignments for pollucite derived from various sources have been published. Some of these are summarized in Table 1. Palmer *et al.*[17] were the first workers to report a tetragonal room-temperature structure for pollucite based on neutron powder diffraction, with the transition from the high-temperature cubic *Ia-3d* phase observed at around 373K. Yamase *et al.*[18] later reported a cubic room-temperature phase, with a transition to a tetragonal $I4_1/acd$ phase at 248K. An $I4_1/acd$ phase is generally observed in the decreasing-temperature transition from cubic to tetragonal in leucite ($KAlSi_2O_6$)[17, 19], but no other investigators have observed this space group in the pollucite system. Xu *et al.*[19] used synchrotron XRD to refine structural parameters in the $I4_1/a$ space group, and found somewhat different unit cell dimensions to those calculated by Palmer *et al.*, with a predicted cubic-tetragonal transition temperature of approximately 301K. Gordon *et al.*[22] studied geopolymer-derived pollucite (crystallized at 1400°C) by Rietveld refinement of synchrotron XRD results, and observed a cubic (*Ia-3d*) structure at room temperature. Gallagher and McCarthy[16] synthesized pollucite by high-temperature crystallization from a range of different oxide precursors, and observed cubic structures with lattice parameters that varied slightly depending on the preparation method. This variation was attributed to minor stoichiometric variations, with slightly Cs-deficient structures showing a smaller unit cell size.

These apparent discrepancies in symmetry, unit cell dimensions and transition temperatures have been ascribed to possible slight differences in sample composition or Si/Al ordering due to different synthesis conditions[19]. Earlier X-ray investigations may not have had sufficient resolution to observe the very slight tetragonal distortion in this material due to instrumental limitations. Also, the sample used by Palmer *et al.*[17] contained a small (~1%) amount of both K and Ca, which may have contributed to an

increased tetragonal distortion. However, one of the samples of Gallagher and McCarthy [16] was found to be cubic despite containing significantly more cationic contaminants that the sample of Palmer *et al.*[17].

Table 1. Summary of published structures for pollucite at or near room temperature

	Náray-Szabó (1938)[29]	Newnham (1967)[30]	Taylor & Henderson (1968)[21]	Palmer *et al.* (1997)[17]	Yamase *et al.* (2000)[18]	Xu *et al.* (2002)[19]	Gordon *et al.* (2006)[22]
a,b (Å)	13.74	13.682	13.673	13.65199	13.6645	13.6731	13.6744
c (Å)	13.74	13.682	13.673	13.72126	13.6645	13.6921	13.6744
Vol (Å^3)	2593.9	2561.23	2556.2	2557.325	2551.416	2559.77	2556.965
Space group	*Ia-3d*	*Ia-3d*	-	$I4_1/a$	*Ia-3d*	$I4_1/a$	*Ia-3d*
Source	Natural	Natural	Synthetic (gel)	Synthetic (ion exchange)	Synthetic (dry oxides)	Synthetic (sol-gel)	Synthetic (geopolymer)
Temperature	-	-	298K	298K	273K	298K	298K

Due to this uncertainty regarding the exact structure and unit cell dimensions of pollucite, refinements were carried out in PDFFIT for both cubic and tetragonal structures. The fact that the tetragonal distortion of pollucite is so small makes it impossible to choose unequivocally between the two possibilities from the PDF method, so results for both are presented in Table 2 and in Figure 5. For cubic symmetry, the structure was refined starting from the structures of Náray-Szabó[29] and Yamase *et al.*[18], with almost identical results as shown in Table 2. For tetragonal symmetry, refinements were carried out using the structures of Palmer *et al.*[17] and of Xu *et al.*[19] as starting points. In all refinements, isotropic temperature factors B_{iso} were assumed to be identical for all atoms of a particular element within the structure[19]. Individual atom positions within the unit cell were not refined, but rather the lattice parameters and temperature factors only were investigated.

Table 2. Summary of structure refinement results for each symmetry type.

	Cubic (*Ia-3d*)		Tetragonal ($I4_1/a$)	
Starting structure reference	Náray-Szabó (1938)[29]	Yamase *et al.* (2000)[18]	Palmer *et al.* (1997)[17]	Xu *et al.* (2002)[19]
a, b (Å)	13.626(4)	13.625(4)	13.617(21)	13.614(30)
c (Å)	13.626(4)	13.625(4)	13.634(40)	13.622(50)
PDFFIT R-value ($1.5 < r < 20$Å)	0.1824	0.1787	0.2572	0.1353

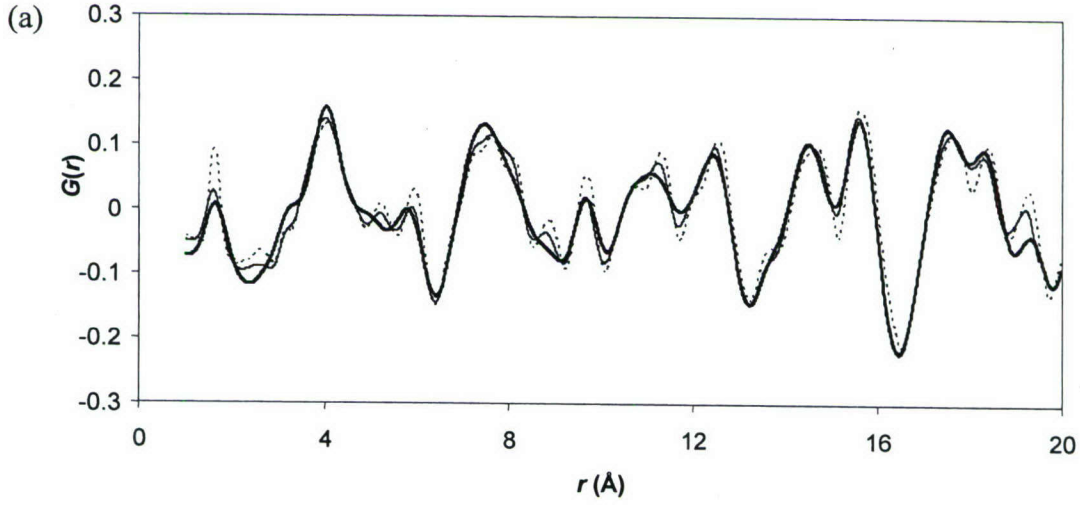

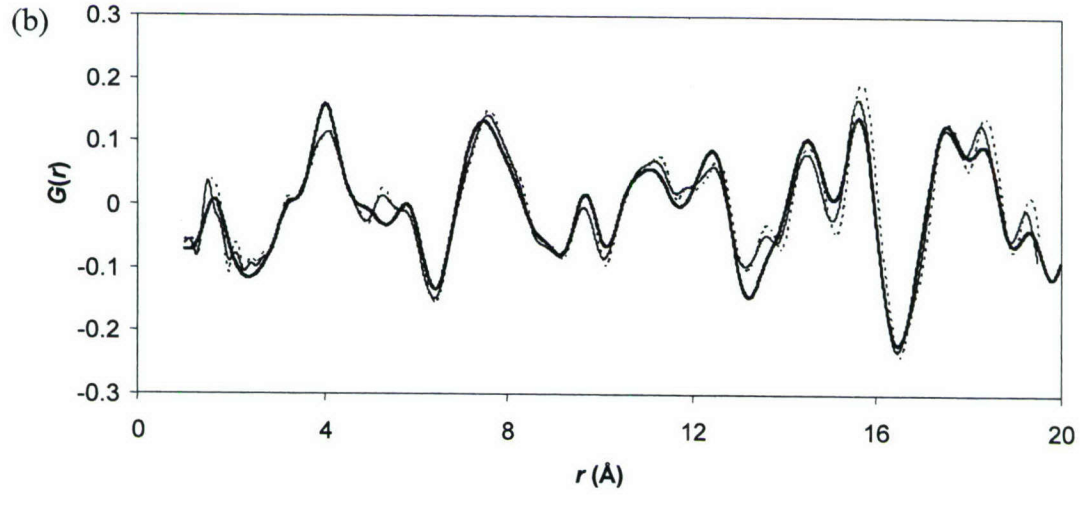

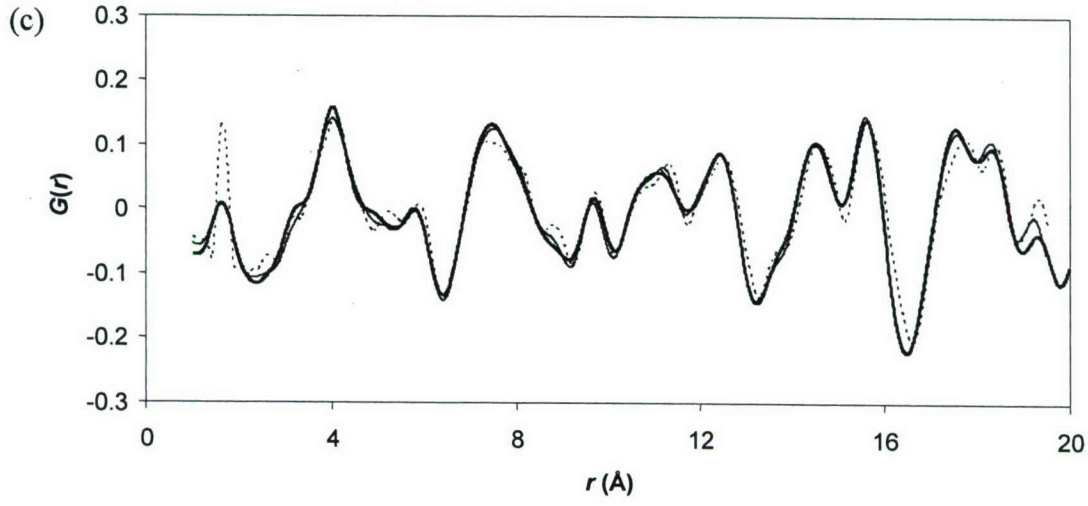

Figure 5. Refined PDFs (thin solid lines) compared to experimental data (thick solid lines), and to those calculated from published structures (dotted lines): (a) cubic symmetry (structure of Yamase *et al.*[18]), (b) tetragonal symmetry (structure of Palmer *et al.*[17]), (c) tetragonal symmetry (structure of Xu *et al.*[19]). For each plot, the refined PDF was calculated starting from the structure shown.

From the results presented in Table 2, it is clear that the real-space Rietveld refinement converged satisfactorily for the cubic case, giving almost identical results regardless of the starting structure, but slightly less so for the tetragonal case. This is shown by the higher uncertainties in the tetragonal lattice parameters (errors shown are estimated by PDFFIT during refinement). There is also some variability in the refined B_{iso} parameters (not shown) in the tetragonal cases. Real-space refinement of such a large unit cell (160 atoms) is a non-trivial procedure, and cannot be undertaken without some prior understanding of the system of interest. In particular, the best R-value shown in Table 2 was obtained by refinement of the tetragonal structure using the parameters of Xu *et al.*[19]. However, this structure could not be directly reached by refining from the published structure (which instead resulted in an unphysical structure with $a/c < 1$). Rather, the structure had to be refined starting from the published parameters using only the long-r ($10 < r < 20$Å) component of the PDF data, forcing the a/c ratio to take a reasonable value. Only then was the full range of the PDF data was used, refining from this calculated 'intermediate-refined' structure, which gave the results presented in Table 2. Difficulty in refining tetragonal structures for pollucite has also been reported by Xu *et al.*[19], who were unable to obtain convergence in a reciprocal-space refinement of a

tetragonal structure starting from the parameters of Palmer *et al.*[17], and instead used a cubic structure as the starting point for refinement of their tetragonal structure.

Figure 5 shows that, as expected, the lattice parameters of the refined structures fit the experimental data much better than do the values obtained from the literature. This is particularly visible in the (negative) peak at $r \sim 16.5$Å, where the dotted line representing the literature structure is seen to fall in a distinctly different position to the experimental PDF in all three plots. The refinement starting from the structure of Palmer *et al.*[17] (Figure 5b) is visibly a poorer fit than either of the other refined structures, in agreement with the higher R value for this refinement (0.2572) as shown in Table 2. As a point of comparison, the R values for the published structures are 0.3143 (cubic, structure of Yamase *et al.*[18], Figure 5a), 0.3363 (tetragonal, structure of Palmer *et al.*[17], Figure 5b), and 0.2828 (tetragonal, structure of Xu *et al.*[19], Figure 5c) respectively. The marginally better fit obtained by refinement under tetragonal symmetry (as measured by the r values in Table 2) is not unexpected, given the increased number of degrees of freedom in this refinement. However, the greatly increased error estimates in this refinement mean that this cannot be definitively stated to be the actual structure of the material, given that the refined cubic structure actually falls within the range of the error estimate from the tetragonal refinement. Given that the primary aim of this investigation is to use the PDF method to elucidate the room-temperature geopolymer structure rather than to undertake detailed analysis of the structure of pollucite, this level of accuracy is more than sufficient here.

It must also be noted that Si/Al ordering has not been described explicitly in the PDF refinement process. A trend towards avoidance of Al-O-Al bond formation has been observed in both crystalline[31] and amorphous[14, 32] aluminosilicates. An NMR study of the leucite-pollucite group of materials has also shown some slight ordering behavior above that which is required for Al-O-Al avoidance[33], which was attributed to "Dempsey's rule"-type behavior (minimization of Al-O-Si-O-Al linkages) [34]. However, given that the X-ray scattering and absorption properties of Si and Al are very similar, the resolution of

the current experiments was not sufficient to allow features due to these two atom types to be distinguished from each other. To resolve such features, Petkov *et al.*[35] conducted experiments with Q_{max} = 40Å^{-1}, and at a temperature of 20K to minimize thermal vibrations. Rowles [11] used Q_{max} = 21Å^{-1} at a temperature of 15K, and was only able to distinguish the Si-O and Al-O bond lengths from each other by careful deconvolution of the final PDFs. Given that the experimental work reported here was undertaken at room temperature, thermal motion of the atoms will render the Si-O and Al-O peaks indistinguishable. The Si and Al atoms present within the unit cell have therefore been distributed randomly across the tetrahedral cation sites, and are treated as a single "T" atom, with characteristics ⅔ Si and ⅓ Al, for the purposes of detailed PDF analysis.

Short-range structure and partial PDFs

Having refined a unit cell structure for the pollucite phase formed by high-temperature crystallization of a cesium aluminosilicate geopolymer, decomposition of the refined PDF into partial PDFs will provide valuable information regarding the identities of each peak in the room-temperature geopolymer structure. The structure that has been selected for this step of the analysis is the one calculated by refinement starting from the tetragonal structure of Xu *et al.*[19] (Figure 5c), as this has the lowest *R*-value and so provides the best fit to the experimental pollucite structure. However, given the relative similarity of all the structures presented in Table 2, it is clear that the other refined structures would also provide similar results. The partial PDF decomposition of this structure, calculated using PDFFIT, is shown in Figure 6.

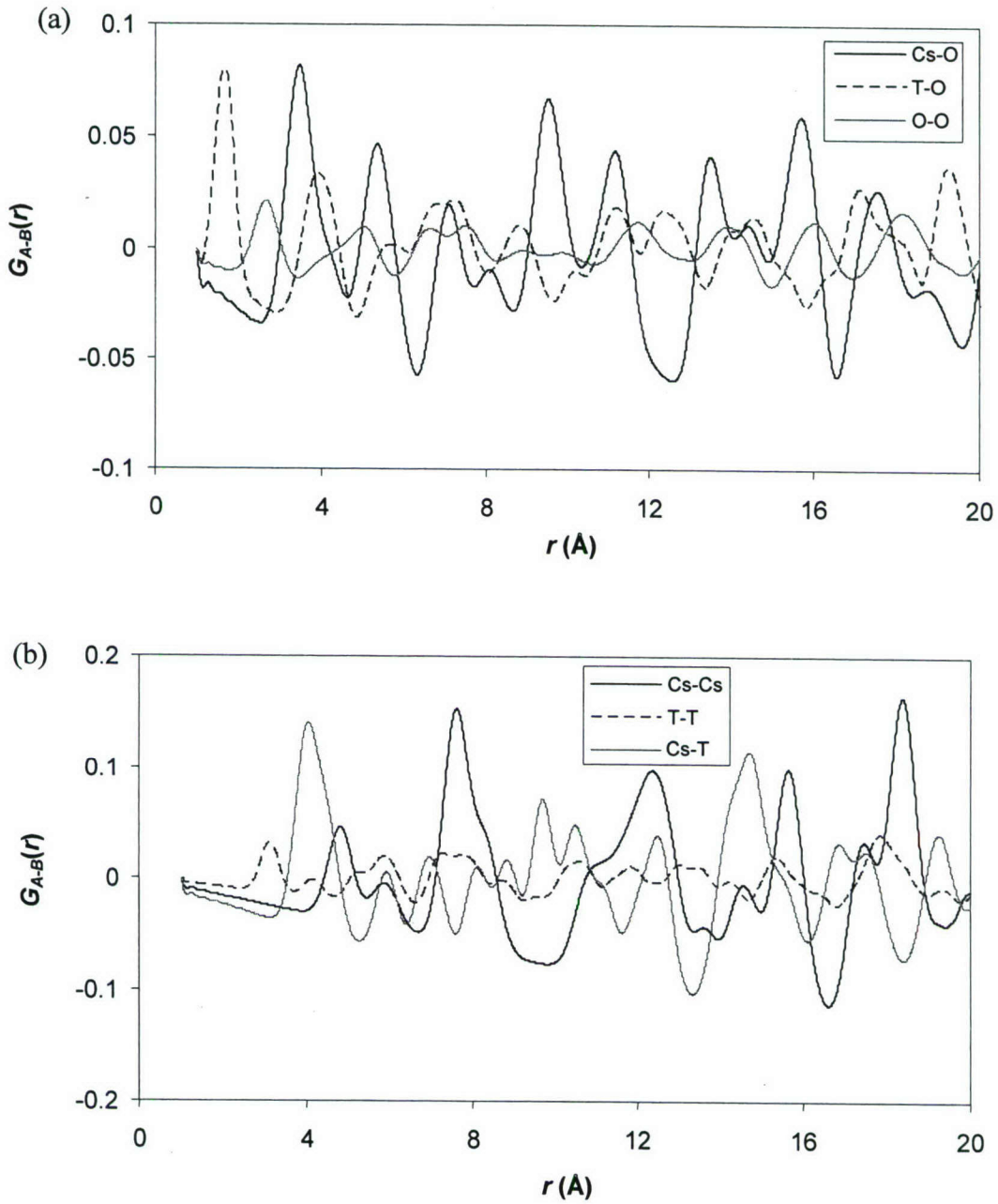

Figure 6. Partial PDF decomposition of the refined pollucite structure: (a) correlations involving O, (b) correlations not involving O. Note the different vertical scales in (a) and (b).

Using these partial PDFs, the relationship between the amorphous room-temperature geopolymer phase and the pollucite formed from it at elevated temperature may now be applied as a means of analyzing geopolymer structure. Specifically, the low-*r* region of

the geopolymer PDF may be fitted as a linear combination of the partial PDFs, and the relative contributions of each atomic pair to the overall structure described in relation to their contributions to the pollucite structure. While it is known that the full PDF is not exactly given by simply summing the contributions of the partial PDFs[2], using this an approximation provides a level of accuracy sufficient for the semi-quantitative analysis conducted here. The region $1.2 < r < 5.0$Å was used as the basis for analysis, as it is the region in which the PDFs shown in Figure 3 displayed significant similarities over the entire temperature range studied. Scale factors for the linear combination of the particle PDFs were calculated by a least-squares fit to the experimental data using the Microsoft Excel Solver package. Figure 7 shows the results of this analysis, and the scale factors used are presented in Table 3. A set of scale factors similarly fitted to the pollucite PDF data are also presented in Table 3 to provide a measure of the accuracy of the linear-combination approximation.

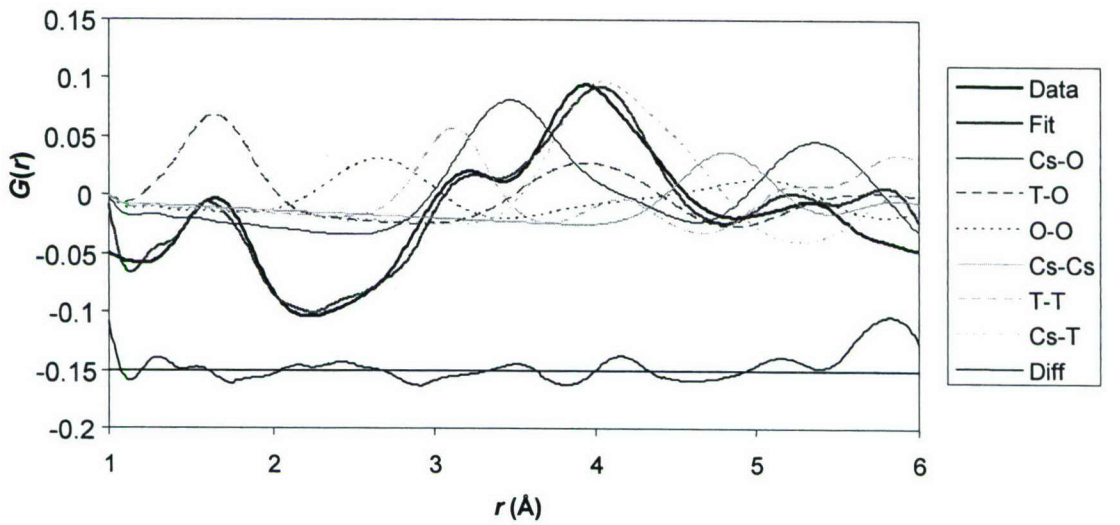

Figure 7. Partial PDFs (thin light or dark gray lines) fitted to the experimental PDF for the room-temperature geopolymer phase (thick lines), with a difference plot (thin black line) offset by -0.15 units.

Table 3. Scale factors for each partial PDF in Figure 7, and for the pollucite structure.

Element pair	Scale factors	
	Pollucite	Geopolymer
T-O	0.963	0.835
O-O	0.985	1.474
Cs-O	0.977	0.993
T-T	1.449	1.795
Cs-T	1.050	0.687
Cs-Cs	0.924	0.810

Comparison between the two set of scale factors in Table 3 provides significant insight into the relative extents of disorder in each atom pair in the heated and unheated geopolymer structures. The fact that almost all the scale factors for pollucite are close to 1.0 shows that approximating the PDF by linear combination of partial PDFs is relatively accurate. The anomalously high scale factor for the T-T correlation is due primarily to the fact that the shoulder in the experimental PDF at ~3.1Å is seen from Figure 5c to be described somewhat poorly by the refined structure. The position of this shoulder corresponds to the main peak in the T-T correlation (Figure 6b), so the high scale factor for this peak is largely an artifact due to the original refinement procedure.

The most significant point that can be drawn from Table 3 is that, while the Cs-O correlation is largely unchanged, the Cs-T and Cs-Cs correlations are much less strong in the amorphous geopolymer than in pollucite. While the Cs^+ cations in pollucite are sitting in strictly-defined positions within the channels in the crystal structure, this is obviously true to a much lesser extent in the less-ordered geopolymer. Cs^+ will still be associated with bridging oxygen atoms within the geopolymer network structure, as was observed for Na^+ by Rowles[11], and the strength of this association will be largely unchanged by the relative crystallinity of the overall structure, leading to an unchanged scale factor for the Cs-O correlation. However, the arrangement of the framework cations around the Cs^+ cation, as well as the arrangement of the Cs^+ cations with respect to each other within the structure, will be significantly less ordered in the amorphous structure. It is also clear

from Figure 7 that the mean Cs-T distance (peak at ~4.0Å) is somewhat shorter in the amorphous geopolymer than in the crystalline pollucite. This is the primary reason for the shift in this peak shown in Figure 4, and may be related to the rapid formation of the geopolymer structure during curing of geopolymers made from synthetic aluminosilicate powders. This very fast setting will mean that some atoms are necessarily trapped in less-than-ideal environments, in this case possibly having less separation between the Cs^+ cations and the highly charged network cations than is structurally ideal. Heating and crystallization will then allow these atoms to take on a more favorable, more separated configuration within the pollucite structure. It is not clear why the O-O correlation should be stronger in the geopolymer than in pollucite, particularly given that the T-O correlation is slightly weaker.

Implications for the current understanding of geopolymer structure

Geopolymers are known to be comprised of a gel-phase binder[10, 36], with possible inclusions of nanocrystallites (often zeolitic in nature)[12] and/or unreacted solid precursor particles[10] depending on the compositions, synthesis conditions and precursor choice. The system selected for investigation here was designed specifically to minimize the level of these inclusions present, with a high-silica composition and low-temperature curing favoring amorphicity[37], and a synthetic solid precursor previously observed to give a very high extent of reaction.[23] It can therefore be confidently asserted that the structure observed is in fact representative of the binder phase within a cesium aluminosilicate geopolymer. The fact that the very short-range order within this binder phase significantly resembles that observed in the crystalline pollucite structure adds further weight to the description of the gel as being similar to 'zeolite precursor' gels.[12]

The absence of any coherent structure in the gel beyond ~8Å, as shown in Figure 3, is consistent with the widely-noted amorphicity of geopolymer gels, and the PDF method thus provides the first direct measure of the length scale on which the structural ordering in geopolymers is observable. A ^{29}Si MAS NMR investigation [38] showed that framework ordering was present on a nearest-tetrahedral-neighbor length scale (~3Å), and a

statistical thermodynamic model developed from those data suggested that some order may extend to the next-nearest-tetrahedral sites (~5-6Å).[14] However, those data were only able to describe the ordering of the tetrahedral cations within the framework, not in the topology of the framework itself. The results of PDF analysis therefore provide a valuable complement to the data obtainable by NMR, and when combined will give a holistic view of the geopolymer gel in terms of both structural and chemical ordering, as well as non-framework cation sites as discussed below. Future extension of PDF analysis to geopolymers containing different alkali metal cations and with different Si/Al ratios will be able to provide a quantitative measure of the variation in ordering behavior with composition, thereby enabling detailed atomic-scale explanation of the observed nano- and microstructural details of these materials.[13]

The observation that the first Cs-O peak position and amplitude are largely unchanged between the geopolymer and pollucite structures also has potentially interesting implications in terms of the hydration of Cs^+ cations within a geopolymeric structure. Barbosa *et al.*[39] postulated a structure for sodium aluminosilicate geopolymers involving hydrated Na^+ cations trapped within the aluminosilicate matrix, charge-balancing the negative AlO_4^- tetrahedra. Duxson *et al.*[40] provided an explanation for the differences between Na- and K-containing geopolymers based on the differences in hydration properties of Na^+ and K^+ cations. It is therefore expected that alkali cation hydration plays a significant role in determining geopolymer structure. Cs^+ cations hydrate much less strongly than Na^+ or K^+ [41], and a hydrated Cs^+ complex may be too large to fit within the geopolymer framework structure, so it is not intuitively obvious whether these cations would be expected to be hydrated within a geopolymer structure.

Any water molecules associated with the Cs^+ cations in the geopolymer structure at room temperature would definitely be released during heating to 1400°C, so the position of the first Cs-O peak in Figure 6a may be taken to be indicative of the distance between a non-hydrated Cs^+ cation and a neighboring framework oxygen atom. The effective charge density of a hydrated ion is reduced by the shielding effects of the water molecules, meaning that a strongly hydrated Cs^+ would be less attracted strongly to the negatively-

charged framework oxygen atom, and therefore would display a longer bond distance than its non-hydrated counterpart in the pollucite structure. The similarities between the Cs-O correlations in the geopolymer and in pollucite suggest that the Cs^+ cations associated with the geopolymer framework oxygen atoms are not strongly hydrated. The absence of any Cs-O correlation at $r < 3.0$Å in Figure 6a also supports this contention, as a fully hydrated Cs^+ cation would be expected to have two water molecules located within this radius.[41] The evidence presented here cannot provide conclusive proof of the hydration state of the Cs^+ cations, but in the absence of a comprehensive published NMR study of cesium aluminosilicate geopolymers, it does provide a highly valuable source of structural information.

Conclusions

Analysis of a cesium aluminosilicate ($CsAlSi_2O_6$) geopolymer by the X-ray pair distribution function technique shows that structural ordering within the geopolymer gel phase is present only up to a length scale of ~8Å. Thermal transformation of the geopolymer to pollucite provides a highly crystalline product, with some structural changes starting to appear from 800°C upwards and essentially full crystallization by 1400°C. The pollucite and the geopolymer show very similar short-range (<5Å) structure, although the positions of the charge-balancing Cs^+ cations do vary. Real-space Rietveld refinement of pollucite lattice parameters from PDF data gives a unit cell that is either cubic or very slightly tetragonal, with refinement to a tetragonal structure giving a better fit to the experimental data but a larger uncertainty in lattice parameters. The PDF method displays great potential as a tool for analyzing geopolymer structures, as it is most sensitive to ordering behavior on a length scale spanning the range in which geopolymers are observed to display an ordered structure.

References

[1]T. Egami, "Atomic correlations in non-periodic matter," *Mater Trans JIM*, **31**[3] 163-176 (1990).

[2]T. Egami and S. J. L. Billinge, *Underneath the Bragg Peaks: Structural Analysis of Complex Materials*. Pergamon Materials Series, 7, Edited by R. W. Cahn, Plenum, Oxford, 2003.

[3]T. Proffen, S. J. L. Billinge, T. Egami and D. Louca, "Structural analysis of complex materials using the atomic pair distribution function - A practical guide," *Zeitschrift für Kristallographie*, **218** 132-143 (2003).

[4]S. J. L. Billinge and M. G. Kanatzidis, "Beyond crystallography: The study of disorder, nano crystallinity and crystallographically challenged materials with pair distribution functions," *Chemical Communications*, 749-760 (2004).

[5]X. Qiu, J. W. Thompson and S. J. L. Billinge, "PDFGetX2: A GUI-driven program to obtain the pair distribution function from X-ray powder diffraction data," *Journal of Applied Crystallography*, **37** 678 (2004).

[6]T. Proffen and S. J. L. Billinge, "PDFFIT, a program for full profile refinement of the atomic pair distribution function," *Journal of Applied Crystallography*, **32** 572-575 (1999).

[7]M. Martínez-Iñesta and R. F. Lobo, "Investigation of the negative thermal expansion mechanism of zeolite chabazite using the pair distribution function method," *Journal of Physical Chemistry B*, **109**[19] 9389-9396 (2005).

[8]M. Martínez-Iñesta, I. Peral, T. Proffen and R. F. Lobo, "A pair distribution function analysis of zeolite beta," *Microporous and Mesoporous Materials*, **77**[1] 55-66 (2005).

[9]V. Petkov, V. Parvanov, P. Trikalitis, C. Malliakas, T. Vogt and M. G. Kanatzidis, "Three-dimensional structure of nanocomposites from atomic pair distribution function analysis: Study of polyaniline and (polyaniline)$_{0.5}V_2O_5$•1.0H_2O," *Journal of the American Chemical Society*, **127**[24] 8805-8812 (2005).

[10]A. Palomo and F. P. Glasser, "Chemically-bonded cementitious materials based on metakaolin," *British Ceramic Transactions and Journal*, **91**[4] 107-112 (1992).

[11]M. Rowles, "The Structural Nature of Aluminosilicate Inorganic Polymers: A Macro to Nanoscale Study". Thesis. Curtin University of Technology, Perth, Australia, 2004.

[12]J. L. Provis, G. C. Lukey and J. S. J. van Deventer, "Do geopolymers actually contain nanocrystalline zeolites? - A reexamination of existing results," *Chemistry of Materials*, **17**[12] 3075-3085 (2005).

[13]P. Duxson, J. L. Provis, G. C. Lukey, S. W. Mallicoat, W. M. Kriven and J. S. J. van Deventer, "Understanding the relationship between geopolymer composition, microstructure and mechanical properties," *Colloids and Surfaces A - Physicochemical and Engineering Aspects*, **269**[1-3] 47-58 (2005).

[14]J. L. Provis, P. Duxson, G. C. Lukey and J. S. J. van Deventer, "A statistical thermodynamic model for Si/Al ordering in amorphous aluminosilicates," *Chemistry of Materials*, **17**[11] 2976-2986 (2005).

[15]R. M. Barrer and N. McCallum, "Hydrothermal chemistry of silicates. Part IV. Rubidium and cesium aluminosilicates.," *Journal of the Chemical Society*, [12] 4029-4035 (1953).

[16]S. A. Gallagher and G. J. McCarthy, "Preparation and X-ray characterization of pollucite ($CsAlSi_2O_6$)," *Journal of Inorganic and Nuclear Chemistry*, **43**[8] 1773-1777 (1981).

[17]D. C. Palmer, M. T. Dove, R. M. Ibberson and B. M. Powell, "Structural behavior, crystal chemistry, and phase transitions in substituted leucite: High-resolution neutron powder diffraction studies," *American Mineralogist*, **82**[1-2] 16-29 (1997).

[18]I. Yamase, H. Kobayashi, Y. Shibasaki and T. Mitamura, "Tetragonal-to-cubic structural phase transition in pollucite by low-temperature X-ray powder diffraction," *Journal of the American Ceramic Society*, **80**[10] 2693-2695 (1997).

[19]H. W. Xu, A. Navrotsky, M. L. Balmer and Y. L. Su, "Crystal chemistry and phase transitions in substituted pollucites along the CsAlSi2O6-CsTiSi2O6.5 join: A powder synchrotron X-ray diffractometry study," *Journal of the American Ceramic Society*, **85**[5] 1235-1242 (2002).

[20]N. J. Hess, F. J. Espinosa, S. D. Conradson and W. J. Weber, "Beta radiation effects in ^{137}Cs-substituted pollucite," *Journal of Nuclear Materials*, **281** 22-33 (2000).

[21]D. Taylor, "The thermal expansion of the leucite group of minerals," *American Mineralogist*, **53**[9-10] 1476-1488 (1968).

[22]M. Gordon and (co-authors..?), "Thermal expansion of pollucite measured by in-situ synchrotron X-ray diffractometry," *Manuscript in preparation*, (2006).

[23]M. Gordon, J. L. Bell and W. M. Kriven, "Comparison of naturally and synthetically derived, potassium-based geopolymers," *Ceram Trans*, **165** 95-106 (2004).

[24]

[25]M. A. Gülgün and W. M. Kriven, "A simple solution-polymerization route for oxide powder synthesis," *Ceram Trans*, **62** 57-66 (1995).

[26]M. A. Gulgun, M. H. Nguyen and W. M. Kriven, "Polymerized organic-inorganic synthesis of mixed oxides," *Journal of the American Ceramic Society*, **82**[3] 556-560 (1999).

[27]B. H. Toby and T. Egami, "Accuracy of pair distribution function analysis applied to crystalline and non-crystalline materials," *Acta Crystallographic A*, **48** 336-346 (1992).

[28]M. A. Hogan and S. H. Risbud, "Gel-derived amorphous cesium-aluminosilicate powders useful for formation of pollucite glass-ceramics," *Journal of Materials Research*, **6**[2] 217-219 (1991).

[29]S. V. Naray-Szabo, "Die Struktur des Pollucits CsAl2O6 - H2O," *Z. Kristallografiya*, **99** 277 - 282 (1938).

[30]R. E. Newnham, "Crystal Structure and Optical Properties of Pollucite," *The American Mineralogist*, **52**[9 - 10] 1515 - 1518 (1967).

[31]W. Loewenstein, "The distribution of aluminum in the tetrahedra of silicates and aluminates," *American Mineralogist*, **39**[1-2] 92-96 (1954).

[32]S. K. Lee and J. F. Stebbins, "The degree of aluminum avoidance in aluminosilicate glasses," *American Mineralogist*, **84**[5-6] 937-945 (1999).

[33]B. L. Phillips and R. J. Kirkpatrick, "Short-range Si-Al order in leucite and analcime: Determination of the configurational entropy from ^{27}Al and variable-temperature ^{29}Si NMR spectroscopy of leucite, its Cs- and Rb-exchanged derivatives, and analcime," *American Mineralogist*, **79**[11-12] 1025-1031 (1994).

[34]E. Dempsey, G. H. Kühl and D. H. Olson, "Variation of lattice parameter with aluminum content in synthetic sodium faujasites . Evidence for ordering of framework ions," *Journal of Physical Chemistry*, **73**[2] 387-390 (1969).

[35]V. Petkov, S. J. L. Billinge, S. D. Shastri and B. Himmel, "Polyhedral units and network connectivity in calcium aluminosilicate glasses from high-energy X-ray diffraction," *Physical Review Letters*, **85**[16] 3436-3439 (2000).

[36]J. L. Provis, P. Duxson, J. S. J. van Deventer and G. C. Lukey, "The role of mathematical modeling and gel chemistry in advancing geopolymer technology," *Chemical Engineering Research & Design*, **83**[A7] 853-860 (2005).

[37]H. Rahier, W. Simons, B. van Mele and M. Biesemans, "Low-temperature synthesized aluminosilicate glasses. 3. Influence of the composition of the silicate solution on production, structure and properties," *Journal of Materials Science*, **32**[9] 2237-2247 (1997).

[38]P. Duxson, J. L. Provis, G. C. Lukey, F. Separovic and J. S. J. van Deventer, "^{29}Si NMR study of structural ordering in aluminosilicate geopolymer gels," *Langmuir*, **21**[7] 3028-3036 (2005).

[39]V. F. F. Barbosa, K. J. D. MacKenzie and C. Thaumaturgo, "Synthesis and characterization of materials based on inorganic polymers of alumina and silica: sodium polysialate polymers," *International Journal of Inorganic Materials*, **2**[4] 309-317 (2000).

[40]P. Duxson, G. C. Lukey, F. Separovic and J. S. J. van Deventer, "The effect of alkali cations on aluminum incorporation in geopolymeric gels," *Industrial & Engineering Chemistry Research*, **44**[4] 832-839 (2005).

[41]C. S. Babu and C. Lim, "Theory of ionic hydration: Insights from molecular dynamics simulations and experiment," *Journal of Physical Chemistry B*, **103**[37] 7958-7968 (1999).

Section I – Thermal Expansion of Cesium Aluminosilicates

Introduction

Pollucite ($CsAlSi_2O_6$) is a framework aluminosilicate belonging to the feldspathoid group of minerals and is the cesium analog of potassium leucite (KAl_2SiO_6). All leucites have three defined regions of thermal expansion (Fig. 1), separated by an inversion temperature (T_i) and a discontinuity temperature (T_d).[1] Thermal expansions of leucite-type ceramics are the most rapid in Region I until the inversion temperature (T_i), at which the tetragonal structure becomes cubic. The inversion temperatures of leucites are specific to cation chemistry (e.g. K^+, Rb^+, Cs^+). Yanase *et al.* reported the pollucite inversion temperature ($I4_1/acd \rightarrow Ia\text{-}3d$) at 248 K using low-temperature X-ray diffraction (XRD).[2] Earlier workers did not resolve the inversion temperature of pollucite but reported a cubic phase at ambient temperatures.[1, 3, 4] More recently, however, Xu *et al.* and Palmer *et al*, reported that pollucite was tetragonal ($I4_1/a$) at room temperature, where ($c/a \approx 0.10014$) and ($c/a \approx 1.0051$), respectively.[5, 6] Xu et al. estimated the T_i of their pollucite sample to be ~ 301 K from an extrapolation of data taken from Palmer *et al.*

The thermal expansion of leucite ceramics in Region II is significantly lower than in Region I. Taylor and Henderson hypothesized that silica tetrahedral in leucite ceramics unfold and expand throughout Region II.[7] Taylor and Henderson concluded that silica tetrahedral reached a state of maximum expansion when the discontinuity temperature (T_d) was reached and that further expansion of leucite ceramics in Region III was solely the result of increasing inter-atomic bond lengths.[7] Taylor and Henderson reported the pollucite discontinuity temperature to be 190°C; later work by Taylor indicated that the discontinuity temperature was at 170°C.[1, 8] Kobayashi *et al.* offered an alternative view of the thermal expansion of pollucite in Region II, where silica tetrahedral form nine sets of rings, eight A-rings, and one B-ring.[9] In Region II, the A-rings undergo a rapid expansion, while the B-ring contracts until the discontinuity temperature is reached. Base on this model, Kobayashi *et al.* reported a discontinuity temperature of 673 K.[9]

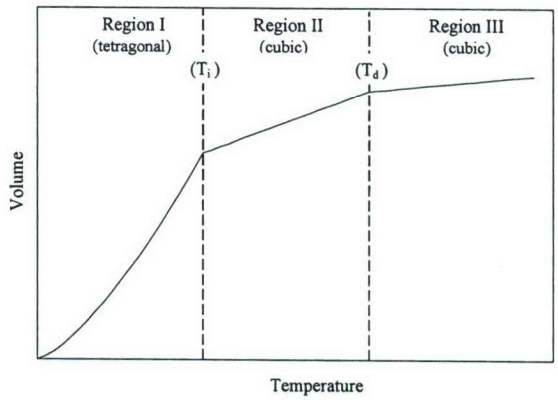

Fig. 2: Generic plot of the thermal expansion of leucite / pollucite ceramics

The thermal expansion of pollucite has been the subject of numerous studies.[1, 2, 8-15] Although individual measurement vary depending on the experimental technique used (e.g. XRD, dilatometer) and sample preparation, there is a general agreement that the thermal expansion is relatively low; Yanase *et al.* reported that the lattice expansion of cubic pollucite was ($\approx$ 0.43%) from 298 – 1273 K using high-temperature XRD.[15]

Pollucite tolerates a high degree of ionic substitution for both the alkali and metallic cations and can incorporate additional silica into the crystal structure. The affect of substitutions and silica dopants on the thermal expansion behavior of pollucite has been studied widely.[6, 8, 11, 12, 14-20] Of particular engineering interest are substitutions and dopants that lower the thermal expansion of pollucite. The incorporation of excess silica into pollucite ($Cs_{0.9}Al_{0.9}Si_{2.1}O_6$) reduced the thermal expansion of pollucite to 0.2% from 278 – 1273 K.[15] Partial substitution of Li^+ for Cs^+ in addition to silica doping lowered the expansion of pollucite to 0.14% from 278 – 1273 K.[15] Replacement of aluminum with boron yielded a cesium borosilicate ($CsBSi_2O_6$) with a negative thermal expansion between 293 – 373 K.[16]

In addition to its unique thermal expansion characteristics, pollucite is the most refractory silicate known ($T_{melt} > 1900^oC$) and has exceptional creep resistance between 1400 – 1500°C, comparable to the two most creep resistant ceramic oxides, mullite and yttrium-aluminum garnet (YAG).[10] The combination of creep resistance, high melting

temperature, and low thermal expansion make pollucite and pollucite glass-ceramics candidate materials for use in ceramic matrix composites (CMCs). The utility of pollucite ceramics for high temperature applications may be limited by the reported volitization of cesia, however.[10, 21]

The thermal expansion of other reported cesium aluminosilicate compounds ($CsAlSi_3O_8$, $CsAl_3Si_3O_{11}$ and $CsAlSi_5O_{12}$) have not been investigated. These compounds may share similar thermo mechanical properties as pollucite but be less prone to high-temperature cesia loss. The purpose of this study is to measure the thermal expansion of chemically prepared cesium aluminosilicate ceramics via high temperature XRD using synchrotron radiation. Complicating the research in this area is the lack of background knowledge via phase diagrams. Only one phase diagram of the Cs_2O-Al_2O_3- SiO_2 system, a theoretical isotherm of at ~ 877 °C, exists in literature.[24]

Experimental Procedures

Cesium aluminosilicate powders (Table 1, Fig. 3) were prepared by the organic, steric entrapment method.[25, 26] The powders were synthesized using metallic salts, aluminum nitrate nonahydrate, 98+% and cesium nitrate, 99% (Sigma-Aldrich, Milwaukee, WI) in combination with Ludox SK colloidal silica (Grace Division, Columbia, Maryland) and Celvol® polyvinyl alcohol ($M_w \approx 35{,}000$ g/mol). Potassium leucite was prepared for comparison purposes (Table 1), substituting potassium nitrate, 99% (Sigma-Aldrich) for cesium nitrate.

Table 1: Aluminosilicate powders produced by the steric entrapment method.

Powder	Nominal Composition	Reported Oxide	Designation
A	Cs_2O - Al_2O_3 - 4 SiO_2	$CsAlSi_2O_6$	Pollucite
B	Cs_2O - Al_2O_3 - 6 SiO_2	$CsAlSi_3O_8$	Cs - Feldspar
C	Cs_2O - Al_2O_3 - 10 SiO_2	$CsAl_3Si_5O_{12}$	Cs – Zeolite
D	Cs_2O - 3 Al_2O_3 - 6 SiO_2	$CsAl_3Si_3O_{11}$	Cs - Mica
K	K_2O - Al_2O_3 - 4 SiO_2	$KAlSi_2O_6$	Leucite

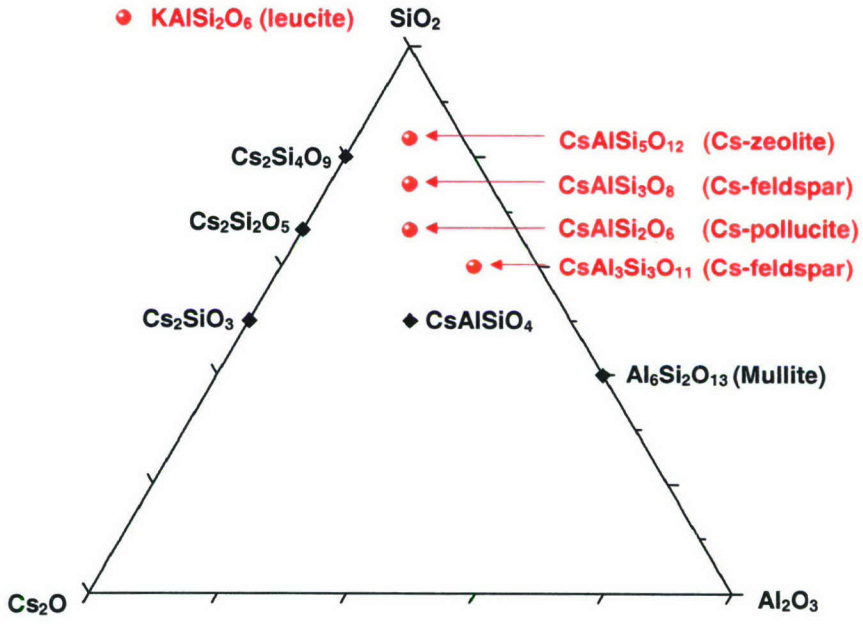

Fig. 3: Ternary phase diagram of the Cs_2O-Al_2O_3-SiO_2 system showing compositions synthesized in this study (●) and other compounds (◆).

The resulting powders were calcined at 800°C for one hour using a ramp rate of 5°C/min in covered platinum crucibles. The powders were then crystallized by heating to 1300°C for five hours at 5°C/min. Initial X-ray diffraction analysis of the heated powders, performed using a Rigaku-D/Max diffractometer (Rigaku Corporation, The Woodlands, TX) showed that single-phase pollucite was not formed. A final heat treatment at 1400°C for ten hours at 5°C/min in platinum crucibles sealed with refractory cement was necessary to form single-phase pollucite. The powders were ground in a mortar and pestle, sieved through –325 (45 μm) stainless steel mesh. Elemental analysis of the powders was performed using a JOEL JSM-6060LV (JOEL USA, Inc. Peabody, MA) equipped with an Oxford Instruments ISIS energy dispersive spectrometer system (EDS) (Oxford Instruments America, Inc., Concord, MA).

In-situ High temperature x-ray diffraction (HTXRD) was performed with synchrotron radiation at the National Photon Source (Argonne, IL). Samples were heated using a quadruple, ellipsoidal, mirror heater furnace that was developed in our research laboratory.[27, 28] Samples were tested using a reflection mode geometry, rocking ± 2° 2θ. The powders were mixed with colloidal platinum powder using a mortar and pestle and heated in a furnace to 450°C to enlarge the platinum crystallite size prior to HTXRD. The temperatures of the samples were determined by the calculating the lattice parameters of the platinum that had been mixed with the ceramic powders. Lattice parameters of the ceramic phases were determined using the Rietveld method with JADE crystallography software (Materials Data Inc., Livermore, California).

Results

Powders A and K crystallized into the single-phase pollucite and leucite, respectively. Higher silica content powders (B and C) formed dual-phase mixtures of pollucite and Cs-zeolite. Powder D, with a composition corresponding to Cs-mica, crystallized into non-stoichiometric pollucite. The lattice spacing of off-stoichiometric pollucites were 0.18 – 0.26% smaller than measured stoichiometric pollucite (Table 2). Comparing powders with identical Al / Cs ratios, the volume of the pollucite and Cs-zeolite decreased with increasing silica content.

Stoichiometric pollucite had the lowest thermal expansion, 1.00% $\Delta V/V_o$ (25 – 1472°C) of all the tested compositions (Fig. 4). An initial, rapid thermal expansion below 300°C was observed in all of the pollucites (Fig. 5). The Cs-zeolite also appeared to have two regions of thermal expansion (Fig. 4). Using a linear fit, the first region, (≤ 813°C) is marked by a thermal expansion rate of 3.74 % $\Delta V/V_o$ (20 – 813°C). The rate of thermal expansion in the Cs-zeolite decreased by 68.8% in the second region (≥ 813 °C). The highest thermal expansion was observed in leucite 6.98 % $\Delta V/V_o$ (20 – 1494°C), followed by the Cs-zeolite 4.68 % $\Delta V/V_o$ (20 – 1408°C). The tetragonal to cubic inversion of leucite took place between 462 and 646°C (Fig. 6, Fig. 4).

Table 2. Lattice parameters of pollucite, leucite and Cs-zeolite at room temperature

Powder	Observed Compounds	a-axis (Å)	b-axis (Å)	c-axis (Å)	Unit cell volume ($Å^3$)
A	Pollucite	13.69639			169.0000
B	Pollucite	13.66207			169.0000
C	Pollucite	13.66074			169.0000
D	Pollucite	13.67119			169.0000
B	Cs-zeolite	16.60886	13.80948	5.03448	169.0000
C	Cs-zeolite	16.74442	13.80156	5.02434	169.0000
K	Leucite	13.08617	13.08617	13.75270	169.0000

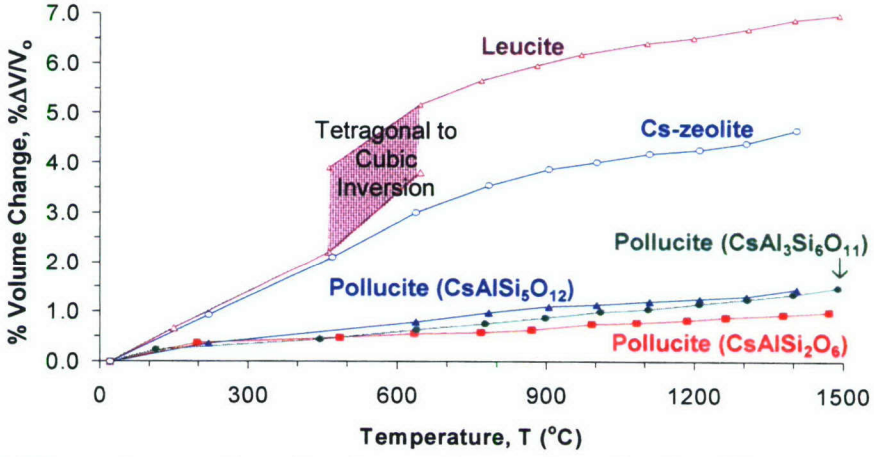

Fig. 4. Thermal expansion of cesium and potassium aluminosilicate compounds

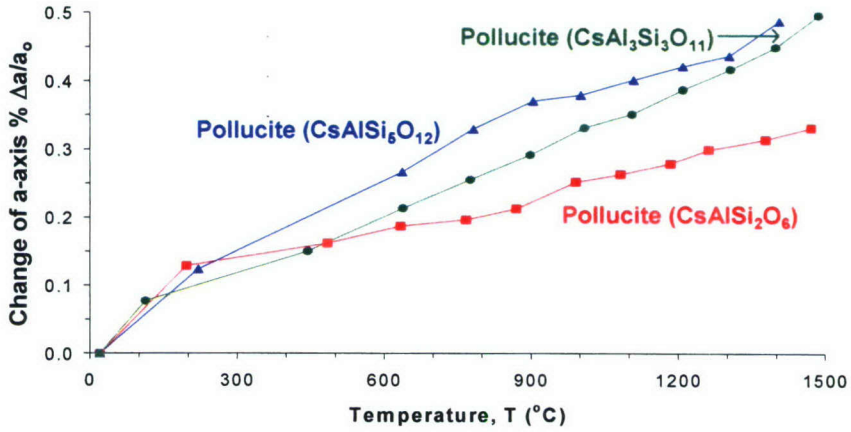

Fig. 5. Thermal expansion of pollucite in stoichiometric pollucite powder ($CsAlSi_2O_6$) in solid solution ($CsAl_3Si_3O_{11}$) and in a dual-phase mixture ($CsAlSi_5O_{12}$).

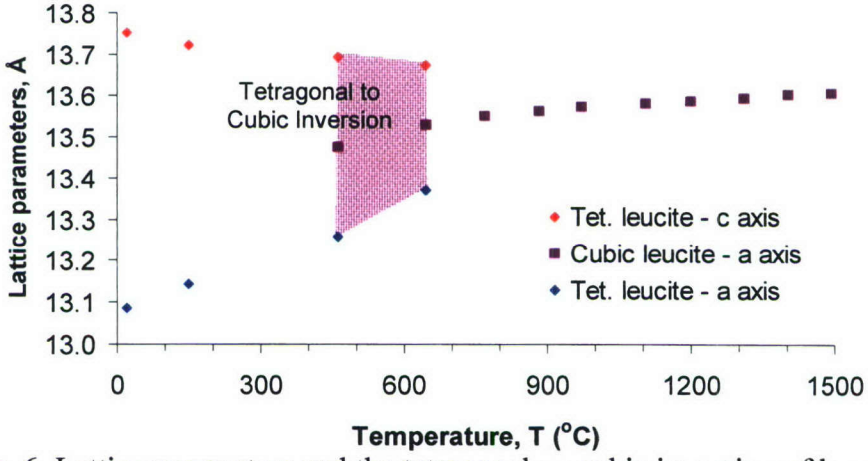

Fig. 6. Lattice parameters and the tetragonal → cubic inversion of leucite

Table 3: Powder compositions based on a series of EDS analyses, ± standard deviations of the measurements (% difference from the expected nominal composition)

Powder	$(Cs,K)_2O$	Al_2O_3	SiO_2
A	1.16 ± 0.12	1.00 ± 0.06	4.39 ± 0.32
B	1.23 ± 0.29	1.00 ± 0.07	5.86 ± 0.39
C	1.00 ± 0.40	1.00 ± 0.37	9.44 ± 2.35
D	0.47 ± 0.29	3.00 ± 0.30	5.40 ± 0.50
K	1.05 ± 0.22	1.00 ± 0.18	3.89 ± 0.22

Discussion

Neither the Cs-feldspar, $CsAlSi_3O_8$ nor the Cs-mica, $CsAl_3Si_3O_{11}$ were detected during the experiment. The absence of the $CsAlSi_3O_8$ phase is due to the sizes of the Li^+ and Cs^+ cations, which are too small and large (respectively) to be integrated into the feldspar structure.[29] The observed absence of the Cs-feldspar structure is consistent with other work.[30] The Cs-mica in Keppler's study was prepared by intercation exchange using hydro thermally prepared paragonite and molten CsCl.[23] It is apparent from this study that Keppler's preparation yielded a non-equilibrium phase. The organic steric entrapment route of processing can only be used to make glassy and equilibrium ceramic phases and was not able produce the structure reported by Keppler.

Kobayashi *et al.* reported the crystallization of single-phase pollucite when prepared from $CsAlSi_{2.5}O_7$ powder.[12] This study suggests that between $CsAlSi_{2.5}O_7$ – $CsAlSi_3O_8$ the pollucite structure can no longer accommodate additional silica without precipitating out the Cs- zeolite. The formation of pollucite with a nominal composition of $CsAl_3Si_3O_{11}$ indicates that the range of the pollucite solid-solution phase is wider than originally known.

The pollucite powder ($CsAlSi_2O_6$) prepared had a smaller lattice parameter than what and lower thermal expansion than anticipated.[3, 15] The smaller observed lattice parameter and lower thermal expansion could be attributed to a minor excess of silica in the pollucite powder, which was supported by EDS analysis of the powder (Table 3). Yanse *et al.* reported a marginal decrease in the lattice constant of pollucite (a = 1.3680(1) and a=1.3679(1) nm) and lower thermal expansion in silica-doped pollucite.[15]

An insufficient number of data points at lower temperatures were taken to identify the discontinuity temperature of the synthesized pollucites. Initial, higher thermal expansions of the pollucites indicated, however that the discontinuity temperatures were below 300°C.

The crystallization of both non-stoichiometric pollucite and cesium-zeolite from powder C was due to a silica deficiency in the powder, indicated by EDS analysis. In general however, EDS results were imprecise. Standard deviations of the alkali (K,Cs) contents of the powders were approximately 30%. Given the limitations of EDS (a surface technique with a high-degree of variability) and the general difficulty obtaining accurate measurements of alkali elements using EDS, the molar ratios presented in Table 3 should be considered only rough approximations.

The observed thermal expansion characteristics of leucite and the inversion temperature was characteristic of literature values.[1, 8]

Conclusion

Neither Cs-feldspar nor Cs-mica crystallized as equilibrium phases in the $Cs_2O - Al_2O_3 - SiO_2$ system. The solid-solution range of pollucite includes both silica-rich ($CsAlSi_{2.5}O_7$) and aluminum rich ($CsAl_3Si_3O_{11}$) compositions. The measured thermal expansion of stoichiometric pollucite was 1.00% $\Delta V/V_o$ (25 – 1472°C). The thermal expansion of cesium zeolite ($CsAlSi_5O_{12}$) was separated into two regions, a region of higher thermal expansion, 3.74 % $\Delta V/V_o$ (20 - 813°C) and a second region with lower thermal expansion, 0.94 % $\Delta V/V_o$ (813 – 1408°C). The unit cell volume of both pollucite and Cs-zeolite decreased with increasing concentrations of silica. The tetragonal to cubic inversion temperature of leucite was between 462 – 646°C, consistent with observations in literature.

References

[1]D. Taylor, "The thermal expansion of the leucite group of minerals," *American Mineralogist*, **53**[9-10] 1476-1488 (1968).
[2]I. Yanase, H. Kobayashi, Y. Shibasaki and T. Mitamura, "Tetragonal-to-cubic structural phase transition in pollucite by low-temperature X-ray powder diffraction," *Journal of the American Ceramic Society*, **80**[10] 2693-2695 (1997).
[3]S. V. Naray-Szabo, "Die Struktur des Pollucits CsAl2O6 - H2O," *Z. Kristallografiya*, **99** 277 - 282 (1938).
[4]R. E. Newnham, "Crystal Structure and Optical Properties of Pollucite," *The American Mineralogist*, **52**[9 - 10] 1515 - 1518 (1967).

[5]D. C. Palmer, M. T. Dove, R. M. Ibberson and B. M. Powell, "Structural behavior, crystal chemistry, and phase transitions in substituted leucite: High-resolution neutron powder diffraction studies," *American Mineralogist*, **82**[1-2] 16-29 (1997).
[6]H. W. Xu, A. Navrotsky, M. L. Balmer and Y. L. Su, "Crystal chemistry and phase transitions in substituted pollucites along the CsAlSi2O6-CsTiSi2O6.5 join: A powder synchrotron X-ray diffractometry study," *Journal of the American Ceramic Society*, **85**[5] 1235-1242 (2002).
[7]D. Taylor, "The thermal expansion behaviour of framework silicates," *Mineralogical Magazine*, **38**[297] 593-604 (1972).
[8]D. Taylor, "Thermal-expansion data .15. complex oxides with the leucite structure and frameworks based on 6-membered rings of tetrahedra," *British Ceramic Transactions and Journal*, **90**[6] 197-204 (1991).
[9]H. Kobayashi, I. Yanase and T. Mitamura, "A new model for the pollucite thermal expansion mechanism," *Journal of the American Ceramic Society*, **80**[8] 2161-2164 (1997).
[10]R. S. Hay, T. A. Parthasarathy and J. R. Welch, "Creep and stability of pollucite"; pp. 89-104 in Ceramic Transactions, Vol. 52, *Low-Expansion Materials* Edited by D. P. Stinton and S. Y. Limayme, American Ceramic Society, Westerville, OH, 1995.
[11]H. Kobayashi, T. Terasaki, T. Mori, H. Yamamura and T. Mitamura, "Thermal-expansion characteristics of Li-replaced type pollucite (Cs1-XLixAlSi2O6) powder," *Nippon Seramikkusu Kyokai Gakujutsu Ronbunshi-Journal of the Ceramic Society of Japan*, **99**[12] 1274-1276 (1991).
[12]H. Kobayashi, T. Terasaki, T. Mori, H. Yamamura and T. Mitamura, "preparation and thermal-expansion behavior of excess SiO2 pollucite powders," *Nippon Seramikkusu Kyokai Gakujutsu Ronbunshi-Journal of the Ceramic Society of Japan*, **100**[1] 91-93 (1992).
[13]D. W. Richerson and H. F. A., "Synthesis and thermal expansion of polycrystalline cesium minerals," *Journal of the American Ceramic Society*, **55** 269-272 (1972).
[14]I. Yanase, H. Kobayashi and T. Mitamura, "Thermal expansion property of synthetic cubic leucite-type compounds," *Journal of the Ceramic Society of Japan*, **108**[1] 26-31 (2000).
[15]I. Yanase, S. Tamai and H. Kobayashi, "Low-thermal-expansion properties of sodium- and lithium-substituted cubic cesium leucite compounds," *Journal of the American Ceramic Society*, **86**[8] 1360-1364 (2003).
[16]R. S. Bubnova, N. K. Stepanov, A. A. Levin, S. K. Filatov, P. Paufler and D. C. Meyer, "Crystal structure and thermal behaviour of boropollucite CsBSi2O6," *Solid State Sciences*, **6**[7] 629-637 (2004).
[17]D. Mazza and M. LuccoBorlera, "On the substitution of Fe and B for Al in the pollucite (CsAlSi2O6) structure," *Journal of the European Ceramic Society*, **17**[14] 1767-1772 (1997).
[18]I. Yanase, H. Kobayashi and T. Mitamura, "Thermal property and phase transition of the synthesized new cubic leucite-type compounds," *Journal of Thermal Analysis and Calorimetry*, **57**[3] 695-705 (1999).
[19]I. Yanase, H. Kobayashi and T. Mitamura, "Synthesis of cubic Cs2FeSi5O12 powder in Ar atmosphere and its thermal expansion property," *Journal of the Ceramic Society of Japan*, **108**[7] 677-680 (2000).

[20]I. Yanase, N. Miyashita, H. Kobayashi, F. Noguchi and T. Mitamura, "Synthesis and thermal expansion property of cubic Cs2MSi5O12 (M = Cd, Ni, Zn) powders," *Journal of the Ceramic Society of Japan*, **106**[11] 1099-1103 (1998).
[21]I. MacLaren, J. Cirre and C. B. Ponton, "Hydrothermal synthesis of pollucite (CsAlSi2O6) powders," *Journal of the American Ceramic Society*, **82**[11] 3242-3244 (1999).
[22]V. D. Borutskaya, *Akad. Nauk SSSR* **222** 150 (1975).
[23]H. Keppler, "Ion exchange between dehyroxylated micas and salt melts and the crystal chemistry of the interlayer cation in micas," *American Mineralogist*, **75** 529-538 (1990).
[24]T. B. Lindemer, T. M. Besmann and C. E. Johnson, "Thermodynamic review and calculations - alkali-metal oxide systems with nuclear-fuels, fission-products, and structural-materials," *Journal of Nuclear Materials*, **100**[1-3] 178-226 (1981).
[25]M. A. Gulgun, M. H. Nguyen and W. M. Kriven, "Polymerized organic-inorganic synthesis of mixed oxides," *Journal of the American Ceramic Society*, **82**[3] 556-560 (1999).
[26]S. J. Lee and W. M. Kriven, "Crystallization and densification of nano-size, amorphous cordierite powder prepared by a solution-polymerization route," *Journal of the American Ceramic Society*, **81** [10] 2605-2612 (1998).
[27]L. F. Siah, W. M. Kriven and J. Schneider, "In situ, high-temperature, synchrotron, powder diffraction studies of oxide systems in air, using a thermal-image furnace," *Measurement Science & Technology*, **16**[6] 1291-1298 (2005).
[28]P. Sarin, W. Yoon, K. Jurkschat, P. Zschack and W. M. Kriven, "Quadrupole Lamp Furnace for High Temperature (up to 2050K) Synchrotron Powder X-Ray Diffraction Studies in Air," *Review of Scientific Instruments*, (submitted).
[29]F. Liebau, *Structural Chemistry of Silicates*. New York Springer-Verlag. 250 - 252. 1985
[30]C. L. Liu, S. Komarneni and R. Roy, "Seeding effects on crystallization of KAlSi3O8, RbAlSi3O8, and CsAlSi3O8 gels and glasses," *Journal of the American Ceramic Society*, **77**[12] 3105-3112 (1994).